UNIVERSITÀ
DEGLI STUDI
FIRENZE

DOTTORATO DI RICERCA IN
INGEGNERIA INDUSTRIALE E DELL'AFFIDABILITÀ

CICLO XXVII

COORDINATORE Prof. Maurizio De Lucia
REFERENTE Prof. Mario Tucci

Navigation Systems for Unmanned Underwater Vehicles

Settore Scientifico Disciplinare ING-IND/13

Dottorando
Dott. Riccardo Costanzi

Tutor
Prof. Benedetto Allotta

Coordinatore
Prof. Maurizio De Lucia

Anni 2012/2014

Al Mare,

alla bellezza vera delle Sue molteplici espressioni,

ed alle storie che custodisce nella Sua pace.

Riflessioni

Giunto, infine, agli ultimi momenti del percorso dei miei studi, questa pagina di riflessioni assume per me una notevole importanza perché è scritta con l'intento di raccogliere e descrivere l'insieme di sensazioni ed impressioni che il rapporto con le persone che ho avuto la fortuna di incontrare negli anni ha suscitato in me.

Vorrei qui manifestare il mio ringraziamento verso il gruppo di persone con le quali ogni giorno ho modo di interagire all'interno del Dipartimento di Ingegneria Industriale dell'Università di Firenze ed in particolare verso tutti i ricercatori ed i professori del laboratorio di Modellazione Dinamica e Meccatronica per la positiva e coinvolgente atmosfera che vi si respira e per aver facilitato ed alleggerito, grazie a questo, il lavoro che sono riuscito a svolgere.

Nel particolare, il mio grande riconoscimento va al Prof. Benedetto Allotta che, grazie al suo lavoro ed alla sua passione per questo, è riuscito a far crescere notevolmente e rapidamente il gruppo di ricerca di cui faccio parte; tengo molto al rapporto umano e professionale di reciproca fiducia che nel tempo si è instaurato. Allo stesso modo tengo a manifestare qui l'apprezzamento che provo per il rapporto, di amicizia, prima che lavorativo, che mi lega ad alcuni "colleghi", attuali e passati, del laboratorio: Gregorio, prima guida e poi esempio da seguire; Alessandro, presente costantemente nel confronto tanto professionale quanto personale; Marco e Niccolò, dai quali ho imparato davvero molto sia dal punto di vista tecnico che umano; Fabio, Jonathan, Enrico, Roberto e Francesco, che mi hanno dimostrato di riconoscere e di coltivare sia il valore dell'amicizia che quello del lavoro.

Un ruolo fondamentale nella mia formazione e nella mia crescita è stato svolto dal rapporto di collaborazione con tutti gli studenti che ho avuto la possibilità di seguire durante i loro lavori di tirocinio e tesi presso il laboratorio. Molto importanti e formative sono state, senza dubbio, le collaborazioni con i gruppi di ricerca guidati dal Prof. Andrea Caiti, Prof. Nicola Casagli e Prof. Luigi Chisci e con i ricercatori che lavorano nei rispettivi gruppi, primi tra tutti Davide, Francesco e Claudio.

Il fine ultimo, legato all'archeologia sottomarina, dei progetti (THESAURUS e ARROWS) nell'ambito dei quali ho lavorato principalmente, mi ha dato la possibilità di incontrare ed interagire con personalità che operano in questo affascinante campo. Tra le varie persone conosciute, le due più significative, per l'interesse che hanno suscitato in me rispetto a questo settore di ricerca, sono Pamela Gambogi, coordinatore del Nucleo Operativo Subacqueo della Soprintendenza Archeologica della Toscana e Jacob (Koby) Sharvit, direttore della Underwater Archaeology Unit della Israel Antiquities Authority.

Una parte di queste pagine non può non essere dedicata agli amici con i quali ho la fortuna di condividere tutto ormai da molti anni: Beniamino, Luca, Niccolò, Daniele, Sara e Alberto hanno rappresentato e rappresentano, anche quando le vicende delle nostre vite ci hanno portato a vivere a molti chilometri di distanza, una parte fondamentale dell'essenza della mia vita. Insieme, fondamentale per me, oggi come quasi dieci anni fa quando ci siamo conosciuti sui banchi dell'università, è l'amicizia con Alessio, Irene, Oriana, Luana, Federica, Frank e Tancredi, fondata su un sincero affetto e, per questo, sopravvissuta intatta alla fine degli studi insieme.

Vorrei, poi, spendere qualche parola per la mia famiglia, i miei genitori e

mio fratello, per esprimere la mia sincera riconoscenza per i valori che mi hanno sempre comunicato e per avermi insegnato ad affrontare la vita col sorriso, lavorando per il perseguimento dei miei desideri, delle mie ambizioni e delle mie passioni, sempre appoggiandomi e supportandomi. Infine, qualche riga per ringraziare Francesca, accanto a me da quasi cinque anni ormai, per avermi mostrato, in questo inizio di viaggio insieme, aspetti ed angoli del mondo e sentimenti puri che non avevo mai conosciuto prima.

A tutte le persone citate, direttamente o indirettamente, va il mio sincero ringraziamento perché è grazie anche all'incontro con loro che, con la presente tesi, si conclude questo mio percorso.

Firenze, 21 Dicembre 2014 *Riccardo*

Contents

Abstract

This thesis collects the experiences and the works that I carried out in the field of Underwater Robotics during the three years of my Ph.D. study period at the Mechatronics and Dynamic Modelling Laboratory (MDM Lab) of the DIEF (Department of Industrial Engineering - Florence, former Department of Energy Engineering) of the University of Florence, between the 2012 and the 2014.

During this period, the research group of the MDM Lab has been actively involved in the design, construction and control of UUVs (Unmanned Underwater Vehicles), underwater vehicles without a pilot on board, within the framework of several projects. UUVs are classified into two main categories:

- **ROVs (Remotely Operated Vehicles) -** the pilot is a human being who guides the vehicle interfacing with a control console on the support ship. The ROV is always connected to the ship through an umbilical cable that has the double functionality of supplying the required power and of ensuring a continuous data exchange with the surface.

- **AUVs (Autonomous Underwater Vehicles) -** in this case the vehicles are fully autonomous and they do not require the involvement of an operator for the motion and the payload control. No cable is required so an AUV can perform a mission even far away from the deployment place with the only constraint of preserving enough energy (usually stored in batteries placed on board) to reach the recovery point.

The projects, involving the MDM Lab during the years 2012-2014, dealt with both the types of UUVs. In particular, the group began dealing with the research in the field of Underwater Robotics with the awarding of the

THESAURUS (TecnicHe per l'Esplorazione Sottomarina Archeologica mediante l'Utilizzo di Robot aUtonomi a Sciami) project started in March 2011, funded by Regione Toscana. Within THESAURUS (successfully concluded at the end of the 2013 summer), MDM Lab was partner of a consortium coordinated by Centro Enrico Piaggio of the University of Pisa. The goal of the THESAURUS project was to develop multidisciplinary scientific methodologies useful to individualize, survey, register and document artefacts and underwater wrecks of archaeological, historical-artistic and anthropological value. One of the means to be developed within the framework of the THESAURUS project to successfully achieve its aims was a small team of AUVs, equipped with optical and acoustic payload sensors, capable of cooperating for a common purpose, exploiting also the possibility of communicating among themselves through acoustics means. The MDM Lab role within the project included the design, the development and the construction of the AUVs of the team in addition to the implementation of the Guidance, Navigation and Control (GNC) software capable of ensuring the AUVs to be able to autonomously travel, in safe conditions, along a desired trajectory.

During the last year of the THESAURUS project, MDM Lab began working on the ARROWS (ARchaeological RObot systems for the World's Seas) FP7 European project as coordinator partner (3 years from September 1st, 2012). The ARROWS project aim is very similar to the THESAURUS one, with some steps forward including the capability of an autonomous dynamical real-time re-planning of a mission based on a distributed ontology world model updated by means of the several cooperating vehicles and shared among themselves. The role of the MDM Lab concerns the design, the development and the construction of a new AUV, with strong characteristics of modularity, and the implementation of the GNC system. This new AUV

has to be integrated within a heterogeneous team of already existing AUVs (owned by other project partners) or developed from the scratch within the framework of ARROWS.

Other vehicles, on which I had the opportunity of working during my Ph.D. study period at the MDM Lab, include a small AUV whose design is closely related to the rules of SAUC-E (Student Autonomous Underwater Vehicle Challenge - Europe), an annual European academic competition organized by the NATO-CMRE (North Atlantic Treaty Organization - Center for Maritime Research & Experimentation) and a small ROV, result of the collaboration with the DST (Dipartimento di Scienze della Terra - Department of Earth Sciences) of the University of Florence which has been specifically designed and built for the monitoring activity of the Costa Concordia wreck, at Isola del Giglio.

For both AUVs and ROVs, a very significant role is played by the navigation system, i.e. the collection of the hardware and the software components to be used for the estimation, moment by moment, of the vehicle pose (comprising both the position and the orientation). In fact, the quality of such a system, if on one hand, affects the performance of the piloting of the vehicle in terms of error between the desired task and the really performed one, on the other side, it interests the quality of the georeferencing process for the acquired payload data. This statement is true for each mobile robot used to acquire information about its working environment, but in the underwater field it represents a very demanding challenge as radio waves are quickly completely absorbed by water so that the GPS signal is not able to reach a vehicle navigating even a few centimeters below the surface.

The subject of this thesis and of my research activity during last three years regards exactly the navigation system for vehicles in the underwater

field. Common navigation techniques are based on sensor fusion strategies, usually exploiting recursive filtering algorithms. In the underwater applications, the state of the art shows how the standard (i.e. the most used) algorithm is the Kalman Filter, in particular the "Extended" version of it as the system is intrinsically strongly non-linear with respect to the state components. The phases of this typology of algorithms are two per each iteration, in particular the *prediction* step that bases the estimation on the knowledge of the model of the dynamical evolution of the system and the *correction* step that updates the estimation through the measures of some quantities related to the state components, obtained by means of the available sensors.

The strategies followed in the framework of the carried out research activity are thus mainly based on two ways. On one hand, the attention has been directed to the development of position measurement techniques (*localization*), alternative to the common and expensive acoustic positioning systems used to replace the GPS, in order to bring an improvement in the correction phase. Along the same way a particular effort has been dedicated to the development of dynamical models (*modelling*) for the vehicle motion enough accurate, but at the same time not too computationally demanding, in order to be used in the prediction phase of the navigation algorithms.
On the other hand, a substantial part of the research activity has been devoted to the study of a proper navigation algorithm itself to investigate the possibility of overcoming the performance generally obtained in the state of the art through the EKF. In particular, the object of the investigation has been the Unscented Kalman Filter (UKF), in the practice almost never used in underwater applications but, representing, for non-linear systems, an advantageous trade-off between computational cost and estimation performance.

The thesis is organized according to the following scheme. Chapter 1 is the introduction used to provide the details of the framework in which this work took place, in particular, a description of the projects and thus of the vehicles will be useful as a basis to understand the succeeding sections, especially the ones about experimental results. Chapter 2 describes the current state of the art as concerns AUVs and ROVs, with particular attention to the topics of navigation, modelling and localization in the field of underwater robotics. Chapter 3 explains some of the limits of the current state of the art about the modelling topic addressed within this work. Chapter 4 explains that an effort is necessary in the field of research to break down the costs due to the use of the acoustic positioning systems. The aim is to identify, for particular common applications, some strategies to exploit less expensive sensors in order to achieve comparable results in terms of position measurement. Chapter 5 describes the process and the reasons that brought to the identification of the UKF as an advantageous alternative to the usually employed EKF. Chapter 6 explains some significant results obtained through simulations and experimental testing campaigns with different vehicles during the missions recently performed. Finally, chapter 7 summarizes the conclusions that can be inferred from the obtained results.

Chapter 1

Introduction

This chapter is the necessary introduction to the description of the carried out work and the research activity. In particular, the purpose of these first pages of the thesis is to provide the details about the framework in which the work took place, both concerning the timing and the activities of the research group. The main features of a Guidance, Navigation and Control System (GNC System) for an underwater vehicle with particular attention to the role of the navigation aspects will be discussed to introduce the description of the state of the art (chapter 2) and the following chapters.

1.1 Overall Framework

The underwater robotics as a research topic was introduced at the Department of Industrial Engineering of Florence (DIEF - former Department of Energy Engineering) in 2011, when a Tuscan Region call was won by a consortium, coordinated by Prof. Andrea Caiti and his research group at Centro Enrico Piaggio of the University of Pisa, and including the DIEF - Mechatronics and Dynamic Modelling Laboratory (MDM Lab). The winning proposal,

in addition to an important part about research in the field of underwater archaeology and to the production of a regional database for knowledge collection and archiving, included the production of a robotics system composed of three Autonomous Underwater Vehicles (AUVs), differentiated as concerns the payload and with communication capabilities, to be employed for monitoring of known submerged sites and the potential discovery of unknown ones. Within the project, baptized **THESAURUS** - TecnicHe per l'Esplorazione Sottomarina Archeologica mediante l'Utilizzo di Robot aUtonomi a Sciami - (figure 1.1) [Allotta and Caiti, 2014], the MDM Lab had the role of designing and assembling the AUVs and of implementing the low level control software, including all the GNC capabilities and the safety logic in order the AUVs to be able of autonomously travelling, in safe conditions, along a desired trajectory. The activity in which my research activity took

Figure 1.1: THESAURUS Project logo and Tuscan Region (project funder) logo

place within the THESAURUS project is the design and the implementation of the GNC system. The outcome of the project includes two vehicles of the same class, named *Typhoon* (figure 1.2), respectively called TifOne and TifTu, that demonstrated to compose a reliable system both during the final demonstration of the project (August 2013) and in the immediately subsequent follow up activities, including various research missions in sea in Italy and abroad in addition to a new project, that has received funding from the European Union's Seventh Framework programme for research,

Figure 1.2: THESAURUS Project - Picture of the team with the TifOne AUV of Typhoon class - Roffia (San Mianiato - Pisa), tests at lake

technological development and demonstration.

One of the most significant initiatives born as follow up of the THESAURUS project is, in fact, the **ARROWS** - ARchaeological RObot systems for the World's Seas -European project (figure 1.3) [Allotta, 2014], started on September 1st, 2012. ARROWS, coordinated by MDM Lab and including

Figure 1.3: ARROWS Project logo and European Commission (project funder) flag

ten partners from Europe, is a project very similar to THESAURUS with some important steps forward within its goals. In particular, the aim is to demonstrate, during the final missions in Sicily (Egadi Islands) and in the Baltic Sea, the advantages for underwater archaeology campaigns of using a heterogeneous team of AUVs (Autonomous Underwater Vehicles), with differentiated capabilities, including three new different vehicles produced within the project itself (MARTA - MARitime Tool for Archaeology, U-CAT - Un-

derwater Curious Archaeology Turtle, A_size AUV; figure 1.4), according to the requirements of the ARROWS Archaeology Advisory Group (AAG), to be integrated with some already existing AUVs owned by the project partners (TifOne and TifTu too).

Figure 1.4: ARROWS Project Vehicles at their intermediate stage

The forward steps include a high-level software capable to reconfigure the mission in real-time according to the ontology stored in a distributed world model populated through a priori known information and the data collected by the AUVs during the mission and shared among themselves through the available communication means. In addition to the coordination role, one of the MDM Lab tasks within ARROWS includes the design and the assembling of MARTA AUV, a vehicle characterized of high modularity and adaptability to the different kinds of archaeological mission. Concerning the software, also in ARROWS, the MDM Lab role includes the design and the development of the low level software with the additional requirement of being compliant

with the modularity feature of the hardware.

During the last years, the MDM Lab research group had the occasion of working on two other vehicles. In 2012 and in 2013, a University of Florence team composed of students, Ph.D. students and researchers, collaborating within the MDM Lab, participated in the **SAUC-E** (Student Autonomous Underwater Vehicle Challenge - Europe) competition among European academical research groups organized by the NATO STO-CMRE (North Atlantic Treaty Organization - Science & Technology Organization - Centre for Maritime Research and Experimentation) in La Spezia, Italy (figure 1.5). The purpose of the competition is to evaluate the capabilities of the presented vehicles of fulfilling some ability trials reproducing real tasks usually involving AUVs in the industrial field. The developed vehicle, achieved after the two years of participation, is called FeelHippo (figure 1.6) and is designed to face the tasks proposed by the SAUC-E competition and to be easily integrated with additional equipment for potential future tasks. The University of Florence team reached the third position in the competition in 2013.

Figure 1.5: SAUC-E Competition Logo and NATO STO-CMRE (SAUC-E Organizer) Logo

The other work that completes the framework of the main activities about Underwater Robotics is the collaboration of the MDM Lab with the DST (Dipartimento di Scienze della Terra - Department of Earth Sciences) of the University of Florence, leaded by Prof. Nicola Casagli. The collaboration took place in the framework of the monitoring of the **Costa Concordia**

Figure 1.6: FeelHippo AUV in the sea and FeelHippo Logo designed and created by Francesca Miotto

wreck in front of Giglio Island, committed to DTS by the Italian Department of Civil Protection (figure 1.7).

Figure 1.7: Department of Earth Sciences, Italian Department of Civil Protection and Costa Crociere Logos

One of the committed activities was the production of a small ROV (Remotely Operated Vehicle) to be involved in the monitoring operations of the zones comprised between the wreck hull and the sea bottom and of the interior areas, both too dangerous for the divers. The collaboration has been about the GNC system for the NEMO ROV (figure 1.9) produced by the DST in the first months just after the Costa Concordia (figure 1.8) disaster. NEMO ROV was successfully tested on the Costa Concordia wreck on May 14th, 2013.

Figure 1.8: Costa Concordia wreck view from Punta Gabbianara (photo by Francesco Mugnai)

Figure 1.9: NEMO ROV

Even if the performance and the functioning of the strategies and of the proposed algorithms are completely independent on the particular software used for the implementation, it is worth to add some words about this aspect. From the beginning of the THESAURUS project until the 2013 Summer, the software on all the vehicles was based on the middleware MOOS[1] (figure 1.10), a framework allowing to develop the vehicle software with a publisher-subscriber architecture that simplifies the integration among the different functions to be included, especially considering that they are developed by different people. MOOS guarantees a soft real-time functioning, no hard

Figure 1.10: MOOS Logo

real-time features are required as in underwater applications the dynamics is very slow and the performance ensured by MOOS with respect to the working frequency of the control system (typically at 10 Hz) is sufficient. Another advantage of using MOOS is that it guarantees a very simplified management of the different computers on board a vehicle (usually at least two - one dedicated to the vital capabilities and one to the payload acquisition and real-time process). Starting from the 2013 Summer, the vehicles software was migrated from MOOS to ROS[2] (Robot Operating System), a similar system capable of better performance as it is not based on a star-like topology as

[1]MOOS Website: www.robots.ox.ac.uk/~pnewman/TheMOOS
[2]ROS Website: www.ros.org

MOOS is, with all the application not exchanging information through a central database but directly. Besides this, ROS has a wider user group and is used for projects of general robotics, not only linked to the underwater environment (figure 1.11).

Figure 1.11: ROS Logo

In order to summarize the timing and the activities in which the carried out research activity has been carried out, two schemes are reported in figure 1.12 and in figure 1.13. The first one is about THESAURUS and ARROWS projects, the second one is instead about the activities of SAUC-E and the Costa Concordia monitoring.

Figure 1.12: Timing of the underwater robotics projects with respect to Ph.D. study period

1.2 AUV Guidance, Navigation and Control

Section 1.1 described the overall framework of the research activity and mentioned the vehicles involved in it. In particular, four different (dimension, weight, propulsion system, maximum depth, shape, etc.) vehicles produced between 2012 and 2014 at the University of Florence, including three

Figure 1.13: Timing of the underwater robotics activities carried out in parallel to the projects with respect to Ph.D. study period

AUVs and one ROV. Independently from the specific considered vehicle, the greatest common divisor is the control system necessary for the motion. The control system scheme for an UUV (Unmanned Underwater Vehicle) coincides with the one of a generic system including automation and is shown in figure 1.14.

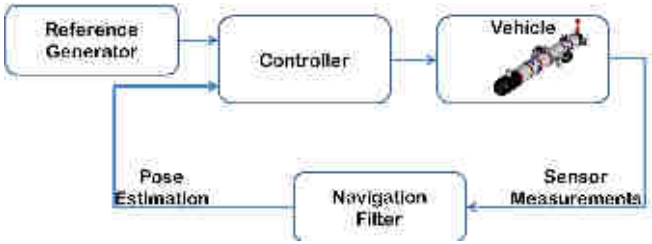

Figure 1.14: Generic Control Scheme

The main components of such a system are the following ones:

- **Reference Generator -** it represents the Guidance part of a GNC system, it contains all the algorithms whose role is to calculate at each instant the reference pose as to ensure the vehicle to comply with the mission requested by a higher level software; in the underwater applications, common imposed requirements are in terms of waypoints to be tracked, constraints on velocity and maximum time.

- **Controller -** it is the software module whose task is to ensure the vehicle to respect the reference trajectory computed by the Reference Generator software; by means of the comparison between the estimated pose and the desired one, the controller calculates suitable signals to be imposed to the vehicle actuators, ideally in order to reduce to zero the tracking error.

- **Vehicle -** this block represents the vehicle, it reacts according to the laws of the mechanics and of the hydrodynamics to the actions generated by the actuators according to the controller outputs. The available sensors are used to measure quantities linked to some of the state components. In simulations, the vehicle in this block is replaced through the dynamical model of the system including the actuators and the sensors.

- **Navigation Filter -** this is the software used to calculate an estimation of the system state and, in particular, of the vehicle pose (position and orientation). This part of the control system is essential for the controller to be fed with a reliable and updated signal describing the current state. If the Navigation Filter produces too high errors in the estimation process, this could lead to the calculation of wrong signals by the controller and in some cases to the instability of the whole system. The estimation of the system state usually takes place through filtering techniques including recursive algorithms based on a Kalman approach [Thrun et al., 2005].

To summarize, in the common control system architecture, the vehicle inter-

acts, directly or indirectly, with the three components of the Guidance, Navigation and Control system. Among the three elements of the GNC system, the most demanding is, for sure, the Navigation system. In fact, concerning the Guidance and Control aspects, standard simple approaches are sufficient to comply with simple tasks, typical of underwater missions that usually are defined as a collection of waypoints to be tracked. In particular, once the high level control system has defined the current target waypoint, the simple strategy of reaching the desired depth and pointing it with the vehicle bow represents a solution for the Guidance problem that, in the absence of additional requirements, satisfies the mission constraints. As concerns the control, the most widely algorithm used is a multivariable SISO (Single Input - Single Output) PID (Proportional Integral Derivative) for each one of the pose elements, rigorously defined in the chapter 2, where the state of the art about the modelling techniques in the underwater environment will be described. It is a reliable solution to the control problem, working properly even with a lot of non-linear systems. These simple solutions are not the only ones, in fact, more sophisticated strategies are described in the literature both about the generation of the reference (e.g. paths defined in three dimensions through elementary geometrical curves as segments or arcs of circumference permit to successfully perform more complex tasks) and the controller (e.g. trajectory tracking or path following approaches based on non-linear laws derived, for example, from the Lyapunov theory can allow the vehicle to satisfy particular time constraints or to counteract marine currents).

On the contrary, for the solution of the Navigation problem, simple strategies valid for wide classes of applications are not identifiable. For sure, a filtering algorithm based on the Kalman theory is the most common solution [Bar-Shalom et al., 2001], but the achievable results are strongly dependent

on the particular typology of the KF (Kalman Filter), on the model used in the prediction step and on the available measurements in the correction one. If, in addition to this aspect, the fact that the controller output, directly acting on the vehicle, is a function of the navigation filter results is considered, it appears clear that the Navigation aspects play the role of the bottleneck concerning the performance of the overall GNC system.

1.3 Navigation Role

As just described, the definition of the Navigation algorithms is the most challenging within the GNC system of a mobile robot in general. In the underwater robotics field, the topic is made even more complicated because of some intrinsic limits introduced by the working environment. The most important is, certainly, the impossibility of exploiting the GPS positioning system as the radio waves are quickly completely absorbed by the water so that the signal is not able to reach a vehicle navigating even a few centimeters below the surface.

The only waves capable of propagating through water for long enough to be exploited for positioning purposes are the acoustic ones. Localization systems based on the acoustic technology are commercially available, even if very expensive, as an integrated solution with the acoustic modems usually used for communication purposes [Di Corato et al., 2014],[Allotta et al., 2014a]. These systems exploit various transducers, whose mutual position is known, capable of acquiring the acoustic signal transmitted by a modem (like the ones mounted on the vehicles) or of transmitting a signal themselves towards a modem. Then, by means of algorithms based on TDOA (Time Difference Of Arrival), TOF (Time Of Flight) or on phase difference, the relative po-

sition of the modem is inferred. Depending on the mutual distance of the transducers, different methods are defined:

- **USBL (Ultra-Short BaseLine) -** all the transducers are integrated in a single device; the common uses see it mounted on a vehicle or placed in water from a boat as a stand-alone module. In this case, the modem on the vehicle has the transmitting role and is localized by the USBL device.
- **LBL (Long BaseLine) -** the transducers are placed in georeferenced positions in the operating zone; in this case, constraints on the allowed area for the vehicles have to be defined in order them not to lose the localization signal. When this solution is implemented, the modem on the vehicle has the receiving role and is able of self-localization with respect to the known nodes of the LBL net.

In the light of the above considerations, the development of the Navigation software appears as the most demanding part in the definition of the whole vehicle control system. From the algorithm point of view, the widest part of examples for position estimation described in the literature takes advantage of strategies based on a Kalman approach. The KF (Kalman Filter) is a recursive algorithm composed mainly of two steps for the computation of an estimation of the system state. Uncertainty associated to the computed estimation is calculated as error covariance. The two steps are:

- **Prediction Step -** the state estimation is calculated exploiting a *model* of the dynamical evolution of the system as a function of the previously estimated state and the current input signals.
- **Correction Step -** the state estimation is updated taking into account the currently available *measurements* according to the function describing the sensors model as a relationship between sensors output and state elements.

The main aim of this thesis is to propose some small steps forward with respect to the state of the art about the algorithm itself and about the model and the measurements that can be used in order to improve the performance of the overall system. The KF usually running on UUV is an EKF (Extended Kalman Filter) as the system dynamics is not linear. In this work, the comparison between this technique, used as a standard, and the UKF (Unscented Kalman Filter) is investigated. The UKF is based on the function called UT (Unscented Transform) instead of a linearization through Taylor series expansions. As result of this implementation, the UKF more accurately captures the true mean and covariance. Moreover, the computational load, even if higher with respect to the one of the EKF, is not too demanding compared to the resources of the PCs usually housed on the vehicles. Despite these considerations, even if UKF is used for mobile robots in general, in the field of underwater robotics it is almost not used in the practice [Barisic et al., 2012]. Results of the comparison will be provided through the use of experimental data collected at sea. The topic of the choice of a model for the prediction step and of the available measurements, in particular classes of applications, for the correction step is addressed and some strategies aiming at avoiding the use of the expensive USBL or LBL systems are proposed.

The aspects of orientation estimation, even if the two problems (position and orientation estimation) are not independent, are usually addressed separately because of the potential error introduced through this kind of approach is negligible with respect to the implied simplification. A considerable part of this work is dedicated to the orientation estimation and to a possible

solution for some of the limits proper of the strategies in the state of the art.

Chapter 2

State of the Art and Theoretical Bases

This chapter of the thesis is dedicated to an exhaustive description of the state of the art concerning the addressed topics. The discussion is divided into three sections, each one dedicated to one of the main topics identified in chapter 1. In particular, section 2.5 deals with the description of the solutions adopted in the literature about the particular *Filtering Techniques* adopted in the process of position and orientation estimation in the field of underwater robotics. Section 2.5 is preceded by sections 2.1 and 2.3 respectively about *Modelling* and *Localization*, fundamental and functional aspects for the navigation algorithm to work properly.

A further section (2.5.2) is dedicated to the orientation estimation strategies, as within the pose estimation process, the orientation and the position of the vehicle are usually independently estimated following different approaches.

2.1 Modelling

This section about modelling for mobile underwater robots aims at defining the state of the art in this field, highlighting the aspects involved in the navigation process. Section 2.1.1 is dedicated to the modelling of the vehicle three-dimensional motion in the water, whereas the following one, section 2.1.2 deals with propulsion system modelling.

2.1.1 Underwater Vehicle Motion

The state of the art about kinematics and dynamics modelling for underwater vehicles, even if not very recent, is represented by the first part of [Fossen, 1994]. [Antonelli, 2006] deals with the topic as functional part of his opera but, from a modelling point of view, no significant steps forward are identifiable.

For the greater part of the applications, for modelling purposes, an underwater vehicle can to be considered as a single rigid body moving in an environment with which interactions cannot be considered negligible, as water is. The introduction of two fundamental reference frames (figure 2.1) will be useful for all the following development of this section and of the overall thesis. The frames are:

- **body-fixed frame -** reference frame with origin O^b placed in the center of mass of the body and axes lined up to the main inertia axes of the body itself. In case of a vehicle of regular shape, the x^b-axis is longitudinal, pointing forward, the z^b-axis is vertical downward and the y^b-axis is set out in order to form a right-handed frame with the other two axes;
- **earth-fixed frame -** inertial reference frame, defined with the origin

O^e placed on the surface and axes lined up to the ones of a NED (North-East-Down) frame. The x^e-axis heads to the north, the y^e-axis to the east and the z^e-axis down.

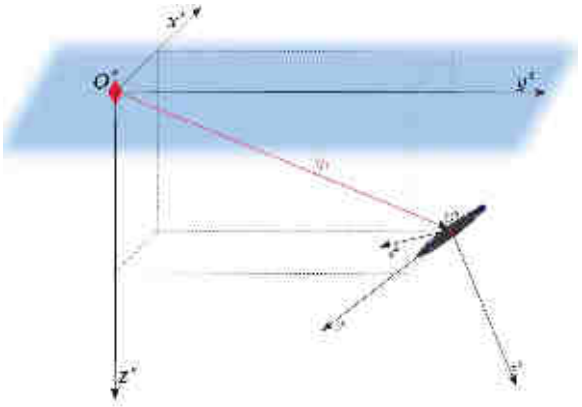

Figure 2.1: Reference frames for system modelling

The modelling is based on the SNAME notation (1950), that defines the following different quantities:

$$\begin{aligned} \vec{\eta} &= \left[\vec{\eta_1}^T, \vec{\eta_2}^T\right]^T \qquad \vec{\eta_1}^T = [x, y, z]^T \qquad \vec{\eta_2}^T = [\varphi, \vartheta, \psi]^T \\ \vec{\nu} &= \left[\vec{\nu_1}^T, \vec{\nu_2}^T\right]^T \qquad \vec{\nu_1}^T = [u, v, w]^T \qquad \vec{\nu_2}^T = [p, q, r]^T \\ \vec{\tau} &= \left[\vec{\tau_1}^T, \vec{\tau_2}^T\right]^T \qquad \vec{\tau_1}^T = [X, Y, Z]^T \qquad \vec{\tau_2}^T = [K, M, N]^T \end{aligned} \tag{2.1}$$

Where the meaning of the introduced symbols is:

- $\vec{\eta}$ - it denotes the position ($\vec{\eta_1}$) and the orientation ($\vec{\eta_2}$), expressed as RPY (Roll-Pitch-Yaw) angles with respect to the earth-fixed;
- $\vec{\nu}$ - it is composed of linear ($\vec{\nu_1}$) velocity and angular ($\vec{\nu_2}$) velocity vectors in the body-fixed frame;

- $\vec{\tau}$ - it includes the vectors of forces ($\vec{\tau_1}$) and moments ($\vec{\tau_2}$) acting on the vehicle in the body-fixed frame.

The kinematic description of the system is the typical one of a rigid-body fully unconstrained capable of moving in the space and is summarized by the following matrix equation that links the system variables at the velocity level:

$$\dot{\vec{\eta}} = J(\vec{\eta})\,\vec{\nu} \tag{2.2}$$

where $J(\vec{\eta})$ is the Jacobian matrix, belonging to $\mathbb{R}^{6\times6}$ and block diagonal, depending on the orientation elements of $\vec{\eta}$:

$$J(\vec{\eta}) = \begin{bmatrix} J_1(\vec{\eta_2}) & 0_{3\times3} \\ 0_{3\times3} & J_2(\vec{\eta_2}) \end{bmatrix} \tag{2.3}$$

with

$$J_1(\vec{\eta_2}) = \begin{bmatrix} c\psi c\vartheta & -s\psi c\varphi + c\psi s\vartheta s\varphi & s\psi s\varphi + c\varphi s\vartheta c\psi \\ s\psi c\vartheta & c\psi c\varphi + s\psi s\vartheta s\varphi & -c\psi s\varphi + c\varphi s\vartheta s\psi \\ -s\vartheta & s\varphi c\vartheta & c\varphi c\vartheta \end{bmatrix}$$

$$J_2(\vec{\eta_2}) = \begin{bmatrix} 1 & s\varphi t\vartheta & c\varphi t\vartheta \\ 0 & c\varphi & -s\varphi \\ 0 & s\varphi/c\vartheta & c\varphi/c\vartheta \end{bmatrix} \tag{2.4}$$

where $s\cdot = sin(\cdot)$, $c\cdot = cos(\cdot)$ and $t\cdot = tan(\cdot)$. Equation 2.4 highlights how the choice of the RPY angles for the description of the vehicle orientation is advantageous as the singular configurations ($J_2(\vec{\eta_2})$ not defined) are all the ones with pitch equal to the right angle ($c\vartheta = 0 \Leftrightarrow \vartheta = \pm\pi/2$), that is when the vehicle is vertical with the bow pointing up or down, a situation that almost never occurs.

As concerns the dynamical model of the vehicle, it is represented by the following, nonlinear 6 DOF (Degrees Of Freedom) equation of motion

expressed in the body-fixed frame:

$$M\dot{\vec{\nu}} + C(\vec{\nu})\,\vec{\nu} + D(\vec{\nu})\,\vec{\nu} + \vec{g}(\vec{\eta}) = \vec{\tau} \tag{2.5}$$

where the new introduced quantities are:

- M - inertia matrix (including added mass)
- $C(\vec{\nu})$ - matrix of Coriolis and centripetal terms (including added mass)
- $D(\vec{\nu})$ - damping matrix
- $\vec{g}(\vec{\eta})$ - vector of gravitational forces and moments
- $\vec{\tau}$ - vector of control inputs

The added mass terms considered in matrices M and $C(\vec{\nu})$ are introduced as a virtual contribution to the vehicle mass used to model the pressure-induced forces and moments, due to a forced harmonic motion of the body, which are proportional to the acceleration of the body.

A description of the contributions to be considered in matrices M, $C(\vec{\nu})$ and $D(\vec{\nu})$ is provided in [Fossen, 1994] and [Antonelli, 2006]. Matrix M, thanks to the definition of the body-fixed frame (whose axes are the principal axes of inertia of the vehicle) is a constant diagonal matrix depending on the mass distribution on board the vehicle. $D(\vec{\nu})$, the damping effects matrix, even if in its general expression is highly nonlinear and coupled, considering two reasonable simplifications - vehicle speed low enough to neglect higher terms than the second one and the presence of at least three symmetry planes in the vehicle shape, can be considered as diagonal with only linear and quadratic damping terms on the diagonal. For $C(\vec{\nu})$, the matrix of Coriolis and centripetal terms, a similar simplification cannot be applied as, by definition, its terms (both in the rigid body contribution and the added

mass one) are out of the diagonal. $\vec{g}(\vec{\eta})$ is the term that takes into account the effects of both the vehicle weight and buoyancy. Considering the vehicle neutral in water ($W = B$, with W and B norm respectively of the weight vector $\vec{W}$ and of the buoyancy vector $\vec{B}$), as the good practice suggests to do in the calibration phase, and defining the vector $\vec{BG} = [BG_x\ BG_y\ BG_z]^T$ as the one between the buoyancy center CB and the gravity center CG, the expression of $\vec{g}(\vec{\eta})$ is simplified as follows

$$\vec{g}(\vec{\eta}) = \begin{bmatrix} 0 \\ 0 \\ 0 \\ -BG_y\ W\ c\varphi c\vartheta + BG_z\ W\ s\varphi c\vartheta \\ BG_z\ W\ s\vartheta + BG_x\ W\ c\varphi c\vartheta \\ -BG_x\ W\ s\varphi c\vartheta - BG_y\ W\ s\vartheta \end{bmatrix} \tag{2.6}$$

The contributions different from zero of the vector $\vec{g}(\vec{\eta})$ are only its angular moment elements. Those are restoring moments that act on the vehicle to bring it in its hydrostatic equilibrium orientation. That implies, as concerns the orientation degrees of freedom, that each action aimed at controlling the vehicle to an orientation different from the equilibrium one has to overcome the effects of the restoring actions. Usually, the calibration of the vehicle buoyancy is carried out in order to have $BG_x = 0$, $BG_y = 0$ and $BG_z > 0$ (buoyancy center placed above the gravity center) so that the values of the hydrostatic orientation equilibrium for roll and pitch degrees of freedom are null and the yaw degree of freedom is not affected by restoring effects.

2.1.2 Propulsion System

The equations of motion for an underwater vehicle are expressed in 2.5; all the terms on the left side of the equation are all contributions describing

the dynamics of a rigid body with 6 DOF moving in the three-dimensional space subjected to hydrodynamic and hydrostatic effects due to the interaction with water. The term on the right is, instead, used to model the actions applied by the propellers to the vehicle expressed in the body-fixed frame, as force and moment components, along the 6 DOF. No method to express the action vector $\vec{\tau}$ with respect to known quantities, usually the propeller rotational speed, is provided by [Fossen, 1994] or [Antonelli, 2006]. The main reference used to derive a law expressing $\vec{\tau}$ as a function of the propeller rotational speed is [Carlton, 2007b]. The various involved quantities are, here, expressed as dimensionless coefficients (J - advance coefficient, K_t - thrust coefficient, K_q - torque coefficient, η - efficiency coefficient). In particular:

$$\begin{aligned} J &= \frac{V_a}{nd} \\ K_t &= \frac{T}{\rho n^2 d^4} \\ K_q &= \frac{Q}{\rho n^2 d^5} \\ \eta &= \frac{K_t J}{K_q 2\pi} \end{aligned} \tag{2.7}$$

where n is the propeller rotational speed [Hz], ρ is the fluid density [kg/m^3], T is the thrust [N], Q is the torque [Nm], d is the propeller diameter [m] and V_a is the advance speed [m/s] (the component of the fluid speed with respect the vehicle that is parallel to the propeller longitudinal direction). Experimentally derived curves expressing the defined coefficient as a function of the advance one, are available in literature and are characterized by patterns analogous to the ones represented in figure 2.2, obtained with K_a 4-70 propeller in nozzle 19A for different pitch/diameter ratios. This kind of approach is characterized by some limits when used for modelling purposes; in particular the main resulting issues are:

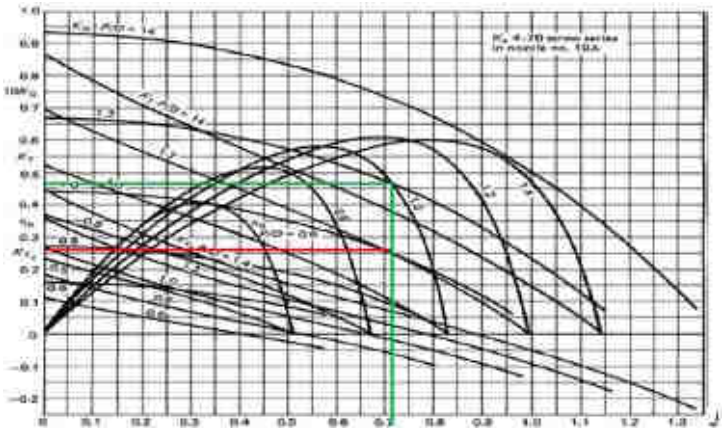

Figure 2.2: Curves expressing the dependency of K_t, K_q and η coefficients by the advance coefficient J for K_a 4-70 propeller in 19A nozzle

- significant difficulties in deriving an analytical, or even numerical, relation between the coefficients from the drawn curves;
- the curves in the charts, in particular the ones related to the thrust coefficient that is the most important from the modelling point of view, are limited to the positive range; that implies that for J values higher than the ones for that K_t is null, the propeller behaviour is not represented;
- the provided curves are related to the first quadrant where all the coefficients are positive and do not represent all the other possible condition; thus even if the first issues were overcome, a model for the conditions related to the missing chart area could not be achieved.

Some works, present in the literature, aim at overcoming the latter identified issue; in particular in [Pivano et al., 2009] the curves for all the four quadrants are experimentally derived; a complete chart, shown by the authors in

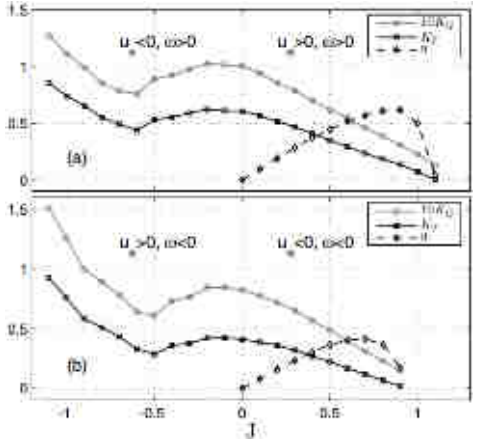

Figure 2.3: Four-quadrant behaviour of a marine propeller [Pivano et al., 2009], u_a in this chart is the same of V_a defined in equation 2.7

it, is here reported in figure 2.3. This is the point at which the literature arrives; it is, for sure, a valuable point as for a lot of standard propeller profiles, a substantial experimental activity completely describes the propeller behaviour, except for the chart areas identified. From the described curves, it would be possible to derive a numerical function expressing the propeller thrust T with respect to the advance velocity V_a and the rotational speed n, e.g. in the form of a look-up table. But, the necessity, as highlighted in the dedicated section 3.1, is to obtain an analytical expression, enough simple to be calculated at each iteration of the recursive pose estimation filter, even penalizing the physical process representation capability of the model. The effort about this aspect of the thesis topic has been dedicated to determine a suitable trade-off between the propulsion model accuracy and its computational simplicity.

2.2 Underwater Sensors

In this section, a qualitative description of the main sensors used for underwater navigation is provided, except for the ones devoted to the localization (position measurement) for that a specific section (2.3) is dedicated.

2.2.1 Inertial Measurement Unit

The term IMU (Inertial Measurement Unit) indicates electronic devices composed of a three-axial accelerometer and a three-axial gyroscope, sensors capable of measuring the dynamical effects which the rigid body, they are mounted on, is subjected to. The dynamical effects, respectively measured, include the absolute acceleration and angular rate expressed in the body-fixed frame. The measure provided by the accelerometers includes also the gravity acceleration as, from the physical point of view, no difference exists between it and the proper acceleration of the sensor. Classical IMUs are very expensive and very accurate devices, instead the modern ones are small, low-cost Micro Electro-Mechanical Systems (MEMS) with the drawback of worse performances. The trade-off between cost, dimension and performance offered by the modern MEMS makes them to be employed on a wide range of mobile robots (underwater or not) for orientation and position estimation purposes.

2.2.2 Magnetometer

Three-axial magnetometers are, in many cases, integrated in the same device with the IMUs. That entails a minimal mounting error between the magnetometer axes and the ones of accelerometers and gyroscopes, that, in the ideal situation, should be aligned in order not to introduce disturbances in the estimation process. This sensor provides a measure of the direction of the local magnetic field expressed in the body-fixed frame. The measured quantity is, ideally, the well known Earth magnetic field in order to exploit the sensor output to estimate the orientation of the rigid body housing it. Experiences on real applications demonstrate that magnetometers are very sensitive to disturbances due to close magnets or ferromagnetic bodies that modify the local magnetic field. When these bodies are rigidly united to the magnetometer during its motion, their effect can be identified and compensated through a calibration phase to be performed before using the measurements.

2.2.3 Depth sensor

The depth sensors are devices able to measure the local pressure. Standard hydrostatic equations are then used to derive the corresponding depth as a function of the fluid density. The measure provided by this kind of sensors is usually very reliable and accurate.

2.2.4 Doppler Velocity Log

The DVL (Doppler Velocity Log) is a sensor based on the principle that an acoustic signal, either transmitted or received by a moving object, is shifted in frequency of an amount proportional to the velocity of the moving object. The DVL can measure the three-axial body-frame velocity with respect to the bottom if the distance from it is limited (usually not more than about 50 m for the common commercially available products). In case the sensor is not able to get the lock to the bottom because of a too high distance from it or particularly hard environment conditions such as the presence of a thermocline or high pressure gradients, some DVL models offer the possibility of getting a velocity measure with respect to the water column. In this case,

the information content is poorer as the vehicle velocity is biased by the water velocity (local current) in the provided measure.

2.3 Localization

The localization techniques for a vehicle moving in the underwater environment rely on acoustic sensors as the acoustic waves are the only ones capable of propagating within the water for a distance long enough. In fact, radio waves, usually used for surface vehicle positioning (e.g. in GPS - Global Positioning System), are quickly completely absorbed by the water. The acoustic localization techniques mainly used in the underwater environment are two (USBL - Ultra Short BaseLine; LBL - Long BaseLine), both of them usually integrated with the vehicle communication system relying on acoustic modems.

2.3.1 USBL Localization

The Ultra Short BaseLine localization is based on a single device integrating both the acoustic transceiver for communication with the compatible acoustic modems and a series (few units, typically 5) of transducers, placed in known relative position, capable of acquiring the signal transmitted by a modem. The signal, transmitted by a modem, reaching the USBL transducers is acquired by them, whose relative distance (baseline) is very short (normally few tens of centimeters - 20-30 cm), and is processed by a dedicated computing unit. This, through the analysis of the TDOA (Time Difference Of Arrival) and the phase difference of the various signals, known the speed of sound in the water, is able to calculate the distance of the transmitting modem and the relative azimuth and elevation angles; in other words, the

position, with respect to the USBL transducers, is determined as spherical coordinates. The USBL transducer is usually mounted in a known position, e.g. on a surface vehicle with GPS available, so that, the position of a vehicle mounting a transmitting modem can be measured in absolute coordinated through geometrical relations. The main positive aspect of an USBL based localization system is that no infrastructures have to be installed in the operational area. The positioning accuracy guaranteed by such a system degrades with the relative distance as, even few degrees of error on the azimuth and elevation angles measurement, can be reflected in some meters of position measurement error when the localized vehicle is far away from the USBL transducer. When a USBL system is used for AUVs, the fact that the measured position is not directly available on board the vehicle, but, a delay of at least some seconds between the measurement instant and the moment when the measure is communicated to the vehicle has to be considered.

2.3.2 LBL Localization

The Long BaseLine localization is based on different transmitter (at least two or three according to the commercial solution adopted) modems placed underwater in well known positions. Periodically, pings are generated by these modems, as response to signals coming from vehicles, and are received by the modem mounted on the vehicle; the relative distance is this way calculated by using the knowledge of the speed of sound in water. Through simple geometrical triangulation algorithms, a dedicated computation unit on board the vehicle is able to calculate its relative position with respect to the fixed transmitting nodes whose absolute position is known. The degree of accuracy, in this case, is more performing than in the USBL case, as the baseline is much longer (up to hundreds of meters). In addition the

achievable precision is not depending on the distance between the vehicle and the fixed nodes. One of the drawbacks in using this solution is that a not negligible amount of work is necessary to install the fixed nodes underwater and to accurately measure its absolute position. Moreover, the choice of this localization methodology necessarily implies a limited operational area depending on the functioning range of the fixed acoustic nodes.

In conclusion, LBL and USBL technologies are complementary efficient solutions for the localization problem for vehicles working in the underwater environment. However, they are characterized by a high cost; in this thesis some alternative solutions have been considered for standard application cases where the use of these kinds of devices can be avoided exploiting other devices already housed on board and already employed for other purposes. Chapter 4 deals with this topic.

2.4 State Estimation Algorithms

This section provides the description of the algorithms commonly used to address the problem of the estimation of the state of a dynamical system. The discrete-time evolution of a dynamical system can be represented through the equations:

$$\begin{cases} \vec{x}_k = f\left(\vec{x}_{k-1}, \vec{u}_k, \vec{w}_k\right) \\ \vec{z}_k = h\left(\vec{x}_k, \vec{\delta}_k\right) \end{cases} \tag{2.8}$$

where, indicating with k the current instant, $\vec{x}_k \in \mathbb{R}^n$ is the state vector, $\vec{u}_k \in \mathbb{R}^p$ is the input vector, $\vec{w}_k \in \mathbb{R}^n$ is the process noise, $\vec{z}_k \in \mathbb{R}^m$ is the measure vector and $\vec{\delta}_k \in \mathbb{R}^m$ is the measure noise.

In the case that f and h are linear functions and $\vec{w}_k$ and $\vec{\delta}_k$ are Gaussian

white noises, the evolution equations can be written as follow:

$$\begin{cases} \vec{x}_k = F_k\vec{x}_{k-1} + B_k\vec{u}_k + \vec{w}_k \\ \vec{z}_k = H_k\vec{x}_k + \vec{\delta}_k \end{cases} \quad with \quad \vec{w}_k \sim N\left(0, Q_k\right), \ \vec{\delta}_k \sim N\left(0, R_k\right) \tag{2.9}$$

where the current state $\vec{x}_k$ linearly depends on the previous state $\vec{x}_{k-1}$ through the state transition matrix $F_k \in \mathbb{R}^{n\times n}$ and on the input signal $\vec{u}_k$ through the control-input matrix $B_k \in \mathbb{R}^{n\times p}$; the process noise $\vec{w}_k$ is Gaussian distributed $(N(\cdot,\cdot))$ with zero-mean and covariance matrix $Q_k \in \mathbb{R}^{n\times n}$. The measure vector at the current instant, $\vec{z}_k$, is, instead, linearly dependent on the current state $\vec{x}_k$ through the observation matrix $H_k \in \mathbb{R}^{n\times m}$; the observation noise $\vec{\delta}_k$ is Gaussian distributed with zero-mean and covariance matrix $R_k \in \mathbb{R}^{m\times m}$. Under these conditions, the Kalman Filter (KF) is demonstrated to be the optimal solution for the estimation problem [Kalman, 1960]. Being $\hat{x}_{k|k}$ and $P_{k|k}$ (the use of the symbol $\vec{}$ for vectors is here and in the following of this section avoided for the sake of notation simplicity) respectively the state and the error covariance at the instant k estimated at the same instant k and z_k the available measures at the k instant, the KF is structured in two phases:

- **KF Prediction Step**
  - $\hat{x}_{k|k-1} = F_k\hat{x}_{k-1|k-1} + B_k u_k$
  - $P_{k|k-1} = F_k P_{k-1|k-1} F_k^T + Q_k$
- **KF Correction Step**
  - $\tilde{y}_k = z_k - H_k\hat{x}_{k|k-1}$
  - $S_k = H_k P_{k|k-1} H_k^T + R_k$
  - $K_k = P_{k|k-1} H_k^T S_k^{-1}$

- $\hat{x}_{k|k} = \hat{x}_{k|k-1} + K_k \tilde{y}_k$
- $P_{k|k-1} = (I - K_k H_k) P_{k|k-1}$

Whether at least one of the assumed hypotheses is not true, an optimal solution in a closed form does not exist.

In the case of non-linear systems with additive noise, i.e. in the form

$$\begin{cases} \vec{x}_k = f\left(\vec{x}_{k-1}, \vec{u}_k\right) + \vec{w}_k \\ \vec{z}_k = h\left(\vec{x}_k\right) + \vec{\delta}_k \end{cases} \tag{2.10}$$

the most widely used estimation technique is the EKF (Extended Kalman Filter), an algorithm derived by the simple KF that is based on the linearization of the system in the last estimated state. The function f is used to directly evaluate the predicted state from the last estimation and, at the same way, h can be used to calculate the predicted measurement as a function of the predicted state. On the contrary, f and h cannot be applied to the covariance computation directly. This problem is solved by means of the computation of the matrix of partial derivatives (the Jacobian), to replace matrices F_k and H_k in the prediction and correction steps of the simple KF:

$$F_k = \left.\frac{\partial f}{\partial x}\right|_{\hat{x}_{k|k-1}, u_k} \tag{2.11}$$

$$H_k = \left.\frac{\partial h}{\partial x}\right|_{\hat{x}_{k|k-1}} \tag{2.12}$$

Concerning the properties of the EKF, it is in general not an optimal estimator. The convergence is not ensured and in case of an initial wrong estimation, the filter may quickly diverge. Moreover the estimated covariance matrix tends to be an underestimation of the real one leading to the risk of becoming, from a statistical point of view, inconsistent. Although no properties are demonstrated, the EKF is the solution used for the most of

the systems that necessitate of an estimation filter, first among all navigation systems and the GPS [Bar-Shalom et al., 2001][Evensen, 2009][Sayed, 2009].

An alternative technique more recently introduced [Julier and Uhlmann, 1997], is the so called UKF (Unscented Kalman Filter). In this case, the filter dynamics is not propagated through a linearization approach, but thanks to a deterministic sampling technique, known as Unscented Transform (UT). It is a derivative-free technique that starting from the mean and covariance of a random variable allows to extrapolate a minimum set of sampling points around the mean to be propagated through a non linear functions. The obtained results can be then used to calculate the mean and the covariance of the random variable propagated through the non linear function.

The UT for a random variable x with mean $\bar{x}$ and covariance P transformed through a function $g(\cdot)$ into the variable y ($g : \mathbb{R}^{n_x} \rightarrow \mathbb{R}^{n_y} \mid y = g(x)$) is defined according to the following steps:

- to generate $2n_x + 1$ samples $\mathcal{X} \in \mathbb{R}^{n_x \times (2n_x+1)}$, the so called σ-points, starting from the mean $\vec{x}$ with deviation given by the matrix square root Σ of P;
- to propagate the σ-points through the transformation function $g(\cdot)$ resulting in $\mathcal{G} \in \mathbb{R}^{n_x \times (2n_x+1)}$;
- to calculate the new transformed mean $\bar{y}$ and associated covariance matrix P_{gg} as well as the cross-covariance matrix P_{xg} of the initial and transformed σ-points.

The Unscented Transform as a function of $\bar{x}$, P and $g(\cdot)$ is represented by:

- $(\bar{y}, P_{gg}, P_{xg}) = UT\left(\bar{x}, P, g\right)$

- $\Sigma = \sqrt{P}$
- $\mathcal{X} = \left[\bar{x} \dots \bar{x}\right] + \sqrt{c}\left[0^{n_x \times 1}, \Sigma, -\Sigma\right]$
- $\mathcal{G} = g(\mathcal{X})$
- $\bar{y} = \mathcal{G} w_m$
- $P_{gg} = \mathcal{G} W_c \mathcal{G}^T$
- $P_{yg} = \mathcal{X} W_c \mathcal{G}^T$

The involved weights c, w_m and w_c are generally a function of the three parameters α, β and κ. Moment matching properties and performance improvements associated to the choice of these parameters are discussed in [Julier and Uhlmann, 2004], [Wan and Merwe, 2001] resorting to specific values of α, β and κ. It is common practice to set these three parameters as constants computing the weights at the beginning of the estimation process.

According to the definition of the Unscented Transform, the main steps of the UKF can be described as follow:

- Prediction Step
  - $\left(\hat{x}_{k|k-1}, P_{k|k-1}\right) = UT\left(\hat{x}_{k-1|k-1}, P_{k-1|k-1}, f(\cdot)\right)$
  - $P_{k|k-1} = P_{k|k-1} + Q$
- Correction Step
  - $\left(\hat{z}_{k|k-1}, S_k, C_k\right) = UT\left(\hat{x}_{k|k-1}, P_{k|k-1}, h(\cdot)\right)$
  - $S_k = S_k + R$
  - $\hat{\vec{x}}_{k|k} = \hat{\vec{x}}_{k|k-1} + C_k S_k^{-1}\left(\vec{z}_k - \hat{\vec{z}}_{k|k-1}\right)$
  - $P_{k|k} = P_{k|k-1} - C_k S_k^{-1} C_k^T$

The main advantages of using the UKF approach instead of the EKF one can be summarized as follow:

- it does not require the calculation of the Jacobians. Therefore the UKF algorithm is very suitable for highly nonlinear problems and represents a good trade-off between accuracy and numerical efficiency;
- being derivative free, it can cope with functions with jumps and discontinuities;
- it is capable of capturing higher order moments of nonlinear transformations better then how the Taylor series based approximations do, as demonstrated in [Julier and Uhlmann, 2004].

In the field of underwater robotics, even if the usually involved computing units that are on board the vehicles are enough performing to deal with the little more computational load required by a UKF with respect to an EKF, the Unscented Kalman Filter is, in the practice, never used on UUVs as in the literature this kind of solution is not reported. The use of the UKF and its comparison with the EKF have been here studied and results on data acquired during field tests are analysed.

2.5 Pose Estimation Algorithms

Pose estimation algorithms are designed to calculate instant by instant the most suitable vehicle pose (orientation and position) according to the knowledge of the evolution laws of the system and to the measurements provided by the available sensors. Even if the time evolution of the position and the orientation of an underwater vehicle is strongly dependent as equations of

motions, 2.2 and 2.5, demonstrate, it is common to separate the two processes for mainly two reasons:

- complexity reduction of the overall system for the estimation, in fact, this way, two different simpler (smaller dimension of the state vectors) systems are faced;
- different algorithms, better performing for a typology of system either the other one, can be applied.

The common way to solve the problem is to obtain the orientation estimation through a dedicated algorithm and to involve its output in the position estimation algorithm as the measurement of a virtual sensor of orientation. In the thesis, this approach is followed: the position and the orientation estimations are independently addressed.

2.5.1 Position Estimation

Position estimation algorithms are used in several applications from years, thus in the literature various contributions about this topic are present. Their implementation depends on the specific application and, in particular, on the available sensor set and the related measured quantities.

In [Barshan and Durrant-Whyte, 1995], an INS (Inertial Navigation System) based on an IMU (Inertial Measurement Unit) for a generic mobile robot is proposed. The IMU includes a three-axial accelerometer and a three-axial gyroscope. The proposed method fuses the acceleration and the angular rate measurements within an EKF (Extended Kalman Filter) running a purely kinematic model with no consideration, in the filter, about the actions (forces or moments) on the system. Trying to apply this strategy to an underwater vehicle, the obtained results appear useless, in fact, because of the poor

degree of accuracy of the common IMUs used on AUVs or ROVs and of the absence of a dynamic model in the prediction step, the estimation error, even in simulations, rapidly grows too much. In the case of underwater vehicles, usually the INS system is aided through the integration of a DVL (Doppler Velocity Log), capable of measuring the velocity of the vehicle in the body-fixed frame $\vec{\nu_1}$; the addition of this kind of measurement improves the performance of the algorithm enough for its use within the motion control loop for significant periods of time, with a very low rate of the drift of the position estimation error [Zhao and Gao, 2004]. This, even if low, is always present; localization measurements, such as the ones provided by a USBL system or a LBL system, are used for its reset as an input of the filter. The problems with this kind of approach born when the DVL, because of the environmental conditions, is not able of getting measurements for a period that may last enough for the accuracy of the estimated position to become too low. This possibility highlights how the involvement of an accurate model to be used in the prediction step of the filter becomes necessary to obtain a position estimation system enough reliable to make the vehicles capable of navigating. The use, in the filter, of a complete dynamic model including propulsion system, based on the theory described in section 2.1, seemed to be a reliable solution; encouraging results were obtained through simulations at the beginning of my Ph.D. study period and published in [Allotta et al., 2012]. The position of the vehicle was correctly estimated along the travelled path during a simulated mission lasting almost one hour and half. An uncertainty about the model parameters of 10% was considered, in order to evaluate the reliability of the proposed method against it. The considered sensor set included an IMU (comprising a three-axial magnetometer), a depth sensor, a DVL and a GPS for the initialization of the filter on the surface. No localization devices,

such as USBL or LBL, were considered as the aim was to evaluate how long the implemented algorithm allows a vehicle navigating underwater without a position estimation error reset. The obtained results are summarized in figure 2.4 where the estimated and the simulated paths are almost indistinguishable because overlapped; the obtained position error evolution is reported in figure 2.5 where the performance of the proposed method clearly appears high as it remains below 1 m for all the simulation period. Considering the

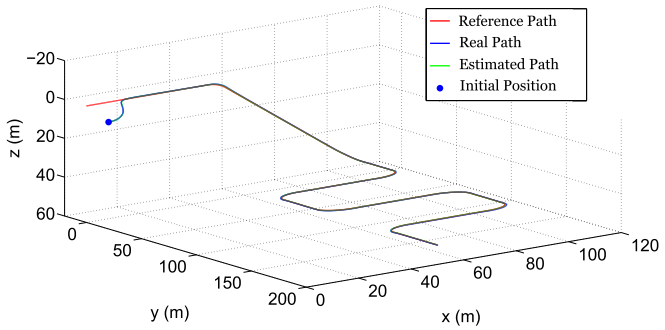

Figure 2.4: EKF based on a complete dynamic model and sensor set including DVL in a simulated mission

encouraging results, the performance was evaluated, still in simulation, also in the conditions of DVL unavailability. The obtained results are represented in figures 2.6 and 2.7 where plots, analogous to the ones in figures 2.4 and 2.5, highlights, also in this case, a good functioning as the error is, as predictable greater than the previous situation, but during all the simulation period does not grow more than 10m. The obtained results convinced to try the use of such an algorithm on a real vehicle; it was firstly tried, off-line, on the TifOne AUV. The experimental results significantly differed from the expected ones as the position estimation error increased too much for the

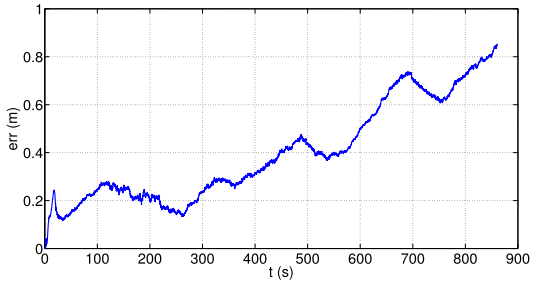

Figure 2.5: Position estimation error of the EKF based on a complete dynamic model and sensor set including DVL in a simulated mission

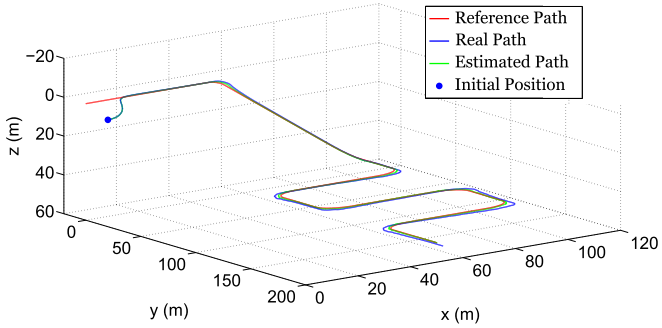

Figure 2.6: EKF based on a complete dynamic model and sensor set not including DVL in a simulated mission

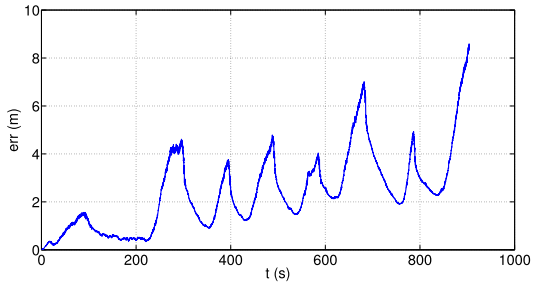

Figure 2.7: Position estimation error of the EKF based on a complete dynamic model and sensor set not including DVL in a simulated mission

filter to be used in the control loop. Results obtained are not here reported as the performance was so bad to make them devoid of meaning, except for the one of a necessary change of strategy. The reason was identified in a discrepancy between the used dynamic model and the real dynamic behaviour of the system. The uncertainty on all the involved parameters led to obtain a model not suitable for the use in the so defined navigation filter.

The described experience suggested to work on defining a trade-off model between the simply kinematic one and the complete dynamic one in order not to fully neglect the effects of the applied forces and moments on the vehicle motion as the use of the first one implies neither to affect the navigation filter with the uncertainties on the model parameters as in the latter. On the other side, the possibility of using a different algorithm from the classical EKF is investigated. Chapters 3 and 5 address these topics.

2.5.2 Orientation Estimation

The orientation estimation is a very important aspect in the framework of the navigation algorithm, as, the accuracy achieved in it affects also

the position estimation algorithm, as the earth-fixed position is intrinsically strongly dependent from the vehicle orientation (equations 2.2 and 2.5). The sensors that are commonly involved in a three dimensional orientation estimation process are a 3D accelerometer, a 3D gyroscope and a 3D magnetometer. Among all the references about sensor fusion algorithms for orientation estimation published in the literature, two particular approaches stand out. The first is a kinematic based EKF [Marins et al., 2001], but the most used algorithm, with properties of convergence demonstrated through a Lyapunov approach, is the NCF (Nonlinear Complementary Filter) proposed in [Mahony et al., 2008]. This second approach and, in particular the explicit version with bias correction, in the thesis, has been assumed as the *de facto* state of the art about the orientation estimation.

The proposed NCF is a recursive algorithm based on the following three relations (for notation simplicity, upper case letters indicate matrices and lower case letters indicate vectors), where the operator $(\cdot)_\times$ indicates the skew symmetric matrix defined for the vector $\cdot = \begin{bmatrix} \cdot_1 & \cdot_2 & \cdot_3 \end{bmatrix}^T$ as $((\cdot)_\times = \begin{bmatrix} 0 & -\cdot_3 & \cdot_2 \\ \cdot_3 & 0 & -\cdot_1 \\ -\cdot_2 & \cdot_1 & 0 \end{bmatrix})$:

$$\begin{aligned} \dot{\hat{R}} &= \hat{R}\left(\left(\Omega^y - \hat{b}\right)_\times + k_P\left(\omega_{mes}\right)_\times\right), \quad \hat{R}(0) = \hat{R}_0 \\ \dot{\hat{b}} &= -k_I \omega_{mes} \\ \omega_{mes} &:= \sum_{i=1}^{n} k_i v_i \times \hat{v}_i, \qquad k_i > 0 \end{aligned} \tag{2.13}$$

where $\hat{R}$ and $\hat{b}$ are respectively the estimated rotation matrix and gyroscopes bias vector; Ω^y is the vector of the gyroscopes measurements and being n the number of directions measurable in the body-fixed frame and constant and known in the earth-fixed frame v_{0i}. For the i-th direction, v_i is the

unit vector corresponding to the known direction measured in the body-fixed frame whereas $\hat{v}_i$ is the same direction estimated through the NCF as $\hat{v}_i = \hat{R}^T v_{0i}$. Finally, k_P, k_I and k_i ($\forall i = 1, \cdots, n$) are positive scalars playing the role of gains regulating the filter dynamics.

Under the condition $n > 1$, in [Mahony et al., 2008] a demonstration is provided, through Lyapunov theory, that the estimation error on orientation and bias $\left(\tilde{R}(t); \tilde{b}(t)\right)$ is locally exponentially stable to $(I; 0_{3\times 1})$. Sensors usually employed to measure known directions with respect to the body-fixed frame are:

- **3D Accelerometer -** it normally measures the proper acceleration of the vehicle biased by the gravity acceleration. Considering the very slow dynamics characterizing a vehicle moving in the underwater environment, the proper acceleration is negligible with respect to the gravity. It is, thus, reasonable to assume that the opposite of the output of the accelerometers is the measure of the acceleration of gravity direction ($\begin{bmatrix} 0 & 0 & 1 \end{bmatrix}^T$ in the earth-fixed frame) with respect to the body-fixed frame.

- **3D Magnetometer -** it provides the measurement of the local magnetic field vector expressed in the body-fixed frame. Its direction is generally variable but can be considered known and constant with respect to the earth-fixed frame over the operating area of an underwater vehicle. All its three components are generally not null in the earth-fixed frame even if the East one is much smaller than the other two to be considered negligible.

Even if the orientation estimation algorithm is well defined and with convergence properties rigorously theoretically demonstrated, some open points

affect the process and are addressed within this thesis:

- **sensors calibration -** the filter good functioning is based on the possibility of measuring, instant by instant, at least two known directions. It has to be ensured that the measurements are not affected by errors, otherwise the estimation converges to orientation values different from the real ones. To achieve this necessary condition, a calibration phase dedicated to the identification and compensation of measurement errors has to be defined. Especially for magnetometers, this phase is crucial and will be addressed in details in a dedicated section.

- k_i **value -** for each positive choice of these gains, the convergence property is ensured and demonstrated. Even in the case of an accurate initial calibration phase, it may happen that during the normal functioning of the system the measurements provided by accelerometers or magnetometers are affected by unpredictable transitory errors. These eventualities have to be detected and the k_i values should be scaled as consequence according to the reliability associated to the measurements. Methods dedicated to this purpose have been studied and tested and are described in details in the following.

- **known directions choice -** the possibility of not using the magnetic field or the gravity acceleration but a function depending on them has been investigated and demonstrates to lead some benefits to the estimation process; the details are presented in the dedicated section.

Chapter 3

Modelling

3.1 Propulsion System Model

The available literature about the propulsion system model offers the possibility of obtaining an accurate description of the relation between the propeller rotational speed and the generated actions (force and moment). The main limit of the available means is that the desired relation can be calculated as a three-dimensional look-up table (the generated force and moment are a function of the advance speed in addition to the propeller rotational speed) starting from the charts about the dimensionless coefficients defined in equation 2.7. The obtained look-up tables, even if accurate, are hardly exploitable e.g. in the prediction phase of an EKF navigation filter where an analytical function describing the model of the system evolution and its Jacobian have to be calculated at each iteration.

This chapter deals with the determination of an analytical expression for the relation between the generated dynamical actions, the propeller rotational speed and the advance velocity. In particular, the analysis is concentrated on the generated force; the generated moments can be, in a first

approximation, neglected as their effect is usually much reduced thanks to a careful mechanical design of the AUV (i.e. for all the vehicles involved in this work, propellers acting on the same degree of freedom are mounted in a counter-rotating fashion in order to limit this undesired effect). To summarize, the aim of the activity described in this section is to determine an analytical expression for the function:

$$T = f\left(n, V_a\right) \tag{3.1}$$

with the same symbol meaning as in section 2.1.

The analysis is strongly based on the trend of the plot expressing the relation between advance coefficient J and the thrust coefficient K_T. Addressing, for the moment, the behaviour in the first quadrant (both coefficients positive), as the plots in figures 2.2 and 2.3 show, K_T is a decreasing linear function of J. From an analytical point of view, this behaviour can be translated in the following algebraic steps, starting from the definition of the coefficients, here again reported to facilitate the comprehension:

$$\begin{aligned} J &= \frac{V_a}{nd} \\ K_T &= \frac{T}{\rho n^2 d^4} \end{aligned}$$

being $-a$ and b the coefficients of the straight line describing this relation ($a, b > 0$), the following expression is valid:

$$K_T = -aJ + b \tag{3.2}$$

through algebraic deductions it is possible to express T as a function of J:

$$\begin{aligned} \frac{T}{\rho n^2 d^4} &= -aJ + b \\ T &= -a\rho n^2 d^4 J + b\rho n^2 d^4 \end{aligned} \tag{3.3}$$

defining the coefficients $m_T(n)$ and $q_T(n)$, depending only on the rotational speed n, as follow:

$$T = \underbrace{-a\rho n^2 d^4}_{m_T(n)} J + \underbrace{b\rho n^2 d^4}_{q_T(n)} \tag{3.4}$$

the result below is achieved:

$$T = m_T(n)J + q_T(n) \tag{3.5}$$

T and J are linearly dependent for each n, with negative slope $m_T(n)$ and positive y-intercept $q_T(n)$. Two points of this straight line are known and can be used to determine the expression of $m_T(n)$ and $q_T(n)$. The straight line crosses the abscissa axis in $(p/d, 0)$ as $T = 0 \Leftrightarrow K_T = 0$ and $K_T = 0$ approximately when $J = p/d \Leftrightarrow V_a = pn$ (the fluid linear momentum is not modified by the propeller). The other known point is the intersection with the ordinate axis; by defining the bollard thrust $T_0(n)$ as the thrust exerted in conditions of null advance velocity ($V_a = 0 \Leftrightarrow J = 0$) with a rotational speed of n, the straight line passes for the point $(0, T_0(n))$.

To summarize, the straight line defined in 3.5 passes through the points:

$$\begin{aligned} (0, T_0(n)) \quad &\Rightarrow \quad q_T(n) = T_0(n) \\ (p/d, 0) \quad &\Rightarrow \quad m_T(n) = \frac{-T_0(n)d}{p} \end{aligned} \tag{3.6}$$

that allow to obtain:

$$T = \frac{-T_0(n)d}{p} J + T_0(n) \tag{3.7}$$

by introducing the explicit expression of J, the straight line equation becomes:

$$\begin{aligned} T &= \frac{-T_0(n)d}{p} \cdot \frac{V_a}{nd} + T_0(n) \\ T &= \frac{-T_0(n)V_a}{pn} + T_0(n) \end{aligned} \tag{3.8}$$

it is possible to further develop the analysis by introducing the explicit expression of $T_0(n)$. Its trend is easily experimentally determinable by measuring the exerted bollard thrust at different rotational speeds [Allotta et al., 2014b]; the relation is approximately parabolic. As an example, in figure 3.1 the curves, experimentally derived for different propellers, showing a parabolic trend, are reported. Thus, the $T_0(n)$ term can be approximated through a

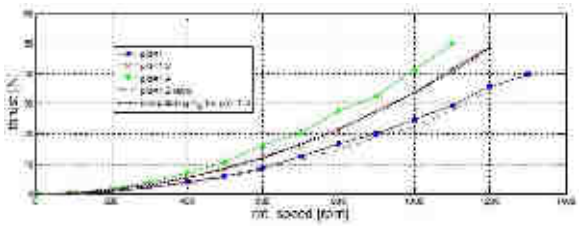

Figure 3.1: Exemple of experimentally derived curves of bollard thrust as function of rotational speed $T_0(n)$ - the used propellers are 5 blades Kaplan with an area ratio of 0.9

parabolic function with the vertex in the origin, defining the second order coefficient k, experimentally calculable:

$$T_0(n) \approx kn^2 \tag{3.9}$$

substituting the expression of equation 3.9 in equation 3.8, the desired result, for the behaviour in the first quadrant, under the constraint $0 \leq J \leq p/d$, is achieved:

$$\begin{aligned} T &= \frac{-kn^2 V_a}{pn} + kn^2 \\ T &= \frac{-knV_a}{p} + kn^2 \\ T &= kn\left(-\frac{V_a}{p} + n\right) \end{aligned} \tag{3.10}$$

In order to generalize the just obtained relation, it is useful to observe the chart in figure 2.3a that reports the experimentally derived behaviour also for $J < 0$. By considering that, during the normal functioning of the propellers on the vehicle, in case that the conditions $J < 0$ and $n > 0$ verify, in the most of the occasions the corresponding working point is close to the ordinate axis (otherwise considerable mechanical stress would affect the propeller itself). Under this reasonable assumption, the behaviour of the thrust coefficient (K_T) and, as consequence, of the thrust (T) can be considered constant. The value that T assumes in the second quadrant is the same assumed on the ordinate axis, i.e. the bollard thrust $T_0(n)$. As concerns, instead, the behaviour for $J > p/d$ and $n > 0$, the contribution due to the propeller is not a positive thrust even if the rotational speed is positive, on the contrary it would tend to decelerate the vehicle imposing a negative thrust. The trend of the curve for this range of values is not explained in the literature, in this thesis it is assumed that the thrust generated for $J > p/d$ is null as negligible with respect to the drag forces due to the interaction of the whole vehicle with the fluid. Another approximation has been done to complete the modelling through an analytical function on the four quadrants, i.e. the propellers have a symmetrical behaviour both for forward and reverse thrust. This is normally true for lateral and vertical thrusters as they use to work in both the ways; it is generally not true for the main propellers of the vehicle, but, being them used mainly in the forward direction, the introduced error through this approximation is considered acceptable.

According to all the proposed considerations, equation 3.10 can be generalized through the following function:

$$T(n, V_a) = sign(n) \cdot \left(k \cdot n^2 \; - \; \frac{k \cdot |n| \cdot g\left(sign(n) \cdot V_a\right)}{p} \right) \tag{3.11}$$

where $g(x)$ is a piecewise defined function as follows:

$$g(x) = \begin{cases} 0 & if \quad x \leq 0 \\ x & if \quad 0 < x \leq |n| \cdot p \\ |n| \cdot p & if \quad x > |n| \cdot p \end{cases} \tag{3.12}$$

achieving, this way, the purpose introduced with equation 3.1.

The obtained function 3.11 fully describes, in an analytical way, the relation that defines the thrust generated by a propeller rotating at a speed equal to n in a fluid moving in the longitudinal direction with a relative velocity equal to V_a. The function is continue but not differentiable; this will influence the way of treating it within the navigation filter.

Once the thrust for each propeller is calculated, they should be suitably combined to obtain the overall effect on the vehicle motion, as the forces and moments acting on it, collected as elements of the actions vector $\vec{\tau}$. Assuming n propellers working on a vehicle, it is possible to collect the related generated thrusts T_i $(i = 1, \cdots, n)$ as components of the vector $\vec{U}$ defined as:

$$\vec{U} \in \mathbb{R}^n \qquad \vec{U} = [\ldots, T_i, \ldots]^T \tag{3.13}$$

Vector $\vec{U}$ and $\vec{\tau}$ are linearly dependent through the constant matrix B, function of the vehicle geometry:

$$\vec{\tau} = B\vec{U} \tag{3.14}$$

the explicit expression of the B matrix is based on the definition of $\vec{P}_{mi}^{\,b}$ and $\vec{n}_{mi}^{\,b}$ respectively the position and the line of action of the i-th motor expressed with respect to the body-fixed frame.

$$B = \begin{bmatrix} A_1 \\ A_2 \end{bmatrix}; \qquad A_1 := \left[\cdots, \vec{n}_{mi}^{\,b}, \cdots\right]; \quad A_2 := \left[\cdots, \left(\vec{P}_{mi}^{\,b} - \vec{O}^{\,b}\right) \wedge \vec{n}_{mi}^{\,b}, \cdots\right] \tag{3.15}$$

the quantities just defined are useful to express the advance speed V_a that appears in function 3.10 as input for T calculation. In particular, being V_{ai} the advance speed to be considered for the i-th motor:

$$V_{ai} = \vec{\nu}_1 + \vec{\nu}_2 \wedge \left(\vec{P}_{mi}^{\,b} - \vec{O}^{\,b} \right) \tag{3.16}$$

This completes the description of the vehicle propulsion system model, providing a method to calculate the inputs $\vec{\tau}$ for the vehicle equation of motion (equation 2.5).

3.2 Sensors Model

In this section, for the sensors introduced in chapter 2, a model to be used in the estimation filters correction step will be provided.

3.2.1 Inertial Measurement Unit

Accelerometers An accelerometer measures the proper acceleration of the rigid body it is mounted on, biased by the opposite of the gravity acceleration ($\vec{g} = \begin{bmatrix} 0 & 0 & 9,81 \end{bmatrix}^T$ m/s in the earth-fixed frame) expressed in the body-fixed frame. The characteristic equation can be represented as follows:

$$\vec{a}^{\,meas} = J_1^T \left(\ddot{\vec{\eta}}_1 - \vec{g} \right) + \vec{b}_a + \vec{\delta}_a \tag{3.17}$$

with $\vec{b}_a$ and $\vec{\delta}_a$ respectively the bias and the measurement noise (zero-mean and Gaussian).

Gyroscopes As concerns the gyroscopes, instead, they measure the angular rate of the vehicle in the body-fixed and their characteristic equation is:

$$\vec{\nu_2}^{meas} = \vec{\nu_2} + \vec{b}_{\nu_2} + \vec{\delta}_{\nu_2} \tag{3.18}$$

with $\vec{b}_{\nu_2}$ and $\vec{\delta}_{\nu_2}$ respectively the bias and the measurement noise (zero-mean and Gaussian). If the accelerometer bias is almost stable, after the initial transitory period, the gyroscope bias is not, thus it has to be estimated online in order to reduce at the minimum the entailed errors.

More precise gyroscopes exploit fiber optics and take the name of FOG (Fiber Optics Gyroscope). The functioning is based on the Sagnac effect present in a Sagnac interferometer. If on one side, its higher precision translates in a reduced measurement noise and stable and low bias, on the other side it entails the introduction in the sensor output of a contribution due to the Earth rotation detected by the sensor and that has to be compensated.

Equations 3.17 and 3.18 highlight that an INS navigation system (section 2.5.1) based only on inertial sensors is intrinsically subjected to unlimited error drift because of the bias components that, even if identified in the calibration phase, cannot be completely compensated [VectorNav-Technologies, 2014]. In particular the following table summarizes this aspect:

Error due to the gyroscope	Error due to the accelerometer
$\delta\vec{v} = \frac{1}{2}\vec{e}_g t^2$	$\delta\vec{v} = \vec{e}_a t$
$\delta\vec{p} = \frac{1}{6}\vec{e}_g t^3$	$\delta\vec{p} = \frac{1}{2}\vec{e}_a t^2$

(3.19)

where $\delta\vec{v}$ and $\delta\vec{p}$ respectively represent the speed and position estimation errors and $\vec{e}_a$ and $\vec{e}_g$ are the residual errors on the measures.

3.2.2 Magnetometer

This sensor provides a measure of the local magnetic field expressed in the body-fixed frame. Defining the local Earth magnetic field expressed in the earth-fixed frame as a constant vector $\vec{m}^{NED} = \begin{bmatrix} m_x^{NED} & m_y^{NED} & m_z^{NED} \end{bmatrix}^T$,

the characteristic equation of the sensor, in absence of external disturbances, is:

$$\vec{m}^{meas} = C_{si}\left(J_1(\vec{\eta}_2)\vec{m}^{NED}\right) + \vec{b}_m + \vec{\delta}_m \tag{3.20}$$

Also in this case the term $\vec{\delta}_m$ is the measurement noise (zero-mean and Gaussian). The term $\vec{b}_m$ is a constant bias on the measure but, for magnetometer, it is not usually introduced only by the sensor itself but it depends by the so called *Hard Iron effects*, distortions created by objects that produce a magnetic field. Matrix C_{si} is used to model the *Soft Iron effects*, commonly caused by metals such as nickel and iron, introducing distortions as deflections or alterations in the existing magnetic field that will stretch or distort the magnetic field depending upon which direction the field acts relative to the sensor. Hard Iron and Soft Iron effects can be identified and compensated through a dedicated preliminary calibration phase.

3.2.3 Depth sensor

The sensors used on underwater vehicles for depth measurement are pressure sensors indeed. The local pressure is then converted in a measure of depth according to the basic hydrostatic relation:

$$p - p_{atm} = \rho g d \qquad \Rightarrow \qquad d = \frac{p - p_{atm}}{\rho g} \tag{3.21}$$

where:

- p is the local pressure (measured by the sensor);
- p_{atm} is the local atmospheric pressure (measured by the sensor during the initialization phase on the surface);
- g is the norm of the gravity acceleration;

- d is the height of the water column above the instrument, i.e. the depth.

The pressure measure p^{meas} is characterized by the following equation:

$$p^{meas} = p + b_p + \delta_p \tag{3.22}$$

with b_p and δ_p respectively bias and measurement noise (zero-mean and Gaussian); it results in the characteristic equation of the depth measurement:

$$z^{meas} = z + \delta_z \tag{3.23}$$

with δ_z measurement noise (zero-mean and Gaussian); no bias has to be considered on the depth measurement as it is obtained through a difference operation between two pressure measurements (the local one and the atmospheric one) obtained by means of the same sensor.

3.2.4 Doppler Velocity Log

A DVL (Doppler Velocity Log) is a velocity sensor based on the Doppler effect affecting an acoustic signal transmitted by a moving object. In particular, the common employment of a DVL for underwater vehicles is with it mounted under the hull pointing the bottom. The device transmits an acoustic signal and by analysing the Doppler effect affecting the echo coming back from the bottom, it computes a measure of the vehicle velocity (three-dimensional) with respect the earth-fixed frame, but expressed in the body-fixed frame. The characteristic equation describing the provided measures is the following one:

$$\vec{\nu_1}^{meas} = \vec{\nu_1} + \vec{b}_{\nu_1} + \vec{\delta}_{\nu_1} \tag{3.24}$$

with $\vec{b}_{\nu_1}$ and $\vec{\delta}_{\nu_1}$ respectively the bias and the measurement noise (zero-mean and Gaussian). The particularity of the DVL is that the related measurement

noise $\vec{\delta}_{\nu_2}$ is characterized by a non constant covariance, i.e. it depends on the norm of the measured velocity according to a function described in the sensor datasheets.

3.2.5 Ultra Short BaseLine System

The USBL transducer is capable of measuring the position of a transmitting compatible modem with respect to itself as spherical coordinates. Defining the azimuth and the elevation angles as α and β and the range as r, if the USBL pose with respect to the earth-fixed frame is $\vec{\eta}^{USBL}$, the measured position of the vehicle housing the transmitter modem is modelled as:

$$\vec{\eta}_1^{meas} = \vec{\eta}_1^{USBL} + J_1(\vec{\eta}_2^{USBL}) \begin{bmatrix} (r+\delta_r)\,(s\alpha+\delta_\alpha)\,(c\beta+\delta_\beta) \\ (r+\delta_r)\,(s\alpha+\delta_\alpha)\,(c\beta+\delta_\beta) \\ (r+\delta_r)\,(c\alpha+\delta_\alpha) \end{bmatrix} \tag{3.25}$$

where δ_r, δ_α and δ_β are the measurement noises (zero-mean and Gaussian) on the related quantities. Equation 3.25 shows how, because of the problem geometry, the noise on the earth-fixed position measurement has not properties of zero-mean neither Gaussian.

3.2.6 Global Positioning System

The GPS, even if not working underwater, equips almost all the UUVs. It is, in fact, usually used for the navigation filters initialization and error reset each time that the vehicle surfaces. The measured position is provided with respect to the geographic coordinate system as latitude and longitude; in order to exploit the provided measure within the navigation filter it is necessary to convert it in order to determine the corresponding earth-fixed coordinates. Standard functions are available to comply with this purpose

(e.g. [UniWisconsin, 2014]). By naming "$LL2NE$" the general function used for the conversion and $\vec{ll}^{\,meas}$ the measure provided by the GPS, the characteristic equation of the sensor can be expressed as:

$$\begin{bmatrix} x \\ y \end{bmatrix} = LL2NE\left(\vec{ll}^{\,meas} + \vec{\delta}^{\,ll}, \vec{O}^{n}_{ll,}\right) \tag{3.26}$$

where $\vec{\delta}^{\,ll}$ is the measurement noise (zero-mean and Gaussian). Because of the non-linearity of the $LL2NE$ function, the resulting measurement noise on $\begin{bmatrix} x & y \end{bmatrix}^T$ is not characterized by the same properties of $\vec{\delta}^{\,ll}$.

Chapter 4

Localization

The localization topic for underwater vehicles navigation is very important as the use of INS based on inertial sensors intrinsically, regardless of the sensor fusion algorithm used, leads to an unbounded growth of the position estimation error, as highlighted in equations 3.19. The availability for the position estimation system of a DVL measuring the vehicle velocity drastically reduces the error drift and allows to navigate for a considerable amount of time without error reset necessity. When an error reset mechanism is important (this happens especially for AUVs that have to autonomously navigate even for long periods), the commercially available solutions are the USBL and LBL systems. If on one hand, the use of such systems ensures high navigation performances, on the other hand, it increases the related costs as the expense to be considered for each of these sensors is in the order of the tens of thousands of euro. As this may not represent a problem for the military applications, for all the other fields where UUVs would be a very useful tool, the high costs represent a real limit. As the projects involving the MDM Lab about underwater robotics are archaeology oriented, a particular effort had been dedicated in orienting the research activity towards a direction that

could lead to the field also an economical benefit.

In particular this section deals with two different real applications, trying to exploit a reduced set of sensors not sacrificing the performance of the navigation system:

- **Cooperative Localization -** the design of the proposed strategy is based on the THESAURUS project that involved the use of three AUVs capable of communicating through acoustic modems and autonomously cooperating to comply with an archaeological mission. The team comprises also a support ship equipped with an acoustic modem, where the operator is able to monitor the mission and to intervene on the desired behaviour of the AUVs if necessary. The aim is to make the vehicles able of correctly estimating their own positions exploiting just the relative distance measurements provided by the acoustic modems, necessarily on board for communication purposes, and a DVL on just one AUV; no USBL or LBL should be used. To comply with this purpose, a cooperative localization algorithm has been studied.

- **Known Structured Environments -** the second proposed strategy is applicable to patrolling tasks, as the one proposed during the SAUC-E competition for FeelHippo AUV and the other participating AUVs. The vehicle had to follow the perimeter of a rectangular basin looking for potential anomalies. The studied strategy is to make the single beam echosounder (a sensor capable of providing the measure of the range from the nearest obstacle on its functioning direction), mounted in forward looking configuration on FeelHippo for obstacle avoidance purposes, able of rotating around its vertical axis. This way, it is able of acquiring information about the shape of the surrounding structures. By means of the comparison between the known environment and the

obtained information, the AUV should be able to calculate its position with respect to the environment itself.

4.1 Cooperative Localization

The proposed cooperative localization strategy, whose relative results have been published in [Allotta et al., 2014c], is based on the exploitation of the acoustic modems used for communication, a fundamental feature for a team of vehicles capable of cooperating. Commercially available acoustic modems are used and they offer the possibility of computing the time of flight from a vehicle to another one. Thus it is possible to calculate the distance between the two vehicles [Singh et al., 2006]. The problem of observability of the relative motion of two AUVs equipped with acoustic modems, configured as range measuring devices, is dealt with in [Arrichiello et al., 2011]. Several researchers have investigated the cooperative navigation between a surface ship and a single AUV, through Synchronous-Clock One-Way-Travel-Time Acoustic Navigation [Eustice et al., 2011], [Webster et al., 2009]. Recently, many interesting and important works concerning underwater cooperative localization and range measurement based localization have been carried out and many bibliographic references can be found in literature [Gao and Chitre, 2010], [Bahr et al., 2009b]. As concerns, instead, range measurement based localization, some interesting approaches are discussed in [Batista et al., 2011], [Parlangeli et al., 2012], [Lee et al., 2007].
[Bahr et al., 2009a] proposed a configuration where a dedicated Communication and Navigation Aid-AUV (CNA) can maintain an accurate estimate of its position through high accuracy sensors, such as DVL, and can enable a much larger group of vehicles with less sophisticated navigation suites to

maintain an accurate position, too. The proposed technique is based on a set of distance measurements among four vehicles that travel on the same working area. A geometrical algorithm, fed with the distance measurements, is then able to calculate the relative positions of all the vehicles with respect to the one that works on the surface and that has access to the GPS signal. Thus, differently from the approaches in the literature that use range measurements as input of the navigation filter, the proposed method uses the range measurements to perform a geometrical algorithm, the outputs of which (the position estimates) are used in the correction step of the navigation Kalman filter.

The approach proposed relies on AUVs with low-cost instrumentation: each of them is equipped with a low-cost IMU, a compass and depth sensor, but only one of them, the master, has a high accuracy navigation sensor such as the DVL. The system used to highlight the performance of the proposed algorithm is composed of three AUVs and a surface support ship equipped with GPS, but the results could be generalized to a system with a general number of vehicles, at least one of which with the DVL on board. The core of the localization algorithm is the *Tetrahedron-based Position Estimator*, a geometric algorithm that is performed on the master AUV. Part of the necessary data is measured on other AUVs and it should be made available to the master AUV by means of communication. The paper investigates some of the limits imposed by communication, providing a strategy to overcome this problem.

No constraints about the path or hypotheses on mutual distance among AUVs are necessary for the proposed algorithm; particularly, the vehicle trajectories may be completely general and no limitations on the variation of the related distances is required. The algorithm has been tested in a

simulated scenario, exploiting the model of the Typhoon AUV, and results will be described in the following chapter 6 where also the robustness of the procedure against numerical noise and model uncertainties have been tested. At the same time, the performance of the new algorithm based on the Tetrahedron-Based Position Estimator has been compared with those of the standard localization procedures to highlight the impact of the innovative algorithm.

All the Extended Kalman Filters used for navigation purposes are based on a purely kinematic model, in order to evaluate the performance of the proposed cooperative localization algorithm not affected by the particular choice of the involved dynamical model.

Before describing the studied method, a further useful reference system is defined in addition to the two ones in section 2.1.1:

- **Support frame** n **-** The origin, O_n, is fixed with respect to the surface support ship with axes aligned with the NED (North-East-Down) system: x^n axis pointing towards North, with y^n axis pointing towards East and z^n pointing towards Down.

According to the definition, it is possible to express the n-frame position of an AUV in the earth-fixed frame through a simple translation. In this section the position of a vehicle with respect to the n-fixed frame is indicated with the symbol p, its derivative with respect to the time (velocity) with the symbol v and its second derivative with respect to the time (acceleration) with the symbol a.

4.1.1 Sensors

Sensors used in the simulated scenario are the ones described in section 3.2, they are summarized in table 4.1 with their typical functioning frequencies. If the functioning of all the other sensors has been exhaustively described,

Sensor	Update Rate	Reference frame
IMU	100 Hz	Body
Magnetic Compass	100 Hz	Body
Pressure Sensor	10 Hz	Earth
DVL	7 Hz	Body
Acoustic Modems	medium: 0.1 Hz	-

Table 4.1: Commonly Used Underwater Vehicle Navigation Sensors

the acoustic modem used as a range sensor need some further words about its integration in the overall system.

Acoustic Modems as Range Sensors The acoustic modems used for communication purposes usually has the ability to embed a time stamp into the data packet allowing the receiving modem to calculate the mutual distance only by means of the TOF (Time Of Flight), calculated comparing the time stamp of the received message with the current time and by exploiting the knowledge of the speed of sound in the water. This kind of implementation is strongly based on an accurate synchronization of the vehicle clocks, that is achieved by setting the on board time equal to the GPS one each time that the GPS is available and always before starting a mission. This way the error between the PC clocks remains negligible [Caiti et al., 2013].

The implemented simulated system is based on the assumption that each vehicle can calculate its distance from the other vehicles of the fleet, while

it receives data, with an update period, that can be reasonably considered around 10 s [Bahr et al., 2009a]. In this work the update time is simulated as a Gaussian white noise with mean equal to 10 s and standard deviation equal to 1 s. This choice turns out to be suitable for this kind of applications because such a period is much greater than the time of flight necessary for the communication among the vehicles. The communication system is based on a Time Division Multiplexing (TDM) scheme with only one vehicle allowed to communicate at a time. A time slot of 15 s is dedicated to the communication from each vehicle; during this period the AUV communicates, in broadcast, necessary data with a time stamp and all the other vehicles are able to receive transmitted information and to calculate the corresponding distance. This way, collisions on the acoustic channel and consequently packet loss are minimized. Message loss and distance measure loss due to the channel conditions have been, instead, considered. As concerns data to be transmitted for the purpose of localization, these are very few as will be clear by the algorithm description, thus problems of saturation of the communication channel have not be considered (the datasheet of the Evologics modems mounted on Typhoon class AUVs states that the acoustic connection can work up to up to $13,9$ kbit/s).

Each underwater vehicle is able to communicate with a surface vehicle too. In the simulated scenario of this work the range measurement $\bar{d}^{ij}$, which is the distance between AUV_i and AUV_j, is affected by a Gaussian white noise with a constant standard deviation as in [Eustice et al., 2011]. In standard conditions a bias error may affect the distance measures. However this can be identified and compensated through a measurement of the sound speed depending on water temperature, salinity and pressure [Mackenzie, 1981].

4.1.2 Architecture for Communication and Estimation

The architecture for the estimation of position, velocity and orientation for each AUV, is based on sensor fusion techniques and communication among the AUVs.

The localization algorithm is distributed among all vehicles, particularly:

- AUV_1, the master vehicle, estimates its own position and, by means of *Tetrahedron-Based Position Estimator*, calculates an estimate of other AUVs' positions;
- Other AUVs estimate their own positions.

The architecture of communication, so that each vehicle gets the needed data, directly measured on other vehicles, available on board, is explained in section 4.1.2. In the following subsections the main modules of the architecture of estimation are described.

Orientation Estimation

The *Orientation Estimation*, depicted in figure 4.1, implements the orientation estimation algorithm called *Non-linear Complementary Filter*, described in section 2.5.2. By means of a 3D gyroscope, a 3D accelerometer and a 3D magnetometer, an estimation of the rotation matrix R_b^n expressing the orientation of the body-fixed frame with respect to the n-frame can be obtained. The algorithm is able to estimate on-line the bias of the gyroscope, too.

Position and Velocity Estimation - Vehicle 1

The master AUV of the fleet, called AUV_1, has a more sophisticated navigation suite, since it owns the DVL sensor. Its architecture of estimation for position and velocity is composed of four parts, figure 4.2:

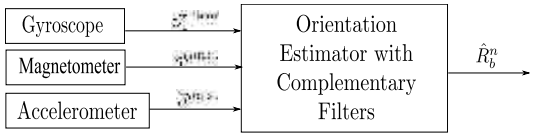

Figure 4.1: Orientation estimation

- a kinamtic based Kalman Filter of extended version for the INS of the AUV_1,
- a simple Kalman Filter for the estimation of the AUV-to-AUV ranges,
- a Dead-Reckoning algorithm propagating an estimation of the position of the other AUVs,
- a Tetrahedron-Based position estimator.

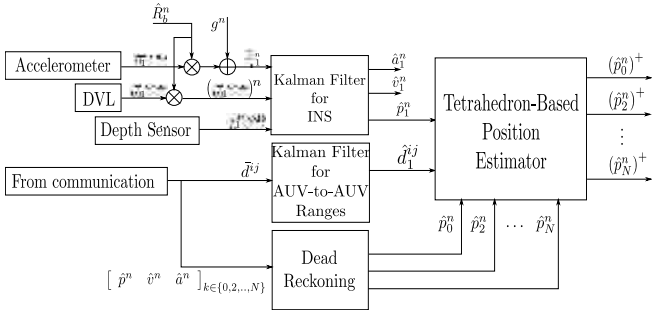

Figure 4.2: Position and Velocity Estimate - Vehicle 1

The first module, Kalman Filter for the INS of the AUV_1, implements an EKF [Barshan and Durrant-Whyte, 1995] which propagates a state composed of the position, velocity and acceleration, by means of the inertial sensors, the DVL and the depth sensor measurements. In order to consider

the different update rate of the sensors, the sensor noise covariance matrix R is adaptive to their occurrence. The next two modules have been implemented in order to circumvent that all dead-reckoning and range measurements cannot be gathered instantaneously to the *Tetrahedron-based Position Estimator*. The Kalman Filter for the estimation of the AUV-to-AUV ranges builds up the distances, propagating a model based on a constant rate. No constraints about the path or hypotheses on mutual distance among AUVs are necessary for the proposed algorithm; particularly the vehicle trajectories may be completely general and no limitations on the related distances is required. Whenever a task of communication with another AUV occurs, the measurement update of the KF takes place and it gets possible to calculate a new value for the distance rate, through the incremental ratio

$$\dot{\bar{d}}^{ij}(k) = \frac{\bar{d}^{ij}(k+\tau) - \bar{d}^{ij}(k)}{\tau} \tag{4.1}$$

where τ is the time interval between two tasks of communication between the AUV_i and the AUV_j. Range measurements computed by AUV_1 are always used as observations, the distances received by other AUVs, instead, must respect a constraint explained in Subsection 4.1.2. This module is fundamental for the *Tetrahedron-Based estimator*, since the availability of the range measurements is not homogeneous and depends on the occurrence of events of communication with the other AUVs. Dead-Reckoning propagates the position of the other AUVs by means of their last information of the position, velocity and acceleration received by AUV_1 via communication. In figure 4.2 the subscripts $\cdot_i$ with $i = 0, 1, ..., N$ indicate that the related quantity is available on the vehicle i; the subscript $\cdot_0$ refers to the surface support ship, whose position and velocity are measured through the GPS. The complete explanation of the *Tetrahedron-Based estimator* is described

Section 4.1.3.

Position and Velocity Estimation - Other Vehicles

Other AUVs have a lower accuracy in the estimation. Their architecture of estimation for the position and velocity is composed of two Kalman Filters: the first one estimates position and velocity by means of the accelerometer and the depth sensor; the second one estimates all the AUV-to-AUV distances which involve the vehicle, assuming in the used model their derivatives constant.

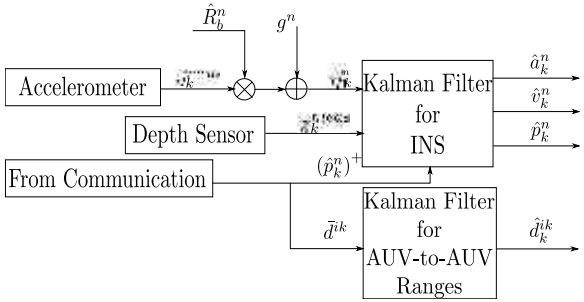

Figure 4.3: Position and Velocity Estimate - Vehicle k

Communication

As shown in figure 4.4 each AUV_i is able to communicate through acoustic modems both with the other AUV_j and the surface support ship. Each edge of the communication graph is called v_{ij}.

The different line section indicates three different situations:

- *Dotted line*: AUVs without DVL communicate each other, without exchanging any information. The receiver AUV_j calculates the range measurement $\bar{d}^{ij}$, where $i, j \neq 1$,

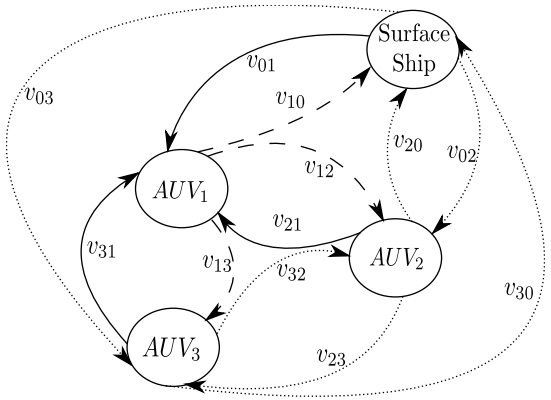

Figure 4.4: Communication Architecture - Particular situation of three AUVs

- *Solid line*: AUVs without DVL communicate with AUV_1, sending a packet of information v_{i1}, which includes the estimates of the position, velocity, acceleration and all the last range measurements it owns. Briefly $v_{i1} = \left\{\hat{p}_i^n, \hat{v}_i^n, \hat{a}_i^n, \hat{d}_i^{ij}\right\}$, where $i, j \neq 1$ and $j = \{0, .., N\} - \{i\}$. Obviously during this communication AUV_1 is able to calculate the distance $\bar{d}^{i1}$,

- *Dashed line*: AUV_1 communicates with the other AUVs, sending a packet of information v_{1i}, which includes the estimate of the position of AUV_i elaborated by the *Tetrahedron-based Position Estimator*. Briefly $v_{1i} = \left\{(\hat{p}_i^n)^+\right\}$, where $i \neq 1$.

A time stamp is associated to each range measure. AUV_1 exploits this value to decide whether to use the distance $\bar{d}_i^{ij}$ as an observation of the Kalman Filter for the AUV-to-AUV ranges: it happens if the time stamp associated

with the distance received $\bar{d}_i^{ij}$ is more recent than the time associated with the distance value $\bar{d}_j^{ij}$ previously received and already used as an observation.

4.1.3 Tetrahedron-based Position Estimator

The *Tetrahedron-based Position Estimator* is the core of the innovative proposed algorithm. The range measurements are not directly used in the localization filter but they are the input of a geometrical algorithm able to calculate the position of all the AUVs on the working scenario with respect to the surface support ship whose position is known by means of the GPS signal. These indirect measures of position are then used in the correction step of the Kalman navigation filter.

The *Tetrahedron-based Position Estimator* is a geometric algorithm that takes advantage of the acoustic measures of the distances to extend the advantages of the use of DVL to the vehicles that are not equipped with it. The algorithm is implemented on AUV_1. To perform the algorithm, working with a team composed of a minimum of 4 vehicles is necessary. These occupy the four vertices of a virtual tetrahedron. The analyzed system is composed of four vehicles (three AUVs and a surface support ship), even if the algorithm can be generalized to N AUVs ($N \geq 4$).

Problem Description

The goal of the algorithm is to determine an estimate $\hat{\vec{\eta}}_{1i}$ of the positions

$$\vec{\eta}_{1i} = \begin{bmatrix} x & y & z \end{bmatrix}_i^T \tag{4.2}$$

(with $i = 1, 2, 3$) of the three AUVs with respect to the earth-fixed frame. These coordinates, according to the definition of n frame and earth-fixed frame, are calculated by adding $\vec{\eta}_{10}$ to $\vec{p}_i^{\,n}$, the position of the i-th vehicle

with respect to the n frame. A measure of $\vec{\eta}_{10}$ is provided by the GPS, that is available for the surface vehicle. The *Tetrahedron-based Position Estimator* directly calculates an estimation $\hat{\vec{p}}_i^{\,n}$ of the positions

$$\vec{p}_i^{\,n} = \begin{bmatrix} x_i^n & y_i^n & z_i^n \end{bmatrix}^T \tag{4.3}$$

According to the definition of the n frame, the surface support ship has constant coordinates with respect to it, $\vec{p}_0^{\,n} = \begin{bmatrix} 0 & 0 & 0 \end{bmatrix}^T$. The following quantities, estimated on board by means of the Kalman Filters described in Section 4.1.2, are used as inputs for the *Tetrahedron-based Position Estimator*:

- the estimations of the position for each vehicle
- the estimations of the distances among all vehicles $\hat{d}^{ij}$

Since the quantities, used in this section, are all calculated on AUV_1, the subscript $\cdot_1$ of the generic expression $\hat{d}_1^{ij}$ will be omitted in the following of this section.

Algorithm

The algorithm is based on the definition of a new frame, called A frame (figure 4.5), which allows to easier express the positions of the vehicles. The A frame has its origin in $\vec{p}_0$, x^A axis so that $\vec{p}_1$ belongs to it, y^A axis so that $\vec{p}_2$ belongs to $x^A y^A$ plane with a positive coordinate y_2^A and z^A axis consequently.

Considering A frame, the positions of the AUVs can be defined as follows:

$$\vec{p}_i^{\,A} = \begin{bmatrix} x_i^A & y_i^A & z_i^A \end{bmatrix}^T \tag{4.4}$$

with $i = 1, 2, 3$. An estimate of the elements of $\vec{p}_i^{\,A}$ is calculated in terms of

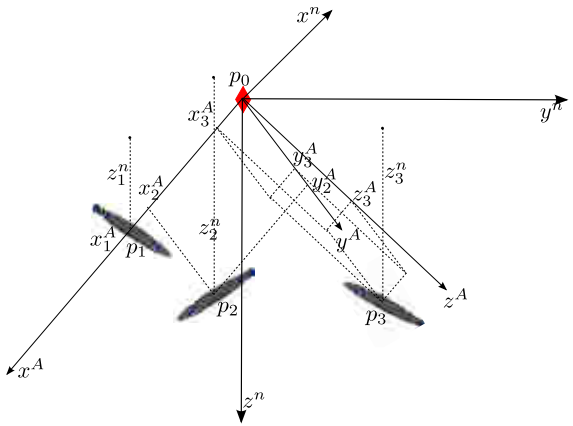

Figure 4.5: Definition of A frame

the estimated distances among vehicles:

$$\begin{aligned}
\hat{x}_1^A &= \hat{d}^{01} \\
\hat{y}_1^A &= 0 \\
\hat{z}_1^A &= 0 \\
\hat{x}_2^A &= \frac{\hat{d}^{01^2} + \hat{d}^{02^2} - \hat{d}^{12^2}}{2\hat{d}^{01}} \\
\hat{y}_2^A &= \sqrt{\hat{d}^{02^2} - \hat{x}_2^{A^2}} \\
\hat{z}_2^A &= 0 \\
\hat{x}_3^A &= \frac{\hat{d}^{01^2} + \hat{d}^{03^2} - \hat{d}^{31^2}}{2\hat{d}^{01}} \\
\hat{y}_3^A &= \frac{\hat{x}_2^{A^2} + \hat{y}_2^{A^2} - 2\hat{x}_2^A\hat{x}_3^A + \hat{d}^{03^2} - \hat{d}^{23^2}}{2\hat{y}_2^A} \\
\hat{z}_3^A &= \pm\sqrt{\hat{d}^{03^2} - \hat{x}_3^{A^2} - \hat{y}_3^{A^2}}
\end{aligned} \tag{4.5}$$

In case that the configuration is singular (AUV_2 belonging to the x^A axis or AUV_3 belonging to the x^Ay^A plane) the tetrahedron degenerates in

a non solid figure. It is possible to notice this issue if the arguments of the roots in $\hat{y}_2^A$ and $\hat{z}_3^A$ are zero; in this case the *Tetrahedron-based Position Estimator* is bypassed. In the case that, because of numerical issues or of the sensor noise, the same arguments became negative the tetrahedron algorithm is bypassed too. An effective way to face singular cases, even if not frequent, would certainly give to the algorithm a greater robustness; at the moment, when the algorithm notices to be in one of these cases, it simply bypass the Tetrahedron-based Position Estimator. Future development will certainly include improvements in this sense. The sign of $\hat{z}_3^A$ cannot be uniquely determined on the basis of the distances. This is an ambiguity about the shape of the estimated tetrahedron. The way to solve this ambiguity is presented at the end of this subsection.

Since both n frame and A frame have the same origin, they differ for a rotation. The rotation matrix R_A^n links the position of the vehicles between n frame and A frame:

$$\hat{\vec{p}}_i^n = R_A^n \hat{\vec{p}}_i^A \tag{4.6}$$

with $i = 1, 2, 3$. Thus, once R_A^n is calculated, it is possible to get the result. From equation 4.6, replacing the expressions of equation 4.5:

$$\begin{bmatrix} \hat{x}_1^n \\ \hat{y}_1^n \\ \hat{z}_1^n \end{bmatrix} = \begin{bmatrix} R_{11} & R_{12} & R_{13} \\ R_{21} & R_{22} & R_{23} \\ R_{31} & R_{32} & R_{33} \end{bmatrix} \begin{bmatrix} \hat{x}_1^A \\ 0 \\ 0 \end{bmatrix} \tag{4.7}$$

Element R_{31} can be calculated by the knowledge of $\hat{z}_1^n$ and $\hat{x}_1^A$:

$$R_{31} = \frac{\hat{z}_1^n}{\hat{x}_1^A} \tag{4.8}$$

Similarly, for elements R_{32} and R_{33}

$$R_{32} = \frac{\hat{z}_2^n - R_{31}\,\hat{x}_2^A}{\hat{y}_2^A} \tag{4.9}$$

$$R_{33} = \frac{\hat{z}_3^n - R_{31}\,\hat{x}_3^A - R_{32}\,\hat{y}_3^A}{\hat{z}_3^A} \tag{4.10}$$

The elements of R_A^n, already determined, are not sufficient to uniquely determine the orientation of A frame as to n frame. In fact, only two out of three degrees of freedom have been solved. The third degree of freedom, the rotation around a vertical axis passing through the origin of the frame, is still to be determined.

This issue is solved through the use of the estimate of the position of AUV_1, that, thanks to DVL, is more accurate than the ones of the other vehicles. Specifically, using $\hat{x}_1^n$ and $\hat{y}_1^n$ components, it is possible to obtain elements R_{11} and R_{21} of the rotation matrix.

$$\begin{aligned} \hat{x}_1^n = R_{11}\,\hat{x}_1^A \quad &\Rightarrow \quad R_{11} = \frac{\hat{x}_1^n}{\hat{x}_1^A} \\ \hat{y}_1^n = R_{21}\,\hat{x}_1^A \quad &\Rightarrow \quad R_{21} = \frac{\hat{y}_1^n}{\hat{x}_1^A} \end{aligned} \tag{4.11}$$

Five of the nine elements of the rotation matrix R_A^n have been calculated; the other four can be uniquely determined using the properties of the rotation matrices.

The obtained rotational matrix may not be part of the special orthogonal group SO(3) due to numerical issues in the calculation of their elements. The problem is the well known "Procrustes Problem". In the proposed algorithm, the obtained matrix is thus projected on SO(3) by using the singular value decomposition of the matrix itself $R_A^n = U\Sigma V^*$; the projection of the matrix on SO(3) is obtained by replacing matrix Σ with the unit matrix I_3.

In order to complete the solution of the problem, it is necessary to solve the ambiguity concerning the sign of $\hat{z}_3^A$. The $x^A y^A$ plane divides the space

into two halfspaces: the problem is to determine which of two halfspaces AUV_3 belongs to. In order to overcome this issue, the positions $\hat{\vec{p}}_i^n$ of the vehicles, estimated on AUV_1, can be used. Even if these positions are not exact, they can be used to solve the problem of the sign, as follows

$$sign\left(\hat{z}_3^A\right) = sign\left(\hat{\vec{p}}_3^n \cdot \left(\hat{\vec{p}}_1^n \times \hat{\vec{p}}_2^n\right)\right) \tag{4.12}$$

If the dot product is equal to zero, AUV_3 belongs to the plane of division and the tetrahedron becomes degenerate on it. Thus, the quantity in brackets is an index of how much the system is close to a singular configuration. So that quantity can be used to decide if it is not advantageous to use the *Tetrahedron-based Position Estimator*. Specifically, if

$$\hat{\vec{p}}_3^n \cdot \left(\hat{\vec{p}}_1^n \times \hat{\vec{p}}_2^n\right) < \epsilon_t \tag{4.13}$$

where ϵ_t is a constant tolerance, the estimate algorithm is rejected, until the vehicles reach a configuration sufficiently far from the singularity.

AUV_1 plays a key role in the team, thanks to the valuable set of navigation sensors, including DVL, that it has on board. The doubt that it is better to make play this role to the Surface Ship may rise because of the continuous availability of the GPS signal that ensures a higher degree of accuracy in its localization. This is not possible because of two reasons:

- the estimated position of AUV_1 is used to solve the last degree of freedom of the tetrahedron in the space so that to determine uniquely its configuration. The degree of freedom is the one around the vertical straight line passing through the Surface Ship. Thus, it is not possible to substitute AUV_1 with the Support Ship in this role because, by definition, it belongs to the vertical axis around which the ambiguity is defined. In case that also AUV_1 belongs to it, the rotational matrix R_A^n

results undetermined and the *Tetrahedron-based Position Estimator* is bypassed.

- AUV_1 is also the best vehicle on which to calculate the *Tetrahedron-based Position Estimator* algorithm because it always has available a recent and reliable estimation of its position to determinate the configuration of the tetrahedron in the space.

The algorithm is based on the determination of the orientation of a tetrahedron in the space through the calculation of the SO(3) rotation matrix that represents it. Other angular representations, that in certain circumstances, may be particularly compact and efficient (axis-angle, quaternion, etc. requiring a lower number of parameters to describe the orientation), but at this stage of the research the use of a complete representation method, as rotation matrix is, has been preferred both because it permits to avoid potential singularities and discontinuities and because it allows to simply calculate the fundamental geometric parameters of the algorithm.

The algorithm can also be used with teams consisting of more than 4 vehicles. In this case, *Tetrahedron-based Position Estimator* is implemented between the surface vehicle and the three closest AUVs. For each other pair of AUVs, a set of four vehicles can always be formed with the surface support ship and AUV_1; the same algorithm is performed for each set.

4.2 Known Structured Environments

This section describes the localization strategy based on low-cost sensors usually available on board for obstacle avoidance necessities for vehicles, such as FeelHippo, during patrolling missions of well-known structured environments such as harbours or docks.

The aim is to demonstrate that an AUV, even if equipped with a low-cost set of sensors, by taking advantages from the knowledge about structured environment, can achieve a good self-localization avoiding the use of the expensive standard devices. In addition to the sensors for orientation and depth estimation, FeelHippo is equipped with a single beam acoustic sensor (Imagenex 852 ultra-miniature echo-sounder). The sensor periodically emits an acoustic signal and is able to measure the strength of the echo coming from up to 500 different points in the sensing radius (for a range of 50 m maximum). The echo-sounder is able to rotate around its vertical axis; its angular position can be controlled thanks to a servo motor mounted inside the vehicle hull (figure 4.6).

Figure 4.6: The rotating echo-sounder system

Thanks to this setting, the studied ALS (Acoustic Localization System) can be used for a 2D mapping of the surrounding environment and for self-localization within it. The 2D mapping is a procedure periodically performed to detect the environment structures, a priori known; the period corresponds to the necessary time for the echosounder to perform a complete rotation. The absolute direction of the sensor head on the horizontal plane is always known as the sum of the vehicle yaw angle and the feedback provided by the

servomotor about its current coordinate. The acquired data, associated to the orientation of the sensor compared to the North, can be collected in an image (figure 4.7 taken in the MDM Lab testing pool), where, according to a gray scale from black to white, the color of each pixel is proportional to the strength of the echo coming from the related point. Distortions due to

Figure 4.7: Acoustic image of the MDM Lab testing pool

the vehicle movement during a complete acquisition are negligible, since the vehicle typical operating speed results negligible compared the sensor range (50m for the considered one) and the necessary time for a complete rotation (< 10 s for the system here considered). The algorithm of localization consists of different steps: the first processing phase is oriented to the identification of the pixels belonging to the edges of the structures. A pixel is considered part of the edge of a structure if the gradient of the echo strength calculated along a centrifugal direction has a local maximum. To avoid to consider the

echo reflections instead of real edges, for each direction it is considered a real positive only the one nearest to the center. Once a new image containing only the positive points has been identified, this is processed through the Hough transform in order to locate potential straight line belonging to the structured environment (known a priori) in the "visual" field of the echo-sounder. In the obtained Hough space, the points of intersection of the deduced curves correspond to lines in the original image. The parameters of the line are uniquely determined from the coordinates of the intersection point in the Hough space. The a priori knowledge of the environment, e.g. of the directions of the walls of a harbour, permits to reduce the area of the Hough space where to look for intersection points, giving more robustness to the method. Figure 4.8 qualitatively shows the processed image of a rectangular basin with one edge aligned with the East-West direction ($\pi/2$ rad) and two edges aligned with the North-South direction (0 rad). In the related Hough space, the corresponding points can be searched in two bands around the 0 rad and the $\pi/2$ rad.

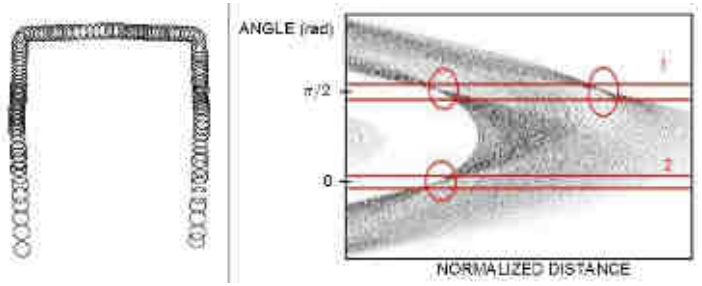

Figure 4.8: Hough Transform of the pre-processed image

Once the straight lines belonging to known structures are identified, the absolute position of the vehicle with respect to the environment can be de-

termined by means of the comparison between the on-line acquired map and the known one about the working area. This strategy has been validate during the SAUC-E 2013 competition and the related results are reported in chapter 6

Chapter 5

Navigation Algorithm

This chapter about the navigation algorithms studied and developed within the last three years of Ph.D. research period is divided into two sections according to the consideration stated in chapter 2. In fact, even if the dynamic evolution of position and orientation is strongly intrinsically coupled, it is advantageous to address independently the two problems and to use the output of the orientation estimation algorithm as the measurements provided by a virtual orientation sensor in the position estimation filter.

5.1 Pose Estimation Algorithms

The first section, here proposed, is about position estimation (section 5.1.1). It describes the choices about process model and sensors model to be integrated both in the EKF and in the UKF structures shown in the dedicated section 2.4. The second one (section 5.1.2) describes instead some proposed modifications from which the most used orientation estimation filter in the literature would benefit in terms of reliability and accuracy.

5.1.1 Position Estimation

This section is in particular divided in three parts, dealing respectively with:

- **choice of state variables -** it is a very important aspect as expressing the system evolution with respect to a group of variables instead of a different one, even if the achieved description is complete, may lead to a much more complicated implementation of the necessary algorithms;
- **definition of the system evolution model -** as anticipated in chapter 2, this is a crucial aspect that has to be considered. In fact, a too poorly representative model, as a merely kinematic model is, may lead the filter to diverge. Similarly, divergence may derive by the use of a complete and detailed dynamic model characterized by a general uncertainty that is too high because of the presence of too many parameters hard to be identified;
- **definition of the sensors model -** here, according to the description of the general model of the sensors usually involved in the underwater navigation, provided in section 3.2, the expression of the measure function $h(x_k)$ will be derived.

State Variables

As concerns the linear motion components, the proposed filter structure is based on a state vector containing the three earth-fixed vehicle coordinates ($\vec{\eta}_1 = \begin{bmatrix} x, & y, & z \end{bmatrix}^T$). At the velocity level, as measurements may be provided by the DVL, it is convenient, in order to obtain a simple measure model (function $h(x_k)$), to include in the state vector the vehicle body-fixed velocity ($\vec{\nu}_1 = \begin{bmatrix} u, & v, & w \end{bmatrix}^T$). As it is necessary to include a dynamical description in the system model, it is useful to introduce the acceleration level within the state vector; in particular, as the equation of motion (equation 2.5) are expressed as a function of the first derivative of $\vec{\nu}$ vector, its linear part ($\dot{\vec{\nu}}_1 = \begin{bmatrix} \dot{u}, & \dot{v}, & \dot{w} \end{bmatrix}^T$) is here considered.

As concerns, instead the orientation components, even if they are estimated through a dedicated algorithm, it is convenient to introduce them as state elements as the time evolution of the linear part of the system is function of them. As this is the only aim in considering the orientation as a part of the state vector, no angular velocity or higher order derivative are considered, but just the fixed-frame orientation components ($\vec{\eta}_2 = \begin{bmatrix} \varphi, & \vartheta, & \psi \end{bmatrix}^T$).

To summarize, according to the just exposed considerations, the state vector to be considered within the estimation filter (independently from its version) is the following one:

$$x = \begin{bmatrix} \vec{\eta}_1 \\ \vec{\nu}_1 \\ \dot{\vec{\nu}}_1 \\ \vec{\eta}_2 \end{bmatrix} \tag{5.1}$$

that in its explicit version is:

$$x = \begin{bmatrix} x & y & z & u & v & w & \dot{u} & \dot{v} & \dot{w} & \varphi & \vartheta & \psi \end{bmatrix}^T \tag{5.2}$$

The proposed state vector is composed of 12 elements; in the following section 5.1.1, a convenient expression for the model of their dynamical evolution is derived in order to be implemented within the estimation filters.

One further evaluation with respect to the proposed choice is that a filter using this state variable set is characterized also by the benefit of intrinsically estimate also the vehicle body-fixed velocity that is a necessary signal for the implementation of a lot of controller typologies.

System Evolution Model

As anticipated, the process model to be implemented in the position estimation filter of an UUV cannot be neither a purely kinematic model nor a complete dynamic one if an identification process for all the involved parameters has not been successfully carried out. Otherwise the estimation process is too much unstable and the estimated state is easily affected by divergence. The idea leading the analysis carried on in this section is to identify a trade-off solution, capable of sufficiently describe the vehicle motion but not introducing a lot of parameters hardly identifiable and thus affected by uncertainty.

The degree of freedom on which a considerable dynamics takes place is only the longitudinal one, as the vehicle drag along the other directions (especially for the torpedo-shaped ones as Typhoon and MARTA are) strongly dampens the lateral and the vertical motion. On the basis of this reasonable consideration, the proposed model involves a dynamical description of the motion only on the longitudinal degree of freedom, in particular at the

acceleration level as explicitly shown in the following expression:

$$\begin{bmatrix} \begin{bmatrix} x \\ y \\ z \end{bmatrix} \\ \begin{bmatrix} u \\ v \\ w \end{bmatrix} \\ \begin{bmatrix} \dot{u} \\ \dot{v} \\ \dot{w} \end{bmatrix} \\ \begin{bmatrix} \varphi \\ \vartheta \\ \psi \end{bmatrix} \end{bmatrix}_k = \begin{bmatrix} \begin{bmatrix} x \\ y \\ z \end{bmatrix}_{k-1} + \Delta T \cdot J_1\left(\varphi_{k-1}, \vartheta_{k-1}, \psi_{k-1}\right) \cdot \begin{bmatrix} u \\ v \\ w \end{bmatrix}_{k-1} \\ \begin{bmatrix} x \\ y \\ z \end{bmatrix}_{k-1} + \Delta T \cdot \begin{bmatrix} \dot{u} \\ \dot{v} \\ \dot{w} \end{bmatrix}_{k-1} \\ \begin{bmatrix} d\left(X(n_k^1, n_k^2, u_{k-1}), u_{k-1}\right) \\ 0 \\ 0 \end{bmatrix} \\ \begin{bmatrix} \varphi \\ \vartheta \\ \psi \end{bmatrix}_{k-1} \end{bmatrix} + w_{k-1} \quad (5.3)$$

where the new introduced symbols are:

- ΔT is the time period elapsed from the last filter iteration;
- $d\left(\cdot\right)$ is the dynamical equation that calculates the longitudinal acceleration as a function of longitudinal fixed-body thrust X and vehicle advance velocity u;
- n^1 are n^2 are the imposed values for the rotational speed of the propellers acting on the longitudinal degree of freedom, in this case, as all the vehicles considered in this work have two main rear propellers, those are indicated with the numbers 1 and 2 at the superscript.

The expression of the function $d\left(\cdot\right)$ is a simplification of the 6 DOF equation of motion (2.5) along the longitudinal axis considering a quadratic drag effect:

$$\dot{u} = d\left(X, u\right) = \frac{X - \frac{1}{2} A_f C_u \rho u^2}{M_{11}} \quad (5.4)$$

where the new introduced symbols are:

- A_f surface of the frontal area the vehicle
- C_u longitudinal drag coefficient of the vehicle, easily experimentally determinable
- M_{11} the first term of the mass matrix M, the vehicle mass

and, finally, X is calculable, with reference to the function in equation 3.11 as:

$$X = T_1 + T_2 = T\left(n^1, u\right) + T\left(n^2, u\right) \tag{5.5}$$

reasonably assuming that the advance velocity for the vehicle main propellers coincides with the vehicle longitudinal velocity ($V_a \approx u$).

It is worth to note that the term w_{k-1} is the vector representing the process noise on all the state elements and that it takes into account all the approximations assumed on the process model.

Sensors Model

According to the sensors model definition in the dedicated section 3.2, the $h(x)$ function to be considered within the adopted filter, considering all the

possibly available sensors, is the following one:

$$y_k = h\left(x_k\right) + \delta_k = \begin{bmatrix} x^{GPS} \\ y^{GPS} \\ x^{USBL} \\ y^{USBL} \\ \varphi^{NCF} \\ \vartheta^{NCF} \\ \psi^{NCF} \\ u^{DVL} \\ v^{DVL} \\ w^{DVL} \\ z^{DS} \end{bmatrix}_k + \delta_k =$$

$$= \begin{bmatrix} 1 & 0 & 0 & 0 & 0 & 0 & 0 & 0 & 0 & 0 & 0 & 0 \\ 0 & 1 & 0 & 0 & 0 & 0 & 0 & 0 & 0 & 0 & 0 & 0 \\ 1 & 0 & 0 & 0 & 0 & 0 & 0 & 0 & 0 & 0 & 0 & 0 \\ 0 & 1 & 0 & 0 & 0 & 0 & 0 & 0 & 0 & 0 & 0 & 0 \\ 0 & 0 & 0 & 0 & 0 & 0 & 0 & 0 & 0 & 1 & 0 & 0 \\ 0 & 0 & 0 & 0 & 0 & 0 & 0 & 0 & 0 & 0 & 1 & 0 \\ 0 & 0 & 0 & 0 & 0 & 0 & 0 & 0 & 0 & 0 & 0 & 1 \\ 0 & 0 & 0 & 1 & 0 & 0 & 0 & 0 & 0 & 0 & 0 & 0 \\ 0 & 0 & 0 & 0 & 1 & 0 & 0 & 0 & 0 & 0 & 0 & 0 \\ 0 & 0 & 0 & 0 & 0 & 1 & 0 & 0 & 0 & 0 & 0 & 0 \\ 0 & 0 & 1 & 0 & 0 & 0 & 0 & 0 & 0 & 0 & 0 & 0 \end{bmatrix} \cdot \begin{bmatrix} \begin{bmatrix} x \\ y \\ z \end{bmatrix} \\ \begin{bmatrix} u \\ v \\ w \end{bmatrix} \\ \begin{bmatrix} \dot{u} \\ \dot{v} \\ \dot{w} \end{bmatrix} \\ \begin{bmatrix} \varphi \\ \vartheta \\ \psi \end{bmatrix} \end{bmatrix}_k + \delta_k \tag{5.6}$$

The particular choice of the state variables vector leads for all the involved sensors to a linear model equation. That means that the system is not linear just as regards the process evolution and not the measurement model.

The measure noise δ_k does not respect the characteristics of being white and Gaussian noise, but by the analysis of the obtained results, proposed in chapter 6 it appears clear that it does not lead the filter to the instability and to diverge.

The proposed process model and sensors model have been implemented both in an UKF and in an EKF to compare the achievable performance. In both the cases, for each correction step it is necessary, because of the asynchronism of the different sensors, to verify which measurements have been updated during the last functioning period ΔT and to eliminate the rows in the equation 5.6 relative to the missing measurements.

5.1.2 Orientation Estimation

This section of the thesis is dedicated to the study of an orientation estimation algorithm that aims at overcoming the potential practical issues implied by the filters proposed in the literature, especially the one that has recently become a standard reference in the field, i.e. the NCF (Nonlinear Complementary Filter) proposed in [Mahony et al., 2008] and described in section 2.5.2.

For this algorithm, the convergence of the estimated orientation to the real one is demonstrated if at least two earth-fixed known directions are measurable with respect to the body-fixed. This is a condition that is normally satisfied by the sensors sets commonly used for orientation estimation purposes, including a 3D gyroscope, a 3D accelerometer and a 3D magnetometer. In fact, through these sensors, the integration of the gyroscope signals can be corrected through the measurements in the body-fixed frame of the directions of the gravity acceleration (through accelerometers, considering

that the dynamics of an underwater vehicle is slow enough for the vehicle proper acceleration to be negligible compared to the gravity acceleration) and the local Earth magnetic field (through magnetometers), both of them known with respect to the earth-fixed frame. Although, in principle, the NCF should work smoothly on such a system, potential issues born, indeed, when the algorithm is applied on the real sensor set, in particular in the field of UUV, where external disturbance sources, especially of magnetic kind, are frequently present. The main error sources are the ones affecting the accelerometer and the magnetometer outputs:

- **Accelerometer -** the assumption that, within the accelerometer measurements, the vehicle proper acceleration is negligible with respect to the gravity acceleration and that, thus, the measured direction is the vertical one is not always true; in fact, in the practice, it may happen that proper acceleration on the horizontal plane makes the measured direction deviate. This phenomenon should be identified in real-time and solution aimed at not considering measurements affected by it within the filter has to be implemented.

- **Magnetometer -** as this sensor cannot distinguish between the Earth's magnetic field and additive magnetic disturbances a procedure to identify the latter and, if possible, to compensate their effect should be implemented. In particular, the effects due to disturbance sources moving jointly with the sensor are, in principle, identifiable during a dedicated calibration phase; potential external disturbances should, instead, be detected and, in case, the measurements acquired in their presence should be avoided by the NCF.

Sensors Calibration and Measurements Process

A first necessary clarification is about the sensors mounting, in particular, all the three sensors (gyroscope, accelerometer and magnetometer) have their three axes aligned with the ones defining the body-fixed frame. The first aspect that is necessary to deal with is the sensors calibration process, in particular with the one of magnetometers, performed in order to identify disturbance sources jointly moving with the vehicle and to compensate their effects on the measurements. This class includes two different typologies of disturbances, introduced in equation 3.20 describing the magnetometer model:

- **Hard Iron disturbances -** permanent magnets and magnetized objects, such as electronic subsystems in the proximity of the sensor, cause the so-called "Hard Iron effect": these objects are the source of a permanent magnetic field, constant in the body-fixed frame. They have the effect of adding a constant bias $\vec{b}^m$ on the magnetometer output.
- **Soft Iron disturbances -** their effect on the measure equation is represented by the matrix C_{si}: the phenomenon is due to ferromagnetic materials close to the sensor (such as iron and nickel) that deviate the local magnetic field by producing an additional contribution whose magnitude is related to the angle of incidence of Earth's magnetic field on the material itself. Hence, this effect changes as the sensor rotates.

The effects of Soft and Hard Iron disturbances can be visualized by rotating the sensor along different directions. By plotting in the three dimensional space the measures acquired during the procedure, the result, in absence of Soft and Hard Iron effects, should be a distribution of points belonging to the surface of a sphere with its center in the origin of the axes. The effect

introduced by Hard Iron disturbances is a shift of the center of the point distribution corresponding to the introduced bias $\vec{b}^m$; on the other hand, the effect of the Soft Iron ones is a deformation of the sphere in a generic ellipsoid, represented by the geometrical linear transformation C_{si}.

If both kinds of disturbance are present, the measurements taken while rotating the sensor in the space would lie on the surface of an ellipsoid centered at a certain offset from the origin. For example, Figure 5.1 shows the magnetometer readings taken while rotating the device by hand in 3D space in a disturbance-free environment; it is easy to note that the measurements lie with good approximation on the surface of a sphere (the radius of the sphere does not reflect the true magnitude of the magnetic field; the scale factor is due to the magnetometer internal settings that cannot be modified by the user). On the contrary, Figure 5.2 reports the measurement of the magnetometer taken in the same geographical locality as in the previous test, but

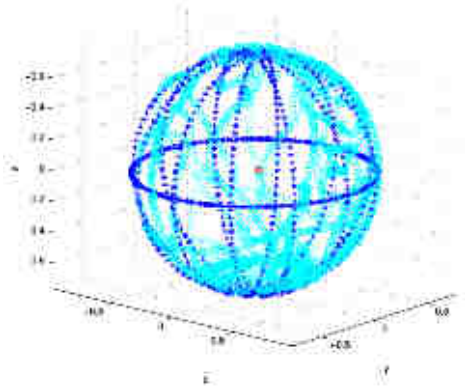

Figure 5.1: Magnetometer readings with no magnetic disturbances - Blue dots belong to a sphere with its center in the origin; light blue dots correspond to magnetometer measurements

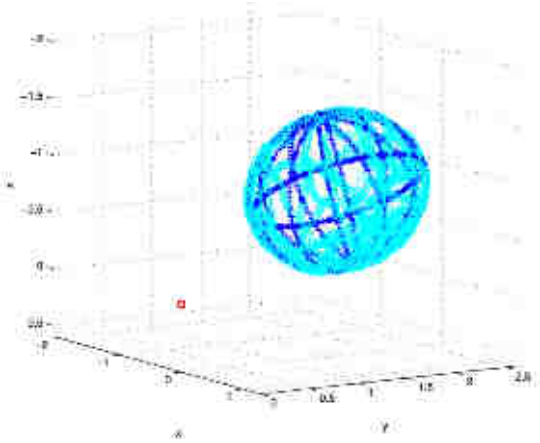

Figure 5.2: Magnetometer readings with magnetic disturbances - Blue dots belong to a generic ellipsoid in the space; light blue dots correspond to the magnetometer measurements; red dot is the origin

after attaching metal objects to the sensor case: in this case, the previously obtained sphere is deformed, and its center is shifted from the origin.

Thus, in general, the set of points, this way generated, lies on the surface of an ellipsoid, defined by $\vec{b}^{\,m}$ and C_{si}; the aim of the magnetometer calibration consists in the definition of a procedure for the compensation of the effect due to this two terms to be used to correctly map every subsequent measurement on the surface of the theoretical sphere. The most common calibration techniques are based on ellipsoid fitting: after collecting measurements while rotating the sensor in a sufficient number of different orientations in the 3D space, the best fitting ellipsoid (in the least square sense) can be identified through its characteristic parameters calculation; once its center, radii and axes are known, the offset and the scaling affecting each measure can be corrected. Whereas this solution to the problem is fairly simple and prove to be

efficient in a large number of application cases, it can be not applicable when the sensor rotation along some axes is constrained. This is the case of the underwater mobile robots field of application. The achievable vehicle configurations are characterized by limited roll and pitch angles range (because of restoring forces described in equation 2.6 desired for vehicle hydrostatic stability). This restriction implies that the measure set that can be used for calibration purposes cannot include enough information content along one of the three space dimensions (the vertical one) to completely identify the shape of the ellipsoid. Hence, the goal becomes to define a simple and fast calibration technique which can approximate the best the theoretical locus on which the uncorrupted measurements lie, by exploiting only data, which approximately derive from measurements performed on the horizontal plane, acquired during a complete turn of the vehicle along its vertical axis.

Assuming the knowledge of the local Earth magnetic field vector thanks to its representation through accurate models described in the literature, and considering that its value does not change enough on the possible operational area of an underwater vehicle not to consider it constant, the expected sphere, in absence of disturbances, is uniquely determined and known as well as the circumference corresponding to the measurements performed with the vehicle (and thus the sensor) belonging to the horizontal plane. Figure 5.3 summarizes this assumption, highlighting that the vertical component of all the performed measurements corresponds to the constant vertical component of the magnetic field with respect to the earth-fixed frame m_z^{NED}. The idea standing at the basis of the proposed calibration procedure is to exploit the knowledge of the position of the circumference represented in red and to determine the ellipse into which it is deformed by Soft and Hard Iron disturbances. Then, through the comparison of the two curves, the goal is

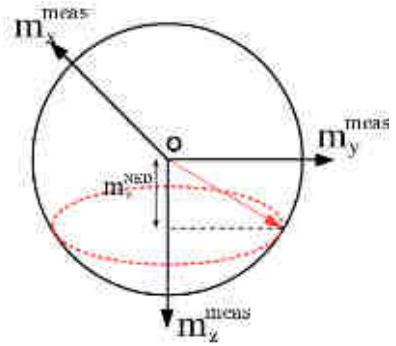

Figure 5.3: Magnetic field measurements performed by rotating the vehicle on the horizontal plane

to determine the geometrical transformation that maps the former onto the latter in order to compensate the disturbances on the measures by applying the inverse transformation to them. The algorithm is composed of the following steps: firstly, the measurement ellipse is rotated so that it lies on a horizontal plane; then, a planar ellipse fitting procedure is applied to determine the center, the radii and the tilt of the ellipse; finally, these quantities are compensated and the measurements are mapped back to the theoretical circle. In the real application of the algorithm, not all the measurements are really taken with the vehicle in exactly null pitch and roll configuration; hence, the magnetometer readings do not perfectly lie on a plane. The first preprocessing step of the calibration algorithm consists in computing the minimal distance plane (in a least square sense) Π that best fits all the points. Such calculation can be executed resorting to linear algebra. Consider the standard plane equation

$$ax + by + cz + d = 0 \tag{5.7}$$

Let $\vec{q} = [x\ y\ z\ 1]^T$ denote a point on the plane, represented as an augmented vector. The vector $\vec{A} = [a\ b\ c\ d]^T$ contains the unknowns of the problem. If point $\vec{q}$ lies on the plane, it verifies the following equation:

$$\vec{q}^T \vec{A} = 0. \tag{5.8}$$

Given N points (the magnetometer readings), the following linear system can be written:

$$Q\vec{A} = \vec{e} \tag{5.9}$$

where

$$Q = \begin{bmatrix} x_1 & y_1 & z_1 & 1 \\ \vdots & \vdots & \vdots & \vdots \\ x_i & y_i & z_i & 1 \\ \vdots & \vdots & \vdots & \vdots \\ x_N & y_N & z_N & 1 \end{bmatrix} \tag{5.10}$$

being each $[x_i\ y_i\ z_i]^T$ a different reading, and $\vec{e}$ a $N \times 1$ vector representing the error to be minimized (if all points lie on the plane, then $\vec{e} = \vec{0} \in \mathbb{R}^{N\times 1}$). The solution of such system is the closest vector to the kernel of Q, which is given by the right-singular vector corresponding to the minimum singular value obtained from the singular value decomposition of Q. The direction of the normal direction to the plane is given by $\vec{n} = [a\ b\ c]^T$; the position of a point $\vec{p}$ on the plane can be determined by assigning two coordinates and calculating the third one by inverting equation 5.7. The projection of a generic magnetometer measure $\vec{m}_i^{meas} = [x_i^{meas}\ y_i^{meas}\ z_i^{meas}]^T$ on Π is then given by:

$$\vec{m}_i^{\Pi} = [x_i^{\Pi}\ y_i^{\Pi}\ z_i^{\Pi}]^T = \vec{m}_i^{meas} - \left(\vec{n}^T\left(\vec{m}_i^{meas} - \vec{p}\right)\right)\ \vec{n} \tag{5.11}$$

The determination of the plane containing the measures allows to calculate the necessary rotation for them in order to align Π itself with the horizontal

plane. Defining the axis-angle rotation matrix $R(\theta_\Pi, \vec{a}_\Pi)$ representing a rotation of θ_Π angle around the $\vec{a}_\Pi$ axis, the new set of points $\vec{m}_i^h$ is obtained through:

$$\vec{m}_i^h = R(\theta_\Pi, \vec{a}_\Pi)\vec{m}_i^\Pi \tag{5.12}$$

Finally, a standard ellipse fitting procedure can be applied to determine the best fitting ellipse (in the least square sense) to the points. Without going into details (see [Fitzgibbon et al., 1999], [Halíř and Flusser, 1998] for theoretical proof), given the ellipse defined by the implicit equation

$$Ax^2 + Bxy + Cy^2 + Dx + Ey + F = 0 \tag{5.13}$$

and a set of M different points $m_i^h = [m_{i,x}^h \; m_{i,y}^h \; m_{i,z}^h]^T, \; i = 1, \cdots, M$, the best fitting ellipse is obtained by solving the following generalized eigenvalue problem:

$$S\vec{X} = \lambda K\vec{X} \tag{5.14}$$

$$\vec{X}^T K\vec{X} = 1 \tag{5.15}$$

where $\vec{X} = [A \; B \; C \; D \; E \; F]^T$ is the vector of unknowns (the coefficients of the ellipse equation), λ is a scalar value, S is the scatter matrix built from measurement:

$$S = Y^T Y \in \mathbb{R}^{M\times 1} \tag{5.16}$$

$$Y = \begin{bmatrix} (m_{1,x}^h)^2 & m_{1,x}^h m_{1,y}^h & (m_{1,y}^h)^2 & m_{1,x}^h & m_{1,y}^h & 1 \\ \vdots & \vdots & \vdots & \vdots & \vdots & \vdots \\ (m_{i,x}^h)^2 & m_{i,x}^h m_{i,y}^h & (m_{i,y}^h)^2 & m_{i,x}^h & m_{i,y}^h & 1 \\ \vdots & \vdots & \vdots & \vdots & \vdots & \vdots \\ (m_{M,x}^h)^2 & m_{M,x}^h m_{M,y}^h & (m_{M,y}^h)^2 & m_{M,x}^h & m_{M,y}^h & 1 \end{bmatrix}, \tag{5.17}$$

and K is the constraint matrix defined as follows:

$$K = \begin{bmatrix} 0 & 0 & 2 & 0 & 0 & 0 \\ 0 & -1 & 0 & 0 & 0 & 0 \\ 2 & 0 & 0 & 0 & 0 & 0 \\ 0 & 0 & 0 & 0 & 0 & 0 \\ 0 & 0 & 0 & 0 & 0 & 0 \\ 0 & 0 & 0 & 0 & 0 & 0 \end{bmatrix} \tag{5.18}$$

The resulting ellipse coefficients can be conveniently converted to center $[Cx \; Cy]$, radii $[Rx \; Ry]$ and tilt α of the ellipse (the latter indicating which axes the ellipse is scaled along) [Wolfram-MathWorld, 2014]; once these quantities are known, the points can be mapped on the circumference by using the following transformation:

$$\vec{m}_i^c = R_z(\alpha) \begin{bmatrix} r/Rx & 0 & 0 \\ 0 & r/Ry & 0 \\ 0 & 0 & 1 \end{bmatrix} R_z^T(\alpha) \left(\vec{m}_i^h - \begin{bmatrix} C_x \\ C_y \\ 0 \end{bmatrix} \right) \tag{5.19}$$

where $R_z(\alpha)$ denotes a rotation around the vertical axis of an angle α. The vertical offset on the vertical axis can be computed as the difference between the z coordinate of the points $\vec{m}_i^h$ and the component m_z^{NED}. By correcting the offset, the overall correction transformation is obtained through the steps in equations 5.11, 5.12 and 5.19. A scheme that summarizes the steps of the proposed calibration procedure is shown in figures 5.4 - 5.7.

Through the just explained procedure, the Soft and Hard Iron disturbances due to elements jointly moving with the vehicle are compensated. It is, on the contrary, intrinsically impossible to compensate the disturbances due to external bodies. Their presence is not uncommon, e.g. an important part of THESAURUS and ARROWS projects is dedicated to modern wrecks

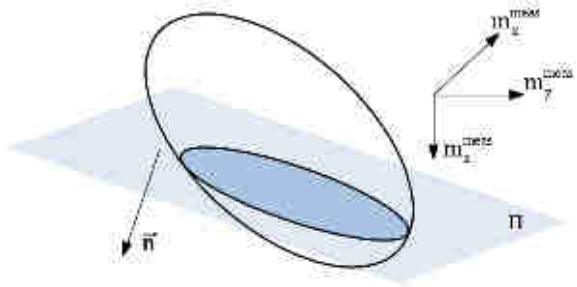

Figure 5.4: Minimal distance plane

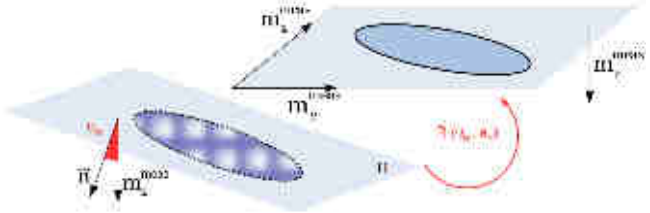

Figure 5.5: Alignment with the horizontal plane

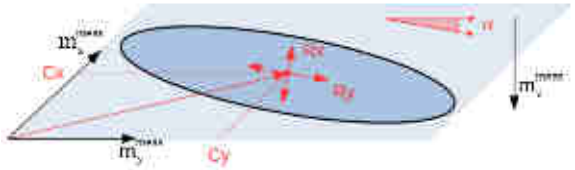

Figure 5.6: Ellipse fitting

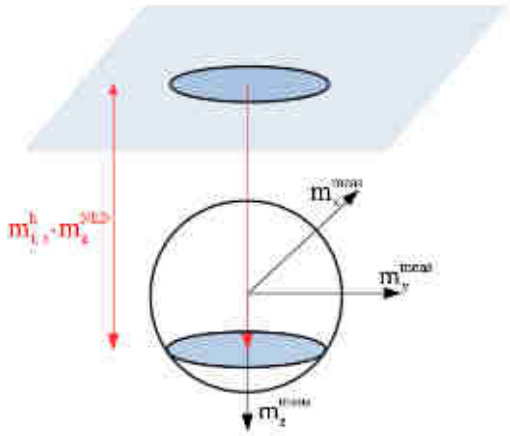

Figure 5.7: Vertical offset correction

completely made of metal that represent a unavoidable source of disturbance. The only possible countermeasure, when this situation is detected, is to avoid the use of magnetometers. The result of such a countermeasure is a rapid error drift due to the integration of the measurement noise of the MEMS gyroscope. In order to be reliable against these situations, the sensor set is integrated with a single-axis Fiber Optic Gyroscope (FOG), with its working axis aligned with the vehicle vertical direction (the yaw degree of freedom is, in fact, the one along which the magnetometer correction has its effects). The FOG is a very accurate and reliable instrument based on the Sagnac effect in the Sagnac interferometer. The noise affecting it is very low, thus through its use the risk of the unacceptable growth of the integration error, during the periods when the magnetometer is not considered, is avoided. However, the use of such a device has to be subject to a data processing before being considered within the NCF. In fact, the bandwidth

of a FOG is enough wide to include in its measures a contribution due to the Earth's angular velocity, thus producing a nonzero output of up to $15°$ per hour, even if it is stationary with respect to the earth-fixed frame. This effect can, however, be compensated exploiting the knowledge of the latitude at which the sensor is operating and the information about its roll and pitch angles. With reference to figure 5.8: it is assumed that the sensor is

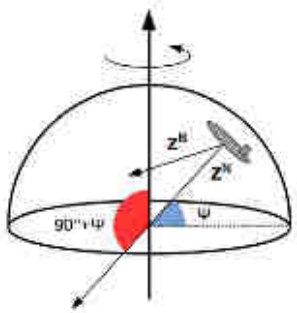

Figure 5.8: FOG correction term computation

operating in the northern hemisphere; however, the compensation procedure is conceptually the same on the whole planet surface. Let $\vec{\omega}_E$ denote Earth's angular velocity; its magnitude is then

$$\omega_E = ||\vec{\omega}_E|| \cong 7.2921 \cdot 10^{-5}\ rad/s \tag{5.20}$$

The latitude Ψ is supposed to be known. The compensation algorithm is composed of two steps: firstly, $\vec{\omega}_E$ is projected onto the local vertical axis; then, on the basis of roll and pitch values, the magnitude of the resulting vector is projected onto the body-fixed frame vertical axis and subtracted from the sensor output. The magnitude of Earth's angular velocity projected

onto the earth-fixed vertical axis is given by

$$\omega_E^{\perp} = \omega_E\ cos(\pi/2 + \Psi) \tag{5.21}$$

in order to determine the desired correction term, this quantity has to be multiplied by the result of the dot product $\left(\vec{z}^N\right)^T \vec{z}^B$, where $\vec{z}^N$ is the unit vector indicating the vertical axis of the earth-fixed frame expressed with respect to it ($\vec{z}^N = \begin{bmatrix} 0 & 0 & 1 \end{bmatrix}^T$) and $\vec{z}^B$ is the vertical axis of the body-fixed frame expressed with respect to the earth-fixed one. $\vec{z}^B$ can be computed by pre-multiplying $\vec{z}^N$ through the composition of the vehicle roll and pitch rotation matrices:

$$\vec{z}^B = (J_1(\varphi, \vartheta, \cdot))^T \vec{z}^N = (R_y(\vartheta) R_x(\varphi))^T \vec{z}^N \tag{5.22}$$

It is easy to verify that the result of the dot product $\left(\vec{z}^N\right)^T \vec{z}^B$ is

$$\left(\vec{z}^N\right)^T \vec{z}^B = J_1(\varphi, \vartheta, \cdot)(3,3) = cos(\varphi) cos(\vartheta) \tag{5.23}$$

In conclusion, the compensated FOG measurement is given by:

$$\omega_{FOG}^c = \omega_{FOG} - \omega_E^{\perp} cos(\phi) cos(\theta)\ , \tag{5.24}$$

where ω_{FOG} indicates the uncompensated reading.
After the correction has been applied, highly accurate measurements can be obtained: in the considered case study, mere integration over time of the compensated measurement while the device was held stationary showed an angle drift of about $2°$ per hour.

As concerns the accelerometers, during the calibration phase, when vehicle proper acceleration is maintained low, the mean of the acquired measures is stored as $\vec{a}_{mean}$ in order to exploit it during the estimation process to evaluate in real-time whether the current sensor outputs are reliable as vertical direction measurements or not.

Known Directions Choice

The NCF standing at the basis of the study proposed in this section relies on at least two directions known in the earth-fixed frame and measurable in the body-fixed frame. The most natural choice, considering the available sensors, is to use the local directions of the gravity acceleration and of the Earth magnetic field. These measures enter in the NCF (equations 2.13) in the correction equation $\omega_{mes} := \sum_{i=1}^{n} k_i v_i \times \hat{v}_i$, where the error between the estimated and the measured directions is evaluated through a sum of cross products.

The proposed choice of the directions implies the use with the gravity acceleration of the component of the local magnetic field that is orthogonal to it instead of the complete one. This is justified through the consideration that the accelerometer signal is more reliable with respect to the magnetometer one, mainly because the former is not affected by external error sources as the latter is. Thus, by using the complete magnetic field measurement, including its vertical component, if in absence of external magnetic disturbances it does not entail further benefits with respect to the information content due to the accelerometer; on the contrary, when the measure is affected by disturbances, errors would be introduced in the orientation correction process. According to this consideration, the magnetic field measurements before being considered in the filter are projected on the horizontal plane defined as the one orthogonal to the acceleration measure:

$$\vec{m}^c_{\perp} = \vec{m}^c - \left((\vec{a}^{\,meas})^T \vec{m}^c \right) \vec{a}^{\,meas} \tag{5.25}$$

with $\vec{m}^c$ complete magnetometer measures compensated through the procedure explained in section 5.1.2. $\vec{m}^c_{\perp}$ is a vector pointing towards the North on the horizontal plane, thus it is compared, within the NCF, with the

$\begin{bmatrix} 1 & 0 & 0 \end{bmatrix}^T$ earth-fixed frame direction, expressed with respect to the body-fixed frame.

Online Gain Scheduling

In the classic formulation of NCF, the gains k_i of the correction term are constant. In the considered case study, this holds true only during the initialization of the filter; then, they are eventually scaled (between zero and the initial value), in order to discard in real-time the unreliable measurements. The procedure is different for acceleration and magnetic field readings.

Acceleration gain The acceleration gain k_1 is defined as linearly decreased if high proper acceleration affects the measure of the gravity acceleration. During initialization of the filter, k_1 is set constant at its initial value determined through a preliminary tuning process; the average value $\vec{a}_{mean}$ of the magnitude of acceleration measurements is computed to be used as a reference term. Then, k_1 is scaled according to the relative difference between the norm of the acceleration measurement and the one of $\vec{a}_{mean}$, previously defined:

$$D_a = \left| \frac{||\vec{a}^{\,meas}|| - ||\vec{a}_{mean}||}{||\vec{a}_{mean}||} \right| \tag{5.26}$$

With reference to figure 5.9, a_{th} represents the threshold value which, if exceeded, causes the decrease of the gain until becoming null starting in correspondence of the maximum value a_{max}. Let k_1^{in} denote the initial (constant) gain; if $a_{th} \leq D_a \leq a_{max}$, $k_1(D_a)$ is set according to the following equation:

$$k_1(D_a) = k_1^{in} \left(-\frac{1}{a_{max} - a_{th}} D_a + \left(1 + \frac{a_{th}}{a_{max} - a_{th}} \right) \right) \tag{5.27}$$

for $D_a < a_{th} \rightarrow k_1 = k_1^{in}$ and for $D_a > a_{max} \rightarrow k_1 = 0$

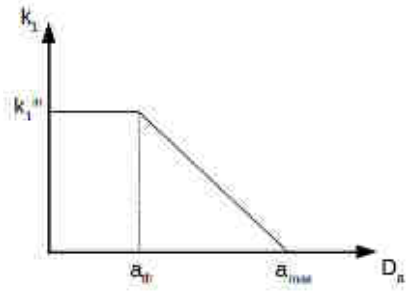

Figure 5.9: Computation of gain k_1.

Magnetic field gain For the magnetometer, a different strategy has been chosen, as it is likely that external disturbances modify the magnetic field direction not varying much its magnitude. In case this happens, the use of a scaling procedure similar to the one adopted for accelerometers would lead to the use wrong information for correction purposes. The idea at the basis of the adopted scaling procedure for magnetometers exploits the availability of the FOG measuring on the heading degree of freedom, the same on which the correction with magnetometers takes place. In particular, the likely assumption on which the strategy relies is that on the brief period the error that can be made because of FOG integration is lower than the one that may be generated by an external magnetic disturbance. Starting from this consideration, the quantity used for the scaling procedure is the angle between the estimated magnetometer direction and the measured one.

The gain k_2 associated to the magnetometer readings increases or decreases according to the value of the angle α^1_{check} between the projection of the corrected measurement onto the horizontal plane and the estimate of the earth-fixed x-axis expressed in the body-fixed frame through the current

estimated orientation:

$$\alpha^1_{check} = arccos\left((\vec{m}^c_\perp)^T \hat{\vec{x}}^N\right) \tag{5.28}$$

where $\hat{\vec{x}}^N = \hat{R}^T \begin{bmatrix} 0 \\ 0 \\ 1 \end{bmatrix}$ is the earth-fixed x-axis expressed in the body-fixed frame. Nevertheless, the experience demonstrated that the use of only α^1_{check} to verify the validity of the magnetometer readings has a drawback; if the magnetic disturbance approaches the sensor very slowly, in fact, the velocity of the drift of the sensor reading may be of the same order of magnitude of the filter dynamics. In this case, a slow but continuous change in the yaw angle is registered, with α^1_{check} remaining close to zero even if a disturbance is present. A second control angle α^2_{check} is, thus, introduced to overcome this problem. The choice of α^2_{check} is based on the following consideration: in a given geographical location the Earth's magnetic field can be considered constant; then, the angle between $\vec{m}^{NED}$ and the vertical direction $\vec{z}^N = [0\ 0\ 1]^T$ is constant. The same angle must be measured between the same vectors measured in the body frame. Hence, α^2_{check} is defined as the difference between the angle

$$\gamma^{meas} = arccos\left((\vec{a}^{\,meas})^T \vec{m}^c\right) \tag{5.29}$$

obtained at each iteration from the dot product of the measured acceleration and the corrected magnetic field and the corresponding expected value

$$\gamma^{NED} = arccos\left((\vec{z}^N)^T \vec{m}^{NED}\right) \tag{5.30}$$

The magnitude of this new defined checking angle is independent from the speed at which a magnetic disturbance is applied

$$\alpha^2_{check} := \left\|\gamma^{meas} - \gamma^{NED}\right\| \quad with \quad 0 \le \alpha^2_{check} \le \pi \tag{5.31}$$

Two threshold values α^1_{th} and α^2_{th} are set; if either one is reached, k_2 is forced to zero in a finite number of iterations. If both angles fall below the threshold values, k_2 is increased back to the initial value. The decrease is much faster than the increase.

Let k^u and k^d denote increase and decrease counters, and let k^u_{max} and k^d_{max} be the number of iterations allowed for the variation of the gain k_2. If k^{in}_2 is the initial value for k_2, then Algorithm 1 illustrates how the magnetometer gain is computed:

Data: k^{in}_2, k^u_{max}, k^d_{max}
Result: gain k_2
if $\alpha^1_{check} > \alpha^1_{th}$ *or* $\alpha^2_{check} > \alpha^2_{th}$ **then**
  $k_2 = k^{in}_2 \left(1 - k^d / k^d_{max}\right)$;
  $k_2 \geq 0$;
  $k^d + +$;
  $k^u = 0$;
else
  $k_2 = k_2 + \left(k^{in}_2 - k_2\right)\left(k^u / k^u_{max}\right)$;
  $k_2 \leq k^{in}_2$;
  $k^u + +$;
  $k^d = 0$;
end

Algorithm 1: k_2 computation.

It is possible for both angles to become greater than the threshold values even if no magnetic disturbances are present; this can occur if large accelerations arise (not likely to happen in the field of underwater robotics) or during motion transients. However, the effect is only temporary and α^1_{check}, α^2_{check} fall again below the threshold in a short amount of time. This solution

may appear quite conservative; nonetheless, if a precise gyroscope is available, it is indeed better to discard good magnetometer readings than running the risk of including corrupted magnetic measurements, thus compromising the accuracy of the yaw estimate. It is worth to note that the proposed weighting strategy, exploiting the defined quantity α^2_{check}, is strongly based on the calibration procedure described in the beginning of this section. In facts its combination with the classical planar calibration procedures (see [VectorNav-Technologies, 2014]) would not work properly as, in this case, the vertical component of the measured magnetic field remains uncalibrated and, as consequence, the angle between measured acceleration and magnetic field is, generally, variable.

In conclusion, in the considered case study ω_{mes} (it is a three dimensional vector, according to the simplified notation introduced in section 2.5.2) has the following explicit expression:

$$\omega_{mes} = k_1 \cdot \left(\vec{a}^{\,meas} \times \hat{R} \begin{bmatrix} 0 \\ 0 \\ 1 \end{bmatrix} \right) + k_2 \cdot \left(\vec{m}^{\,c}_{\perp} \times \hat{R} \begin{bmatrix} 1 \\ 0 \\ 0 \end{bmatrix} \right) \tag{5.32}$$

Experimental results are reported in section 6.4.

Chapter 6

Results

6.1 Involved Vehicles

This first section of the result chapter is dedicated to a brief description of the vehicles involved in the tests described in the following and of the available equipment. The three vehicles mainly used are the Typhoon class TifOne AUV, outcome of the THESAURUS project along with TifTu of the same class but with different equipment (section 6.1.1). The other one is FeelHippo AUV developed within the participation of the University of Florence to the SAUC-E 2013 competition (section 6.1.2).

6.1.1 Typhoon

Typhoon is a middle-sized class AUV, whose features are comparable with other existing AUVs. Considering the vehicle size (length of about 3600 mm, external diameter of about 350 mm, weight of 130-180 kg according to the carried payload) and the achievable performance (reachable depth of about 300 m, at least 8 h of autonomy and a maximum speed of 5-6 kn), the vehicle can be considered an intermediate one compared to the smaller Remus

100 [Packard et al., 2013] and the bigger Remus 600 [Stokey et al., 2005]. Currently, two versions of the Typhoon AUV have been built, characterized by different sensors and payloads. The vehicles are named TifOne and TifTu respectively. In figures 6.1 and 6.2, both the Typhoon CAD design and its final built version (TifOne) can be seen.

Figure 6.1: The Typhoon CAD design

Figure 6.2: The Typhoon final built version - TifOne

The Typhoon AUV has five actively controlled degrees of freedom (DOF) (longitudinal, lateral and vertical translations, yaw and pitch rotations), thanks to four thrusters (two working in lateral direction and two in vertical direction) and two main rear propellers (both working in longitudinal direction). The correct positioning and alignment of the buoyancy and the gravity centres ensure vehicle stability against roll motion.

The system was designed by dividing the on board subsystems in two main categories:

- *vital systems*: all the navigation, communication and safety related components and functions of the vehicle are controlled by an industrial PC-104, called Vital PC;
- *payloads*: all the additional sensors and functions related to variable payloads are managed by one or multiple Data PCs.

The sensor set, useful for navigation purposes, available for Typhoon class vehicles includes:

- **Inertial Measurement Unit (IMU) Xsens MTi -** device including a 3D gyroscope, 3D accelerometer and 3D magnetometer measuring dynamic data at a maximum working frequency of 100 Hz (figure 6.3);

Figure 6.3: Xsens IMU - Datasheet

- **Fiber Optics Gyroscope (FOG) KVH DSP 1750 -** Digital single axis accurate gyroscope based on the Sagnac effect in a Sagnac interferometer, it is used to measure the vehicle angular speed around its

vertical axis in order to obtain a reliable estimation of the yaw angle even in presence of magnetic disturbances (figure 6.4);

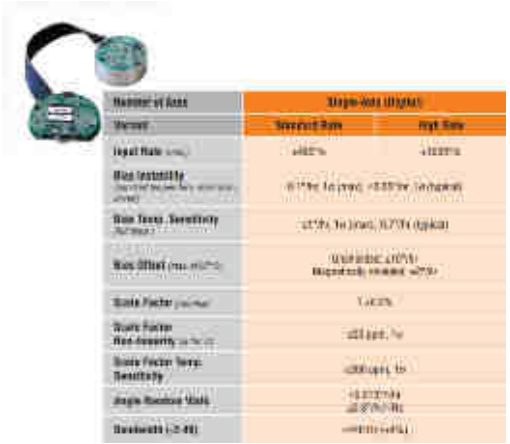

Figure 6.4: KVH DSP 1750 FOG - Datasheet

- **Doppler Velocity Log (DVL) Teledyne Explorer -** sensor measuring the linear body-fixed speed of the vehicle, with respect to the seabed or with respect to the water column beneath the vehicle. Moreover, if it detects the seabed it is also able to measure the distance from it, like an altimeter (figure 6.5);
- **STS DTM depth sensor -** digital pressure sensor used to derive the vehicle depth (figure 6.6);
- **Evologics S2CR** 18/34 **USBL -** ultra short baseline acoustic localization system compatible with Typhoon vehicle class acoustic modems used for communication and cooperation purposes. TifTu houses on

Figure 6.5: Teledyne Explorer DVL - Datasheet

Figure 6.6: STS DTM Depth sensor - Datasheet

board the USBL transducer capable of localizing other vehicles, TifOne houses a modem capable of being localized (figure 6.7);

- **PC-104 GPS Module COM-1289 -** GPS receiver integrated as a module of the on board PC-104 - Vital Computer (figure 6.8).

Table 6.1 summarizes the navigation sensor set available on each of the two existing Typhoon class AUVs.

Figure 6.7: Evologics S2CR 18/34 USBL - Datasheet

Figure 6.8: PC-104 GPS Module COM-1289 - Datasheet

6.1.2 FeelHippo

FeelHippo AUV is a small low-cost AUV developed by the University of Florence student team that participated in the SAUC-E 2013 competition.

Sensor	TifOne	TifTu
Xsens IMU	✓	✓
KVH FOG	✓	×
Teledyne DVL	✓	×
STS DTM	✓	✓
Evologics USBL	Localizable Modem	Localizing Transducer
PC-104 GPS	✓	✓

Table 6.1: Sensors sets for TifOne and TifTu

Its design is oriented to face the tasks proposed by the competition rules, but being easily integrable with potential further features that may be necessary in the future.

Mechanical characteristics FeelHippo central body (figure 6.9) is a plexiglass pipe that contains the instrumental hardware, except for the batteries that are located inside the two Al pipes under the main body. Other parts, e.g. the propellers, the depth sensor and the LED lights, are connected to the main structure by specific plastic (ABS) supports obtained with the 3D printer for rapid prototyping of the MDM Lab. The motion of FeelHippo AUV is under-actuated but sufficient for the classical monitoring tasks and it is given by 4 propellers [Carlton, 2007a] (controlling 4 DOFs of the vehicle):

- two of these are mounted in a V-shape, to control the depth and the lateral movement;
- the other two are horizontal, placed at the two sides of the vehicle, to control the longitudinal motion and the yaw angle.

As concerns the other devices, in the front part of the vehicle there are an echo-sounder sensor and 3 LEDs able to illuminate the water; this solution allows the front camera to get good pictures. In the rear part of the vehicle

Figure 6.9: Feelhippo vehicle in the MDM Lab pool

there are, instead, the depth sensor, a strobe light and another LED light, that illuminates the seabed so that the other camera pointing down can work well. Next to the strobe light there is the transducer of an acoustic modem. Inside the plexiglass pipe the instruments are placed on two plexiglass plates. On the top plate there are: the inertial platform Xsens IMU, a LCD display, a Micro Maestro electronic board for motor control and the computing units. On the bottom plate there are, instead: the acoustic modem board, a DC-DC converter (24V-12V), the motor drivers and the bottom-looking camera. The 4 LiPo batteries are placed inside the Al pipes to obtain a low center of gravity and to facilitate their extraction for charging. The structure of the AUV guarantees:

- ease of assembly;
- ease of access to the internal instruments;
- safe solution thanks to the 24V supply;
- high stability to roll;

- low weight (about 30 kg);
- low cost solution.

Electronics architecture The vehicle is equipped with four 22.2 V LiPo batteries. Each battery can deliver 8 Ah for a total on board energy of about 710 Wh. All the on board modules are supplied by this voltage bus, directly or after a suitable DC-DC converter. The present voltage levels are two, the main one at 24 V and the derived one at 12 V. More than one PC are on board each one dedicated to particular tasks and interfaced from an hardware point of view through Ethernet connection, whereas, through ROS middleware from the software one. The AUV has 4 electric brushless Maxon motors. The chosen model is a sensorless brushless motor capable of 100 W. Despite its small dimensions and low weight this motor provides quite a high torque, also through the associated planetary gearhead (reduction $3.8 : 1$).

6.2 Localization

6.2.1 Cooperative Localization

The validation of the proposed method (section 4.1) has been carried out through simulations performed in Matlab-Simulink^{TM}; a complete model of Typhoon vehicle has been implemented according to the theory described in chapters 2 and 3 and to the vehicle characteristics in section 6.1.

Simulation description

Four vehicles operate on the simulation scenario: three AUVs and a surface support ship (THESAURUS project configuration - section 1.1). The trajectories, chosen for the simulations, imply that vehicle 0, the surface one,

remains stationary, whereas the three AUVs follow the paths shown in figure 6.10. They dive with three different pitch angles and cover an area of 100 m^2 at different depths (AUV_1 at 15 m, AUV_2 at 25 m and AUV_3 at 30 m) with a cruising speed of about 2 kn (≈ 1 m/s).

In order to evaluate the functioning just of the proposed localization strategy, decoupled from the performance of other system modules, the vehicles motion is imposed in open-loop, i.e. the control system is not fed with the output of the navigation filter but it is based on the real followed trajectory obtained as real-time output of the simulation. The used control system is the Multivariable PID proposed in [Fossen, 1994] adapted to an AUV with only 5 DOF actuated as Typhoon AUVs are. The proposed localization algorithm has been tested using the real-time output of the simulated sensors calculated on the followed trajectory. This way, simulations can be used to evaluate the performance of only the localization module, not being part of the control loop. Following the chosen paths, the AUVs do not travel in formation in the sense that the mutual distances and orientation are not constant, so that the performance of the algorithm, which is of geometric type, cannot be affected by it.

Results

Statistical simulations, based on Monte Carlo method, have been realized. Graphs in figure 6.11 represent the evolution of RMS estimate error of position for the three AUVs as to the time, based on a sample of 100 simulations. The first subgraph is about AUV_1: its performance is better than the other two vehicles. This is due to the fact that the DVL, that ensures very small values of the estimation error drift, is present only on it. The performance for the other two vehicles is worse, but the estimation error has not the beha-

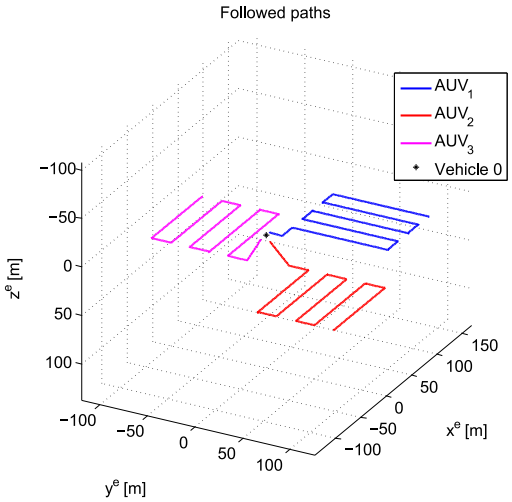

Figure 6.10: Followed paths

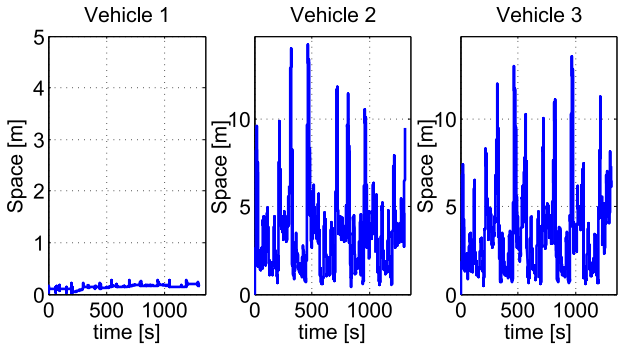

Figure 6.11: Time evolution of RMS estimate error

viour of the unlimited drift which is typical of INS algorithms. Specifically, the estimation error, during more than 20 minutes required to complete the path (the simulations have a duration of about 1300 s), never exceeds the value of 15 m. This error occurs only in correspondence of the curves, when the vehicle has to slow down; the low rate at which new distance measurements are obtained on the vehicles causes a deterioration of their estimates. The graphs highlight one of the strengths of the algorithm, i.e. they show that the method used to estimate the system position is able to recover the accumulated estimation error through a periodic reset.

The AUV localization through dead reckoning based only on inertial sensors would bring to an unlimited drift dependent on the sensors characteristics, according to [VectorNav-Technologies, 2014]. In figure 6.12, the time evolution of the position estimation error for AUV_1 and AUV_2 is overlapped to a band (in red) that represents the error that would be present in case of no reset according to [VectorNav-Technologies, 2014]. In first seconds of simulation the error is higher than the one that would be expected without periodic reset. The reason is that the red line is built taking into account only the error due to the accelerometer bias; in simulations, instead, several non-idealities have been considered as explained in Section 4.1.1. This confirms the robustness of the proposed method. Moreover, it is worth to note that the proposed method does not suffer from the increase of measure error with distance, which is a typical issue of the USBL systems. The usual configuration of these systems is composed of a surface vehicle, equipped with the USBL head, able to measure the relative position of the various AUVs (using the signals coming from the on board acoustic modems).

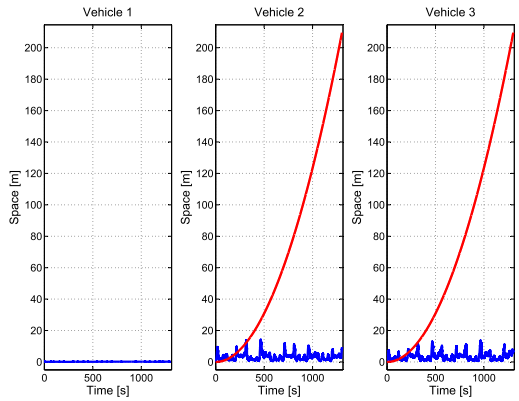

Figure 6.12: Time evolution of RMS estimate error compared to typical error achieved without a position reset

6.2.2 Known Structured Environments

This section describes the validation process for the localization algorithm based on the knowledge of the structures usually present in the working environments (and well known) when UUVs are used for patrolling missions. The presented validation tests have been performed during the SAUC-E 2013 competition, and confirm that FeelHippo, although equipped with a very inexpensive set of sensors, has the potentiality to work autonomously, taking advantages of the information about the surrounding environment. In particular, the ability of the described ALS (section 4.2) to correctly map the basin is demonstrated. The basin is the SAUC-E competition field, located at the NATO Centre for Maritime Research and Experimentation (CMRE). The jury, to evaluate the tasks, uses a very accurate multi-beam system to track the vehicles inside the basin, that has been exploited also as comparison

means to evaluate the potentialities of the proposed system.

In figure 6.13, the comparison between FeelHippo ALS and the acoustic image generated through the jury multi-beam echosounder is shown. Figure 6.13a shows the acoustic image obtained by the echo sounder data acquired by FeelHippo in the competition field. White pixels on the image are the points considered, by the localization algorithm, to belong to an edge of the basin. The center of the red circle represents the current estimated position, whereas the red triangle represents the current field of "view" of the echo sounder. Figure 6.13b shows instead a contemporary acoustic image of the competition field acquired by the CMRE multi-beam sensor for vehicle tracking. The white shadow in the red square is FeelHippo, whereas the other visible big white shadow is a submerged structure devoted to other competition tasks. The results are very encouraging as with the inexpensive proposed system, the mapping of the basin is quite accurate as confirmed by the image overlapping. The "visible" structures are rightly identified. It is also worth to note that the localization algorithm is able to correctly identify the AUV position compared to the surrounding environment. The center of the red circle and the red square are almost coincident.

6.3 Position Estimation

In this part, the navigation system described in section 5.1 will be validated offline for both EKF-based and UKF-based implementations throughout experimental data. Two different missions are here considered for the navigation system validation:

- Final demonstration of the THESAURUS project (Livorno - Italy, August 2013);

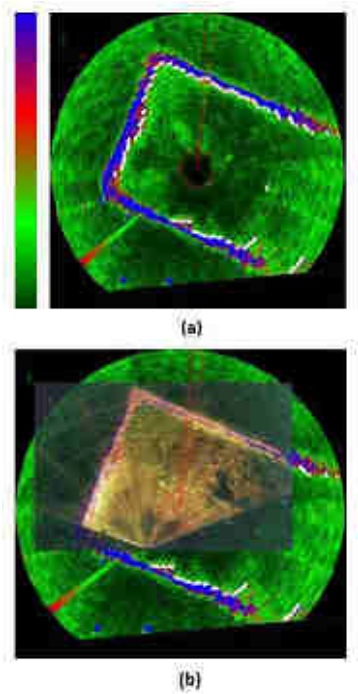

Figure 6.13: Mapping of the CMRE basin: comparison between FeelHippo localization system and NATO one

- CommsNet13 research cruise on board on the NATO Research Vessel (NRV) Alliance (La Spezia - Italy, September 2013).

6.3.1 THESAURUS final demonstration

The experimental data were collected during suitable sea tests performed in Livorno (Italy) in August 2013. Such tests have been carried out in cooperation with *Vigili del Fuoco di Livorno* and *Nucleo Operativo Subacqueo della Soprintendenza Archeologica della Toscana*. Throughout the experiments, the Typhoon AUV TifOne was operated in ROV mode equipped with an IMU, a pressure sensor for the depth, a DVL and a GPS for a total of two missions:

1. WATER SURFACE MISSION: the AUV is guided on the water surface for a total of 1299 s covering a distance of 1012 m. The collected GPS fixes will be used only for initializing the filter and as a benchmark for comparing the two different navigation system implementations. The aim of the mission is to understand the *position drift error* generated during the filtering process. The drift error is due to the fact that the available measurements provided by the exploited sensors (IMU, pressure sensor for the depth and DVL) do not directly provide the position of the AUV.

2. UNDERWATER MISSION: the AUV is guided underwater at a depth of 2 m for a total of 2540 s. The only available GPS fixes are the starting and ending point of the AUV path that are collected since both points are on the water surface. The starting point will be used to initialize the filters, while the ending point will be used to compare the estimation error of the arrival. The aim of the mission is twofold: 1) understand whether or not the filters are capable of reconstructing the shape of the trajectory given by the pilot; 2) understand which filter provides the estimated ending point closest to the

GPS fix and, consequently, the smallest drift error.

Water surface mission In this subsection, the EKF-based and the UKF-based navigation systems will be compared during a water surface mission.

Figure 6.14 shows the estimated Cartesian position coordinates η_{1x}, η_{1y} provided by both navigation system implementations. The GPS measurements η_{1x}^{meas}, η_{1y}^{meas} are also provided for the sake of comparison.

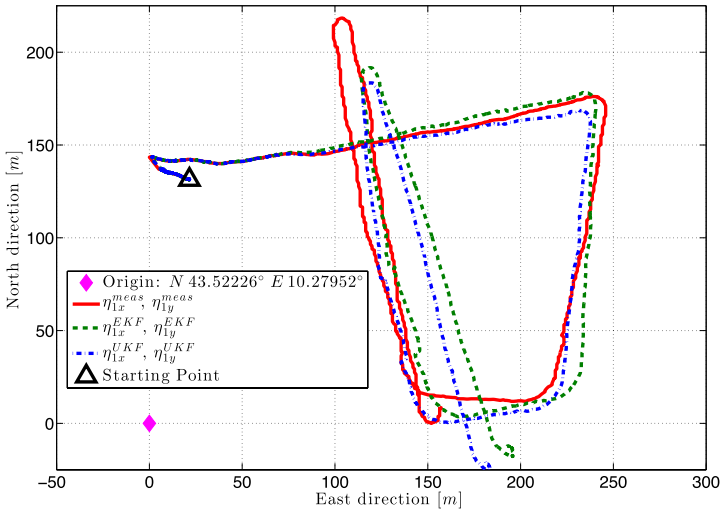

Figure 6.14: AUV trajectory estimated by the classical EKF-based and UKF-based navigation system along with the GPS fixes.

Figure 6.15 respectively shows the EKF and UKF position estimation errors $\|\vec{\eta}_1^{EKF} - \vec{\eta}_1^{meas}\|$ and $\|\vec{\eta}_1^{UKF} - \vec{\eta}_1^{meas}\|$ with respect to the time and to the travelled distance.

The results highlight quite similar performance for both filters, however the error of the UKF presents a flat behaviour in the final part, i.e. starting

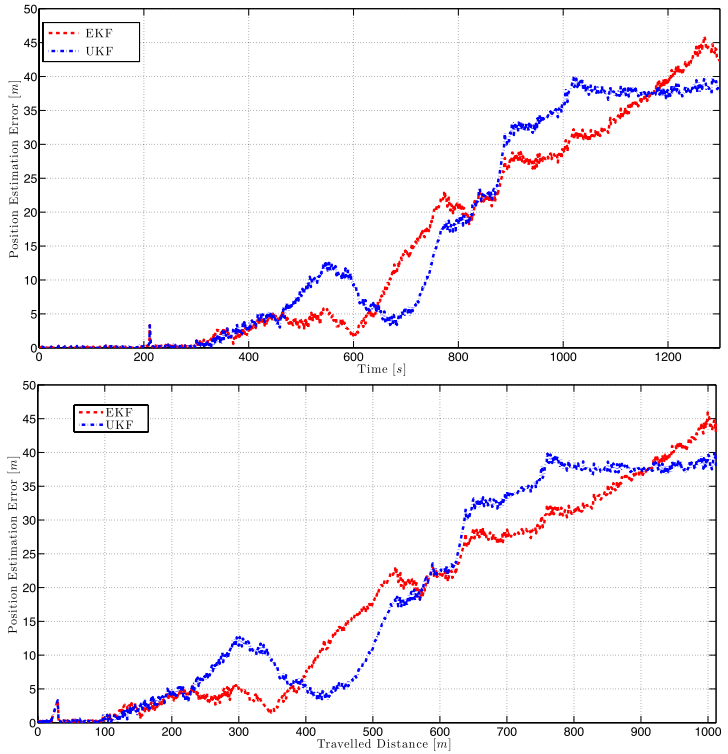

Figure 6.15: Position estimation error as a function of time (up) and of the travelled distance (down).

from time 1000 s (or after having travelled for about 750 m), while the EKF error keeps growing. It is also worth noticing that the shape of the estimated trajectories looks like the one provided by the GPS and that major errors occur when the AUV is turning.

For the sake of completeness the measured and filtered translational velocities $\vec{\nu}_1^{meas}$, $\vec{\nu}_1^{EKF}$, $\vec{\nu}_1^{UKF}$, the vehicle orientations $\vec{\eta}_2^{meas}$, $\vec{\eta}_2^{EKF}$, $\vec{\eta}_2^{UKF}$ and the depths η_{1z}^{meas}, η_{1z}^{EKF}, η_{1z}^{UKF} are reported in figures 6.16-6.21.

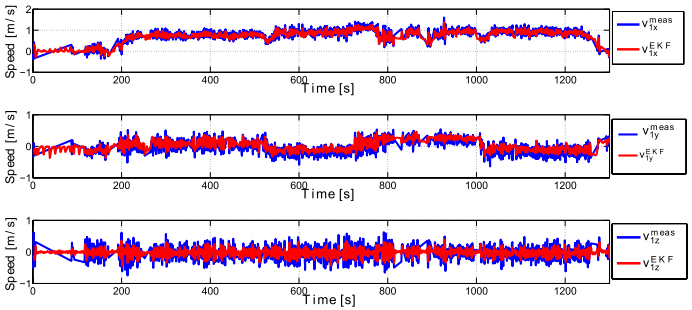

Figure 6.16: Comparison between $\vec{\nu}_1^{meas}$ and $\vec{\nu}_1^{EKF}$

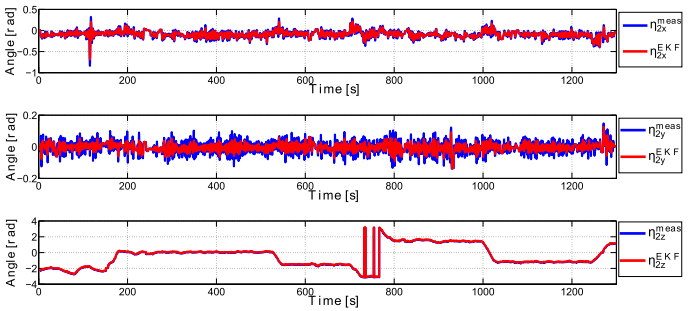

Figure 6.17: Comparison between $\vec{\eta}_2^{meas}$ and $\vec{\eta}_2^{EKF}$

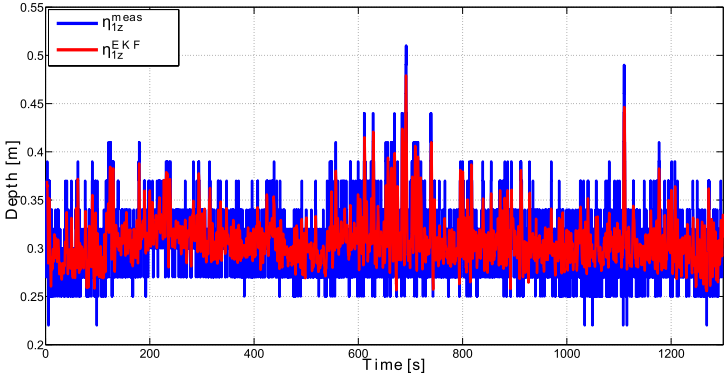

Figure 6.18: Comparison between η_{1z}^{meas} and η_{1z}^{EKF}

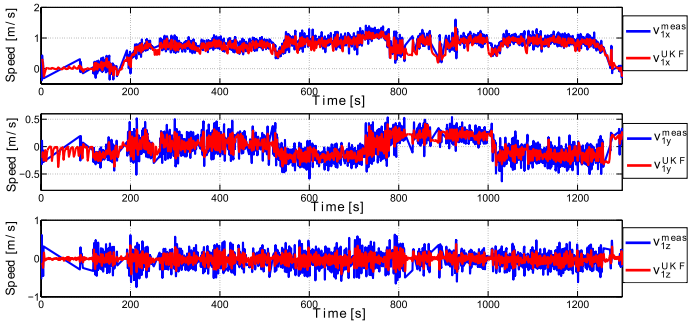

Figure 6.19: Comparison between $\vec{\nu}_1^{meas}$ and $\vec{\nu}_1^{UKF}$

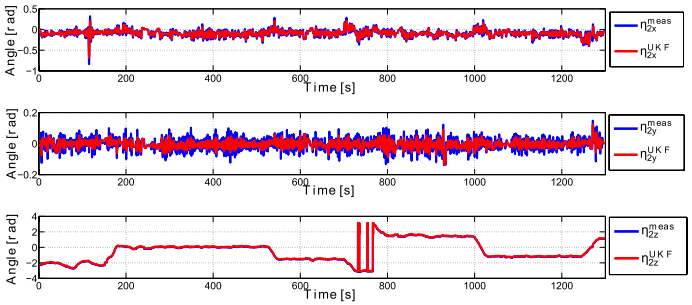

Figure 6.20: Comparison between $\vec{\eta}_2^{meas}$ and $\vec{\eta}_2^{UKF}$

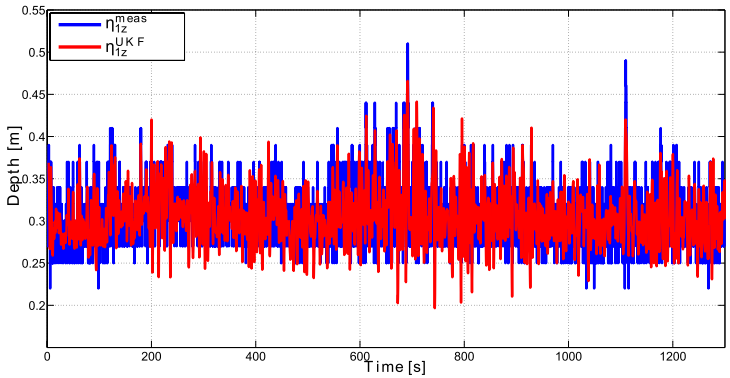

Figure 6.21: Comparison between η_{1z}^{meas} and η_{1z}^{UKF}

Underwater mission In this subsection, the EKF-based and UKF-based navigation systems will be compared during an underwater mission.

Figure 6.22 illustrates the estimated trajectories provided by both EKF and UKF, along with the GPS fix representing the ending point. It is worth pointing out that the trajectory given by the pilot to the AUV involves quite a lot of turning points which, as noticed during the water surface mission described in the previous subsection, are the main sources of error.

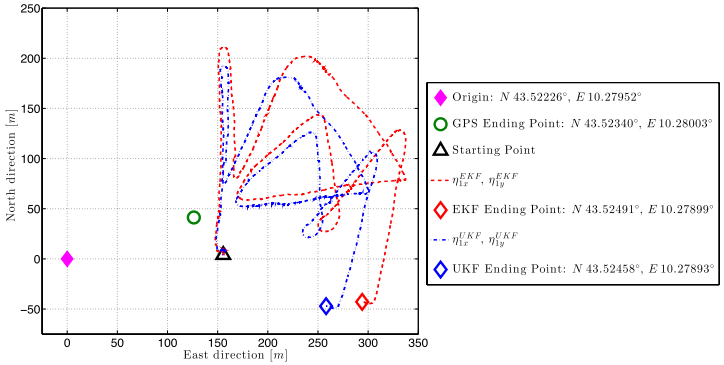

Figure 6.22: AUV trajectory estimated by the classical EKF-based and UKF-based navigation system

Table 6.2 summarizes the ending point estimation errors $\left\|\vec{\eta}_1^{EKF} - \vec{\eta}_1^{meas}\right\|$ and $\left\|\vec{\eta}_1^{UKF} - \vec{\eta}_1^{meas}\right\|$, the estimated covered distances and the error *Growing Rates* (GR) with respect to the duration of the mission and with respect to the estimated covered distance.

The classical EKF-based navigation system shows poorer performance compared to the UKF-based navigation system in terms of ending point estimation error and for both GRs. Therefore, the employment of UKF filter turns out to be quite promising to provide a better accuracy during complex

Table 6.2: Performance summary for both classical EKF-based and UKF-based navigation system.

	Ending point error	Estimated covered distance	GR over time	Distance GR
EKF	187.7 $[m]$	2065 $[m]$	0.074 $[m/s]$	9.1%
UKF	158.7 $[m]$	1953 $[m]$	0.062 $[m/s]$	8.1%

navigation and cooperation tasks and a good trade-off between performance and computational load/implementation complexity.

For the sake of completeness, also the measured and filtered translational velocities $\vec{\nu}_1^{meas}$, $\vec{\nu}_1^{EKF}$, $\vec{\nu}_1^{UKF}$, the vehicle orientations $\vec{\eta}_2^{meas}$, $\vec{\eta}_2^{EKF}$, $\vec{\eta}_2^{UKF}$ and the depths η_{1z}^{meas}, η_{1z}^{EKF}, η_{1z}^{UKF} are reported in figures 6.23-6.28.

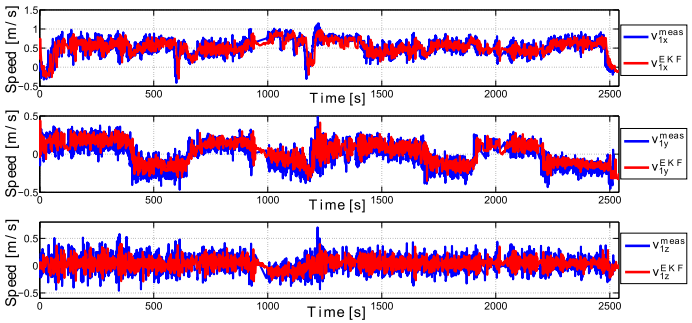

Figure 6.23: Comparison between $\vec{\nu}_1^{meas}$ and $\vec{\nu}_1^{EKF}$

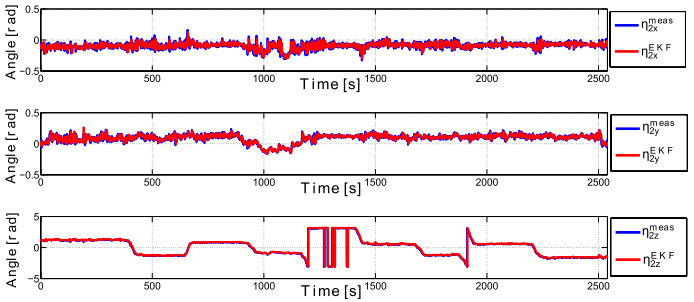

Figure 6.24: Comparison between $\vec{\eta}_2^{meas}$ and $\vec{\eta}_2^{EKF}$

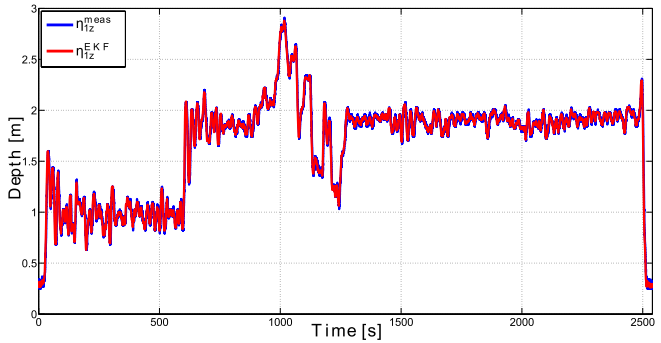

Figure 6.25: Comparison between η_{1z}^{meas} and η_{1z}^{EKF}

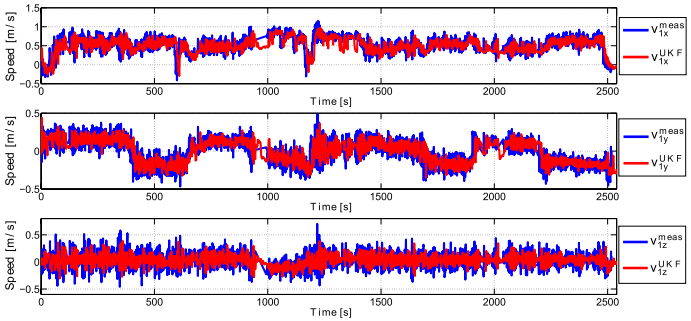

Figure 6.26: Comparison between $\vec{\nu}_1^{meas}$ and $\vec{\nu}_1^{UKF}$

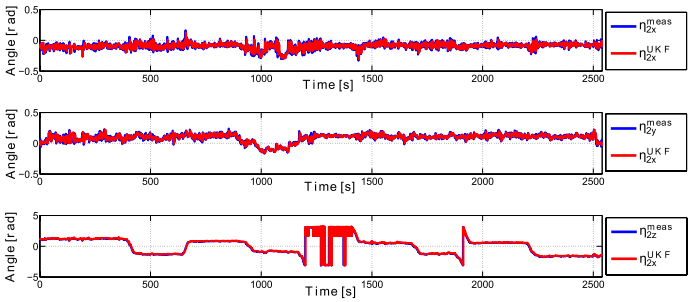

Figure 6.27: Comparison between $\vec{\eta}_2^{meas}$ and $\vec{\eta}_2^{UKF}$

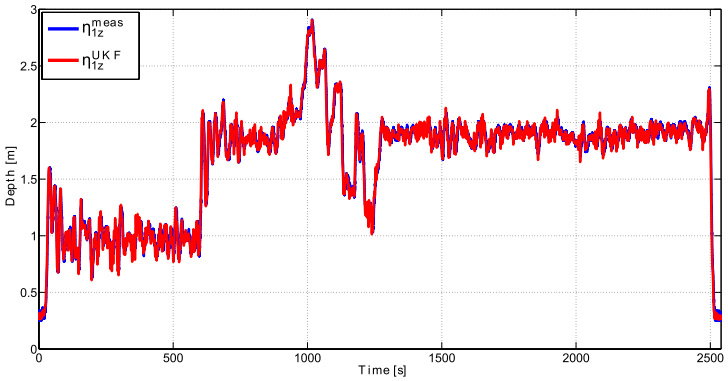

Figure 6.28: Comparison between η_{1z}^{meas} and η_{1z}^{UKF}

6.3.2 CommsNet13

The CommsNet13 experiment took place in September 2013 in the La Spezia Gulf, North Tyrrhenian Sea, with the support of NATO Research Vessel (NRV) Alliance. The experiment was scientifically led by the NATO S&T Org. Ctr. for Maritime Research and Experimentation (CMRE, formerly NURC) and included, among its objectives, the testing of several acoustic communication and localization systems using underwater networks. In fact, in the area, the CMRE has a permanent testbed for underwater networking and communication purposes (LOON - Littoral Ocean Observatory Network). During CommsNet13, the LOON installation consisted of 4 EvoLogics modems, placed on the seabed and cable-connected to the shore (they could be continuously operated and monitored). LOON has been exploited to evaluate the on board USBL systems of the AUVs. The Typhoon class TifTu took part to the experimentation at sea. TifTu was equipped with an EvoLogics acoustic modem/USBL head and navigated within the fixed nodes

Figure 6.29: Layout of the autonomous mission: triangle-shaped path with vertices placed in the waypoints Janus1, M2 and Typhoon1

acoustic network deployed by the CMRE. The LOON modems are compatible with those installed on board the Typhoon, so that the vehicle could use its USBL modem to estimate its relative position with respect to the fixed LOON installation: this allows the comparison between the proposed navigation system and acoustic self-localization as ground truth. Throughout the experiments, TifTu autonomously travelled in dead reckoning and was equipped with the IMU, the pressure sensor for the depth, the GPS sensor (used during the periodic and dedicated resurfacings: one every 2.5 minutes) and the USBL unit (used only as ground truth). TifTu travelled along a triangle-shaped path on the LOON area. The reference path for the underwater mission was defined by three waypoints respectively called Janus1, M2 (position of the second one of the four LOON modems) and Typhoon1. The length of the path side was about 190 m and the mission was performed at the depth of about 4.5 m (see figure 6.29). The TifTu AUV navigated underwater for a total of 1150 s at a speed of 0.6 m/s.

The aim of the mission is twofold: 1) understand whether or not the filters are capable of reconstructing the shape of the desired trajectory during

a navigation task; 2) to understand the *position drift error* generated during the filtering process (using the USBL as reference to evaluate the filter accuracy). The drift error is due to the fact that the available measurements provided by the exploited sensors (IMU, pressure sensor for the depth and GPS only during the resurfacings) do not directly provide the position of the AUV.

The mission In this paragraph, the mission scenario carachterizing the comparison test between the EKF-based and the UKF-based navigation systems will be compared during an underwater mission is described. Figure 6.30 and figure 6.31 show the estimated Cartesian position coordinates η_{1x}^{EKF}, η_{1y}^{EKF} and η_{1x}^{UKF}, η_{1y}^{UKF} provided by both navigation system implementations. The GPS fixes η_{1x}^{GPS}, η_{1y}^{GPS} (during the resurfacings) and the USBL fixes η_{1x}^{USBL}, η_{1y}^{USBL} are also provided for the sake of comparison.

Table 6.3 summarizes the USBL fixes η_{1x}^{USBL}, η_{1y}^{USBL} (used as reference), the estimation error $\left\|\vec{\eta}_1^{EKF} - \vec{\eta}_1^{USBL}\right\|$ affecting $\vec{\eta}_1^{EKF}$ and the estimation error $\left\|\vec{\eta}_1^{UKF} - \vec{\eta}_1^{USBL}\right\|$ affecting $\vec{\eta}_1^{UKF}$.

The classical EKF-based navigation system, representing the standard for the underwater navigation, shows poorer performance compared to the UKF-based one during the whole underwater mission. Therefore, the use of the UKF filter turns out to be quite promising to provide a better accuracy during complex navigation and cooperation tasks and a good trade-off between performance and computational load. For the sake of completeness the measured and filtered vehicle orientations $\vec{\eta}_2^{meas}$, $\vec{\eta}_2^{EKF}$, $\vec{\eta}_2^{UKF}$ and depths η_{1z}^{meas}, η_{1z}^{EKF}, η_{1z}^{UKF} are reported in figures 6.32-6.35: these figures show a good matching with the filtered quantities. The disturbances and noise affecting the behaviour of vehicle orientations and depths are not due

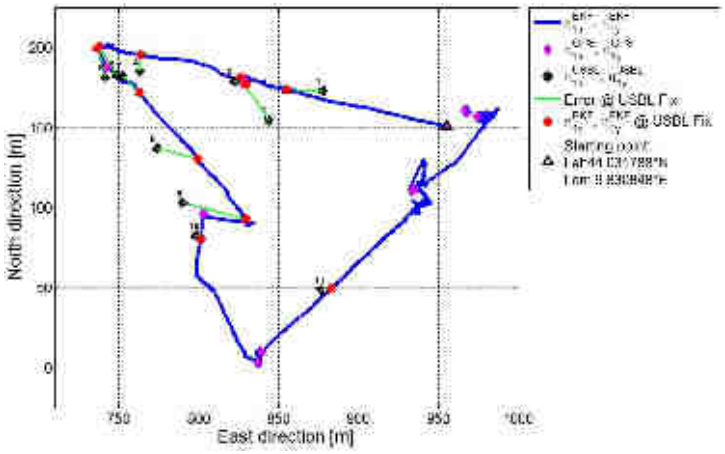

Figure 6.30: AUV trajectory estimated by the classical EKF-based navigation system along with the GPS and USBL fixes (the origin coordinates are: $44.03042984^{o}N$, $9.81893253^{o}E$).

Table 6.3: USBL fixes (η_{1x}^{USBL}, η_{1y}^{USBL}) and errors affecting $\vec{\eta}_1^{EKF}$ and $\vec{\eta}_1^{UKF}$ with respect to the USBL fixes.

Fix	η_{1x}^{USBL}	η_{1y}^{USBL}	Error on $\vec{\eta}_1^{EKF}$ (m)	Error on $\vec{\eta}_1^{UKF}$ (m)
USBL fix $N^{o}1$	44.031985 ^{o}N	9.829877 ^{o}E	22.3	11.1
USBL fix $N^{o}2$	44.031820 ^{o}N	9.829461 ^{o}E	32.4	17.0
USBL fix $N^{o}3$	44.032042 ^{o}N	9.829189 ^{o}E	7.8	7.7
USBL fix $N^{o}4$	44.032093 ^{o}N	9.828454 ^{o}E	10.4	13.6
USBL fix $N^{o}5$	44.032076 ^{o}N	9.828269 ^{o}E	20.7	17.3
USBL fix $N^{o}6$	44.032063 ^{o}N	9.828184 ^{o}E	18.9	20.8
USBL fix $N^{o}7$	44.032069 ^{o}N	9.828319 ^{o}E	14.8	10.6
USBL fix $N^{o}8$	44.031664 ^{o}N	9.828586 ^{o}E	26.4	12.4
USBL fix $N^{o}9$	44.031357 ^{o}N	9.828791 ^{o}E	40.3	18.1
USBL fix $N^{o}10$	44.031175 ^{o}N	9.828890 ^{o}E	4.0	3.8
USBL fix $N^{o}11$	44.030865 ^{o}N	9.829867 ^{o}E	6.6	4.0

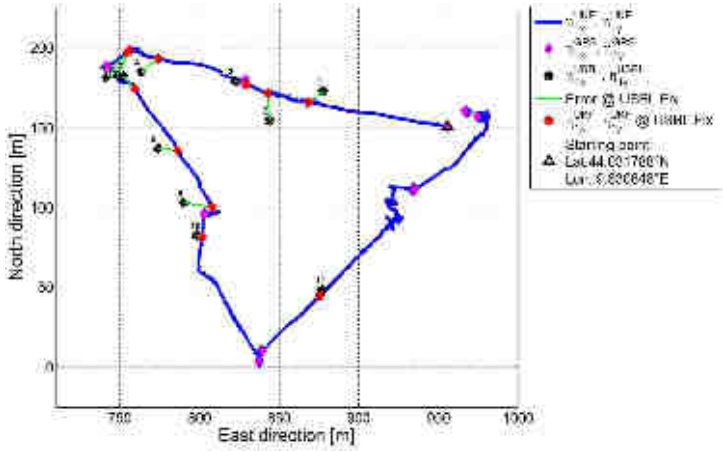

Figure 6.31: AUV trajectory estimated by the UKF-based navigation system along with the GPS and USBL fixes (the origin coordinates are: $44.03042984^{o}N$, $9.81893253^{o}E$).

to the navigation systems proposed, but are caused by the simple navigation system of the real vehicle (pure dead reckoning) and to its simple control system (a PID).

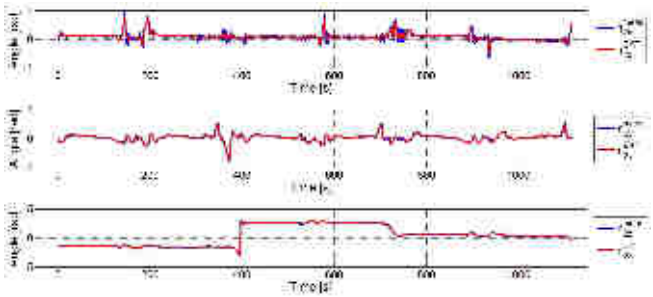

Figure 6.32: Comparison between $\vec{\eta}_2^{meas}$ and $\vec{\eta}_2^{EKF}$

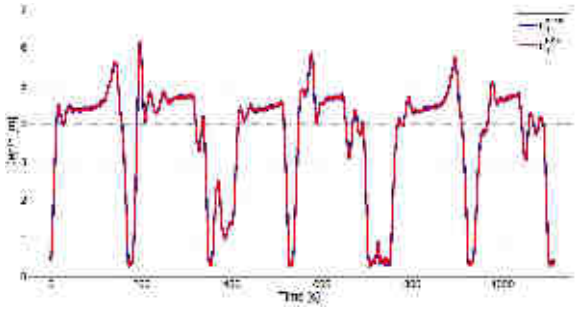

Figure 6.33: Comparison between η_{1z}^{meas} and η_{1z}^{EKF}

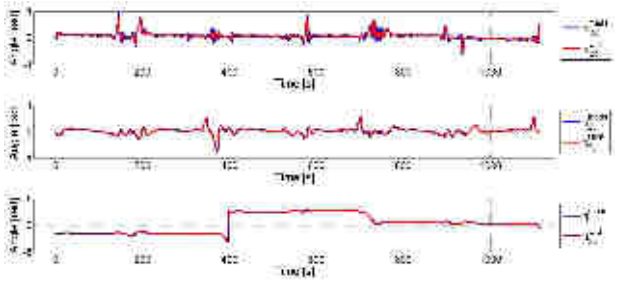

Figure 6.34: Comparison between $\vec{\eta}_2^{meas}$ and $\vec{\eta}_2^{UKF}$

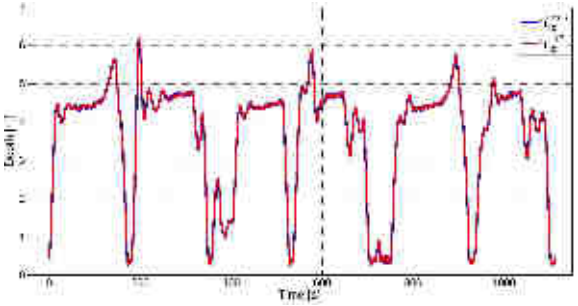

Figure 6.35: Comparison between η_{1z}^{meas} and η_{1z}^{UKF}.

6.4 Orientation Estimation

The performance of the proposed orientation estimation algorithm based on the NCF (section 5.1.2) has been tested on the TifOne AUV, described in section 6.1.1. The sensors involved in the experimental activity exposed in this section are the vehicle on board Xsens IMU and the KVH DSP-1750 single axis FOG (section 6.1.1) mounted with its sensitive axis aligned with the vehicle vertical axis (that coincides with the IMU vertical axis). Xsens MTi includes, as anticipated, a 3-axis gyroscope, a 3-axis magnetometer and a 3-axis accelerometer; in addition, the proprietary software running on it comprises a magnetometer calibration procedure and an attitude estimation algorithm. The DSP-1750 FOG, instead, outputs raw angular velocity data. The tests performed aim at comparing the roll, pitch and yaw estimations provided by the Xsens proprietary algorithm with the corresponding angles obtained through the rotation matrix calculated by means of the proposed algorithm (section 5.1.2).

The first test consists in calibrating the sensor and then completing a whole turn around the sensor vertical direction. Firstly, a complete yaw turn is performed; the sensors data acquired during this phase are used to execute the calibration algorithm explained in section 5.1.2. Subsequently, TifOne is rotated approximately on the horizontal plane and the performance of the proposed orientation estimation algorithm, exploiting the data calibrated through the proposed procedure, is evaluated in absence of considerable external disturbance sources. Let

$$\vec{\eta}_{2filter} = [\varphi_{filter}\ \vartheta_{filter}\ \psi_{filter}]^T$$

denote the roll, pitch and yaw angles extracted from the $\hat{R}$ matrix calculated

through the proposed algorithm, and

$$\vec{\eta}_{2Xsens} = [\varphi_{Xsens}\ \vartheta_{Xsens}\ \psi_{Xsens}]^T$$

be the corresponding angles given by the Xsens internal algorithm.

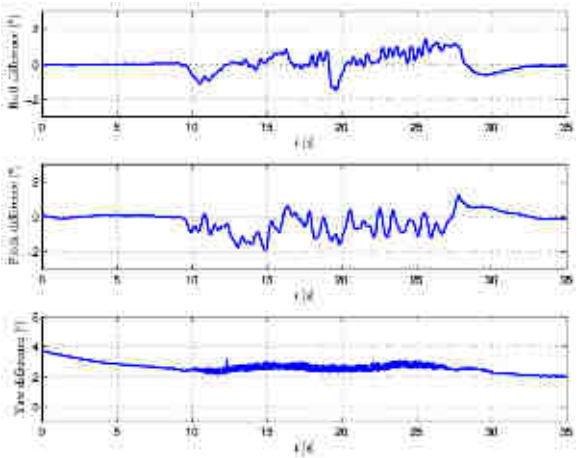

Figure 6.36: $\vec{\eta}_{2diff}$ obtained during the first test

Figure 6.36 reports the three components of the vector $\vec{\eta}_{2diff} = \vec{\eta}_{2filter} - \vec{\eta}_{2Xsens}$ obtained during the first test. Plots show that the roll and pitch difference is small (not exceeding the value of 2°) during all the time necessary to complete the whole circle, leading to the deduction that the performance about the roll and pitch estimates is comparable for the two filters, in absence of external disturbances. The yaw difference is of about 3° almost during all the period. This value corresponds to the local (Tuscan, Italy) magnetic declination angle, due to the displacement between the geographic and the magnetic Earth North. This angle, locally constant and calculable through accurate models [NGDC-NOOA, 2014], is internally compensated within the

Xsens algorithm. Thus, in the light of this consideration, the two algorithms (the one by Xsens and the proposed one) appear to be comparable also on the yaw degree of freedom, in absence of external disturbances. The yaw angle

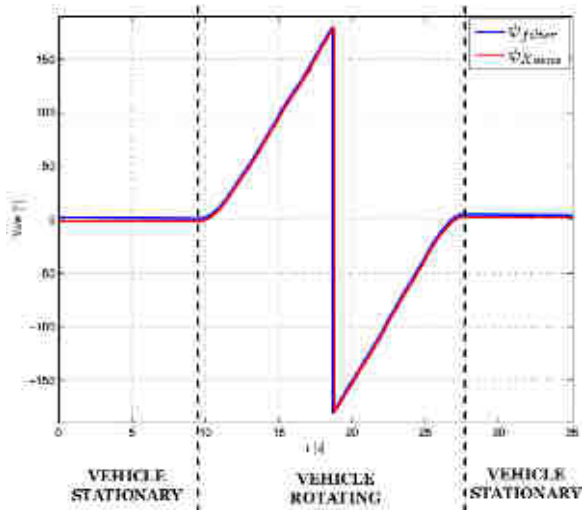

Figure 6.37: Yaw values obtained during the first test

values for the considered algorithms are visible in figure 6.37, highlighting how they almost overlap during the entire test. Regarding the behaviour of the proposed algorithm, figure 6.38 shows the variation of the gain k_2 during the test, along with the two control angles α^1_{check} and α^2_{check}; since large accelerations do not occur, gain k_1 remains stable at its maximum value and is not reported here. The horizontal dashed black lines indicate the threshold values, set at 3° for both angles. During this test, even if considerable sources of magnetic disturbances do not affect the measurement process, it happens that the gain is reduced to zero: comparing figures 6.37 and 6.38, it is possible

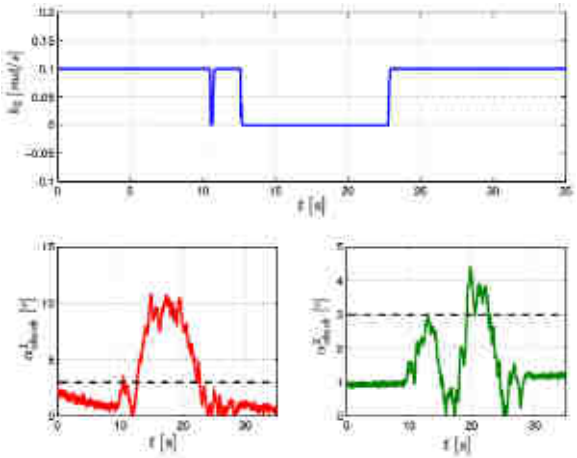

Figure 6.38: k_2 and control angles values obtained during the first test.

to deduce that the yaw estimate relies only on the integration of the FOG for about half of the turn; however, since such device is very precise (with an even increased accuracy after the correction of Earth's angular velocity bias) the result remains very performing.

The second performed test shows how the Xsens algorithm may lead to a not acceptable functioning when magnetic disturbances (be them magnets or ferromagnetic objects) get close to the sensor, causing the output to diverge from the correct attitude. The proposed algorithm, instead, guarantees a correct estimate even in the presence of disturbances. This test is composed of the following steps: without performing a new magnetometer calibration, the vehicle is at first kept stationary until convergence of the filter, then an external magnetic disturbance is artificially introduced (after 17s of testing period) by approaching a piece of metal close to the vehicle; after an amount of time, a clockwise rotation of about 40° is performed, and the metal object

is finally removed (after 55s of testing period). As for the previous test, figure

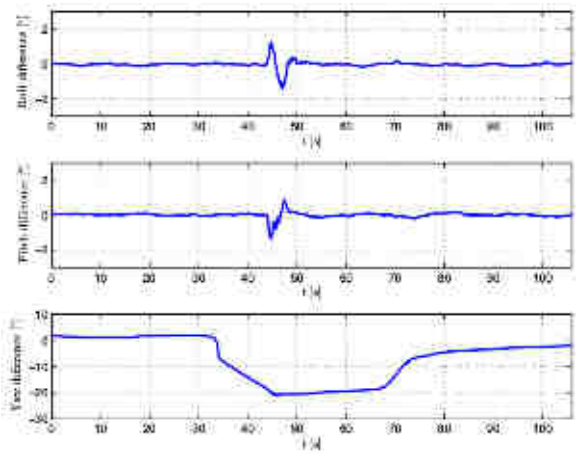

Figure 6.39: $\vec{\eta}_{2diff}$ obtained during the second test

6.39 reports the difference between the outputs of the two algorithms; while φ_{filter} and ϑ_{filter} remain close to the related values estimated by means of the Xsens software, the same does not happen in this case for the yaw estimate, which exhibits a relevant difference, up to 20°.

Figure 6.40 and figure 6.41 show that, when the disturbance of the piece of metal starts affecting the sensor (at about 17s), α^1_{check} and α^2_{check} assume a very high value and the gain k_2 is promptly reduced to zero. The Xsens algorithm, however, does not recognize the disturbance, causing a deviation of the yaw estimate even if the vehicle is kept stationary. When the disturbance source is removed after the rotation, the control angle values both fall below the threshold and the gain k_2 is set to its initial value again. By observing figure 6.40, it is possible to deduce the behaviour of the filter: when k_2 is set to zero, the yaw estimate is computed integrating the FOG readings. While

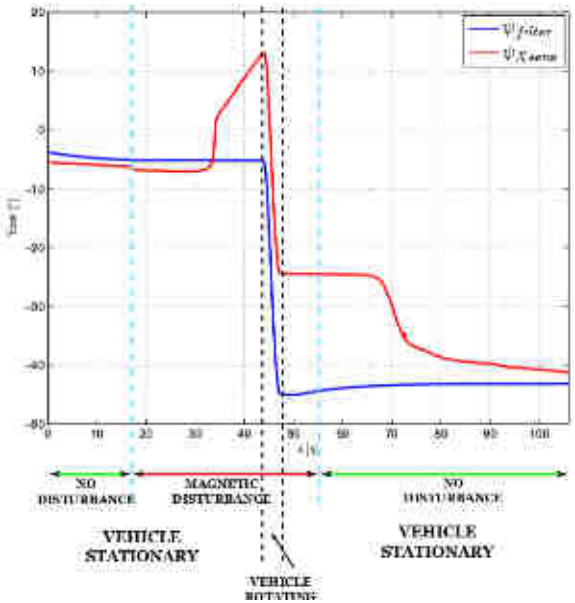

Figure 6.40: Yaw values obtained during the second test

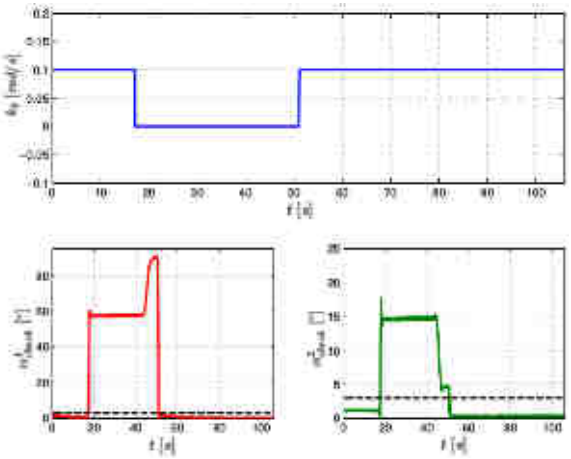

Figure 6.41: k_2 and control angles values obtained during the second test

the vehicle is not rotating, yaw angle exhibits a drift due to integration of the gyroscope measurement noise; however, due to the precision of the device, the deviation in the short term is negligible. This is further supported by the fact that, after the gain is incremented again, the correction applied by the magnetometer does not significantly modifies the current estimation. This is not the case of the Xsens: when the disturbance is added, a significant yaw drift is registered. Even if the IMU gyroscope integration is almost equal to the rotation imposed, when the disturbance is removed the final estimate is affected by the wrong integration initial value. Hence, as reported in figure 6.40, the algorithm slowly converges to the estimate given by the proposed algorithm (with the residual angular difference due to the described magnetic declination angle). Similar tests have been performed to evaluate the reliability of the proposed method; all of them confirmed the results obtained by the analysis here described.

To summarize, the proposed orientation estimation algorithm, based on the NCF presented in section 2.5.2, demonstrated through the carried out experimental activity to be able to overcome the limits of a system based only on MEMS sensors by exploiting the integration of a single axis accurate gyroscope (FOG), aligned with the vertical axis of the vehicle. The implemented system will be employed on MDM Lab UUVs to ensure a reliable orientation estimation with positive effects also on the position estimation, as it is dependent on the former (section 5.1.1). By means of the implemented strategies of signals weighing, the reliability of the orientation estimation is improved, through the proposed algorithm, also in critical conditions when external magnetic disturbances, impossible to be compensated during the calibration phase, affect the measurements.

Chapter 7

Conclusions

In this thesis work, the study about theoretical and practical aspects related to the navigation system for UUVs (Unmanned Underwater Vehicles), carried out at the Mechatronics and Dynamic Modelling Laboratory (MDM Lab) of the Department of Industrial Engineering of the University of Florence during the years 2012-2014, has been described. The work has been developed mainly in the framework of two projects (the Tuscan regional project THESAURUS and the European FP7 project ARROWS) both aimed at exporting the technology of UUVs, in particular AUVs (Autonomous Underwater Vehicles), from classical application fields (e.g. the military and Oil&Gas ones) towards the field of underwater archaeology in order for this fundamental field of culture to take advantage from these tools.

This process, naturally, collides with the different available financial resources in the two fields; thus, the carried out research activity had to take into account this aspect too. The methodology followed to address the emerged research questions has been characterized by the study of the possible solutions, for the limits identified in the state of the art, that could exploit smart and performing algorithms rather than, for example, expensive

sensors or devices in general.

Once identified in the *localization* and the *modelling* two fundamental aspects necessarily affecting the *navigation* performance, the research activity focused much on techniques of vehicle position measurements, alternative to the USBL (Ultra Short BaseLine) and LBL (Long BaseLine) acoustic systems commonly exploited (chapter 4), on the research of a suitable motion model (chapter 3) as on the pure study of performing position estimation algorithms (chapter 5).

In this chapter, a relevant section (5.1.2) has been dedicated to the description of the carried out research activity aimed at defining a reliable orientation estimation system, robust against the potential sources of disturbances that an UUV may have to deal with. An algorithm has been proposed in order to go over the state of the art on the topic and to face all the potential sources of error with particular attention to the rejection of magnetic disturbances affecting the on board compass measures (the importance of this aspect is evident thinking to missions on modern metal shipwreck).

The proposed strategies and algorithms have been characterized through simulations and experimental activities, reported and analysed in chapter 6 dedicated to the achieved results.

As concerns my formation, it has for sure strongly benefited from the experimental testing campaigns and the field missions to which I had the chance to take part during the last three years, as they permitted me to extend my activity from the pure research to the applied research through the comparison with real issues and real needs of the underwater robotics field.

Bibliography

[Allotta, 2014] Allotta, B. (2014). http://www.arrowsproject.eu. *Official Site of the European ARROWS Project*.

[Allotta et al., 2014a] Allotta, B., Bartolini, F., Caiti, A., Costanzi, R., Di Corato, F., Fenucci, D., Gelli, J., Guerrini, P., Monni, N., Munafó, A., Natalini, M., Pugi, L., Ridolfi, A., and Potter, J. (2014a). Typhoon at CommsNet 2013: experimental experience on auv navigation and localization. In *Proceedings of the 19th IFAC World Congress*, Cape Town, South Africa.

[Allotta et al., 2014b] Allotta, B., Bartolini, F., Costanzi, R., Monni, N., Pugi, L., and Ridolfi, A. (2014b). Preliminary design and fast prototyping of an autonomous underwater vehicle propulsion system. *Proceedings of the Institution of Mechanical Engineers - Part M, Journal of Engineering for the Maritime Environment*, DOI 10.1177/1475090213514040.

[Allotta and Caiti, 2014] Allotta, B. and Caiti, A. (2014). http://thesaurus.isti.cnr.it. *Official Site of the Italian THESAURUS Project*.

[Allotta et al., 2014c] Allotta, B., Costanzi, R., Meli, E., Pugi, L., Ridolfi, A., and Vettori, G. (2014c). Cooperative localization of a team of auvs by a tetrahedral configuration. *Robotics and Autonomous Systems*, 62:1228–1237.

[Allotta et al., 2012] Allotta, B., Costanzi, R., Monni, N., Pugi, L., Ridolfi, A., and Vettori, G. (2012). Design and simulation of an autonomous underwater vehicle. In *Proceedings of the European Congress on Computational Methods in Applied Sciences and Engineering, ECCOMAS 2012*, Vienna, Austria.

[Antonelli, 2006] Antonelli, G. (2006). *Underwater Robots*. Elsevier, Amsterdam, Holland.

[Arrichiello et al., 2011] Arrichiello, F., Antonelli, G., Aguiar, A. P., and Pascoal, A. (2011). Observability metric for the relative localization of auvs based on range and depth measurements: Theory and experiments. In *IEEE/RSJ International Conference on Intelligent Robots and Systems (IROS)*, San Francisco, CA, USA.

[Bahr et al., 2009a] Bahr, A., Leonard, J., and Fallon, M. (2009a). Cooperative localization for autonomous underwater vehicles. *The International Journal Robotics Research*, 28:714–728.

[Bahr et al., 2009b] Bahr, A., Walter, M., and Leonard, J. (2009b). Consistent cooperative localization. In *Proceedings of the IEEE International Conference of Robotics and Automation (ICRA)*, Kobe, Japan.

[Bar-Shalom et al., 2001] Bar-Shalom, Y., Li, X. R., and Kirubarajan, T., editors (2001). *Estimation with Applications to Tracking and Navigation*. Wiley and Sons, New York, NY, USA.

[Barisic et al., 2012] Barisic, M., Vasilijevic, A., and Nad, D. (2012). Sigma-point unscented kalman filter used for auv navigation. In *20th Mediterranean Conference on Control & Automation (MED)*, Barcelona, Spain.

[Barshan and Durrant-Whyte, 1995] Barshan, B. and Durrant-Whyte, H. F. (1995). Inertial navigation systems for mobile robots. *IEEE Transactions on Robotics and Automation*, 11:328–342.

[Batista et al., 2011] Batista, P., Silvestre, C., and Oliveira, P. (2011). Single range aided navigation and source localization: observability and filter design. *Systems and Control Letters*, 60:665–673.

[Caiti et al., 2013] Caiti, A., Calabrò, V., Fabbri, T., Fenucci, D., and Munafò, A. (2013). Underwater communication and distributed localization of auv teams. In *Proceedings of IEEE OCEANS 2013*, San Diego, CA, USA.

[Carlton, 2007a] Carlton, J., editor (2007a). *Marine propellers and propulsion*. Elsevier, Amsterdam, Holland.

[Carlton, 2007b] Carlton, J. (2007b). *Marine Propellers and Propulsion, 2nd edition*. Springer-Verlag, Heidelberg, Germany.

[Di Corato et al., 2014] Di Corato, F., Fenucci, D., Caiti, A., Costanzi, R., Monni, N., Pugi, L., Ridolfi, A., and Allotta, B. (2014). Toward underwater acoustic-based simultaneous localization and mapping. experimental results with the typhoon auv at commsnet13 sea trial. In *Proceedings of OCEANS'14 MTS/IEEE St. John's Oceans*.

[Eustice et al., 2011] Eustice, R., Whitcomb, L., Singh, H., and Grund, M. (2011). Experimental results in synchronous-clock one-way-travel time acoustic navigation for autonomous underwater vehicles. In *IEEE International Conference on Robotics and Automation (ICRA)*, Rome, Italy.

[Evensen, 2009] Evensen, G., editor (2009). *Data Assimilation*. Springer Verlag, Heidelberg, Germany.

[Fitzgibbon et al., 1999] Fitzgibbon, A., Pilu, M., and Fisher, R. (1999). Direct least square fitting of ellipses. *IEEE Trans. on Pattern Analysis and Machine Intelligence*, 21.

[Fossen, 1994] Fossen, T. (1994). *Guidance and Control of Ocean Vehicles*. John Wiley and Sons, London, UK.

[Gao and Chitre, 2010] Gao, R. and Chitre, M. (2010). Cooperative positioning using range-only measurements between two auvs. In *Proceedings of IEEE OCEANS 2010*, Sidney, Australia.

[Halíř and Flusser, 1998] Halíř, R. and Flusser, J. (1998). Numerically stable direct least square fitting of ellipses. In *WSCG International Conference in Central Europe on Computer Graphics and Visualization*.

[Julier and Uhlmann, 1997] Julier, S. and Uhlmann, J. (1997). A new extension of the kalman filter to nonlinear systems. *IEEE Transactions on Automatic Control*, pages 182–193.

[Julier and Uhlmann, 2004] Julier, S. and Uhlmann, J. (2004). Unscented filtering and nonlinear estimaion. *Proceedings of the IEEE*, 92:401–422.

[Kalman, 1960] Kalman, R. E. (1960). A new approach to linear filtering and prediction problems. *Journal of Basic Engineering*, 82:35–45.

[Lee et al., 2007] Lee, P. M., Jun, B. H., Kim, K., Lee, J., Aoki, T., and Hyakudome, T. (2007). Simulation of an inertial acoustic navigation system with range aiding for an autonomous underwater vehicle. *IEEE Journal of Oceanic Engineering*, 32:327–345.

[Mackenzie, 1981] Mackenzie, K. (1981). Nine-term equation for the sound speed in the oceans. *J. Acoust. Soc. Am.*, 70:807–812.

[Mahony et al., 2008] Mahony, R., Hamel, T., and Pflimlinn, J. M. (2008). Nonlinear complementary filters on the special orthogonal group. *IEEE Trans. Automat. Control*, 53:1203–1218.

[Marins et al., 2001] Marins, J., Yun, X., Bachmann, E., McGhee, R., and Zyda, M. (2001). An extended kalman filter for quaternion-based orientation estimation using marg sensors. In *Intelligent Robots and Systems, 2001. Proceedings. 2001 IEEE/RSJ International Conference on*, Maui, HI.

[NGDC-NOOA, 2014] NGDC-NOOA (2014). www.ngdc.noaa.gov. *NOAA National Geophysical Data Center - Official Website*.

[Packard et al., 2013] Packard, G., Kukulya, A., Austin, T., Dennett, M., Littlefield, R., Packard, G., Purcell, M., Stokey, R., and Skomal, G. (2013). Continuous autonomous tracking and imaging of white sharks and basking sharks using a remus-100 auv. In *Proceedings of the IEEE OCEANS 2013*, San Diego, CA, USA.

[Parlangeli et al., 2012] Parlangeli, G., Pedone, P., and Indiveri, G. (2012). Relative pose observability analysis for 3d nonholonomic vehicles based on range measurements only. In *Proceedings of the 9th IFAC Conference on Manoeuvring and Control of Marine Craft*, Arenzano, Italy.

[Pivano et al., 2009] Pivano, L., Johansen, T. A., and Smogeli, . N. (2009). A four-quadrant thrust estimation scheme for marine propellers: Theory and experiments. *Control Systems Technology, IEEE Transactions on*, 10.1109/TCST.2008.922602.

[Sayed, 2009] Sayed, A. H., editor (2009). *Adaptive Filters*. Wiley and Sons, Hoboken, NJ, USA.

[Singh et al., 2006] Singh, S., Grund, M., Bingham, B., Eustice, R., Singh, H., and Freitag, L. (2006). Underwater acoustic navigation with the whoi micro-modem. In *Proceedings MTS/IEEE Conference and Exhibition OCEANS 2006*, Boston, MA, USA.

[Stokey et al., 2005] Stokey, R., Roup, A., von Alt, C., Allen, B., Forrester, N., Austin, T., Goldsborough, R., Purcell, M., Jaffre, F., Packard, G., and Kukulya, A. (2005). Development of the remus 600 autonomous underwater vehicle. In *Proceedings of the IEEE OCEANS 2005*, Washington D.C.,USA.

[Thrun et al., 2005] Thrun, S., Burgard, W., and Fox, D. (2005). *Probabilistic Robotics*. The MIT Press.

[UniWisconsin, 2014] UniWisconsin (2014). http://www.uwgb.edu. *University of Wisconsin - Green Bay Web Site*.

[VectorNav-Technologies, 2014] VectorNav-Technologies (2014). http://www.vectornav.com. *Official website of VectorNav Technologies*.

[Wan and Merwe, 2001] Wan, E. A. and Merwe, R. V. D. (2001). *The Unscented Kalman Flter*. S. Haykin Edition, New York, NY, USA.

[Webster et al., 2009] Webster, S., Eustice, R., Singh, H., and Whitcomb, L. (2009). Preliminary deep water results in single-beacon one-way travel-time acoustic navigation for underwater vehicles. In *IEEE/RSJ International Conference on Intelligent Robots and Systems*, St. Louis, MO, USA.

[Wolfram-MathWorld, 2014] Wolfram-MathWorld (2014). http://www.mathworld.wolfram.com. *Wolfram MathWorld - Official Website*.

[Zhao and Gao, 2004] Zhao, L. and Gao, W. (2004). The experimental study on gps/ins/dvl integration for auv. In *Position Location and Navigation Symposium (PLANS)*, Monterey, California.